European Commission funded Enlargement Workshop

Materials resistant to extreme conditions for future energy systems

12-14 JUNE, 2017, Kyiv - UKRAINE

Session 3: Structural materials development for energy applications;

FRACTAL NATURE OF NANO-MICRO STRUCTURE AND ENERGY

V.V. Mitic[1,2*], V. Paunovic[1], Lj. Kocic[1], Hans-J. Fecht[3]

[1]*Faculty of Electronic Engineering, University of Nis, Serbia*

[2]*Institute of Technical Sciences of the Serbian Academy of Sciences and Arts, Belgrade, Serbia*

[3]*Institute of Micro and Nanomaterials, University of Ulm, Ulm, Germany*

Abstract

Fractal microelectronics is a new developing topic that uses fractal nature to improve understanding, analyzing and modeling processes and developing advantageous methods for energy producing, harvesting and storage. In this sense the new experimental-theoretical approach frame methodology is developed by the authors. It includes theoretical models of fractal dimension extraction, building computer models that simulate an energetic source phenomena being studied (energetic cells, solar collectors, wind turbines etc.). The most experiments were done on ceramics capacitors by direct measuring of impedance for given fractal characteristics. The concept design main goal is to predict performances of final products, and their optimization. Through this method and results, we are opening the Fractal microelectronic new frontiers and technological processes, especially specific intergranular relations within grains surfaces coatings and thin film's fractal nature microelectronics. Since the fractal approach offers a coherence on the wide continuous metric scale from macro to micro world, even to nanoscale, it opens the new "window" for further development in achieving universality of relationship between forms and energy in the broad sense as well as miniaturization improvement.

Introduction

Knowledge on morphology of ceramics grains and pores helps in sintering process to be better understood. Real intergrain contact surfaces as highly irregular objects can be described in only adequate way, by using fractal models. Both micro and nanostructure of grains' shapes and intergranular contacts are easy to be reconstructed by fractal analysis/modelling. Here, several variations of the Coble's two-sphere model, are reviewed. Further, the intergranular capacity model has been re-investigated from the point of view of intergranular fractal formations. The area of grains' surface is calculated using fractal correction and fractal dimension. This leads towards a more exact numerical description of ceramics electronics parameters and related properties.

Especially, the role of dielectric constant, being corrected upon intergranular morphology fractal nature causes corrections in Heywang model and Curie-Weiss law.

In order to obtain an equivalent circuit model, an intergranular contacts model for barium-titanate electrical properties characterization is determined and implemented. The improved material prognosis of electronic properties can be given on the basis of micro-nanostructure fractal relations. Considering the obtained results, the new frontiers for deeper and higher level electronics circuit microelectronic integration are established, which is, practically progress towards the new frame of fractal electronics.

The sintering process is characterized by an extreme complexity due to the simultaneous and successive action of elementary mechanisms. Generally speaking, it is very difficult to follow all those actions, and give their qualitative or quantitative descriptions [1-9].

---

1. Coble, R.L., Effects of Particle-Size Distribution in Initial-Stage Sintering, *J. Am. Ceram. Soc.* **56** (9) 461–466 (1973)
2. Coble, R.L., Sintering of crystalline solids. I. Intermediate and final state diffusion models, *J. Appl. Phys.*, **32,** 789–92, (1961).
3. Gibbs, J.W.: Collected Works, Longmans, New York, 1928.
4. Wulff, G. On the question of the speed of growth and the resolution of On the question of the speed of growth and the resolution of crystal surfaces (in German), *Z. Kristallogr*. 34 449–530, (1901).
5. Mitić, V.V., Structures and elektrical properties of $BaTiO_3$ ceramics, Begrade: Zadužbina Andrejević (in Serbian), 2001.
6. Kang, S.J. L., Sintering. Densification, Grain Growth, and Microstructure, Elsevier 2005.
7. DeJonge L., Rahman M.N., Sintering of Ceramics, Handbook of Advanced Ceramics, S.Sowmya et al. (Eds.), Elsevier (78s), 2003
8. Cho, Y.K., Kang, S.L., Yoon, D.Y. Dependence of grain growth and grain-boundary structure on the Ba/ Ti ratio in $BaTiO_3$, *J. Am. Ceram. Soc.*, 87 119-124, (2004).
9. Zhang, D., Weng, G., Gong, S., Zhou D, The kinetics of initial stage in sintering process of BaTiO3 based PTCR ceramics and its computer simulation, *Materials Science and Engineering B*, 99 [1-3] 88-92, (2003)

Ceramic grains contacts are essential for understanding complex electrodynamic properties of sintered materials. Microstructures of sintered BaTiO3-ceramics, observed by SEM method, are characteristic example of complex shape geometry, which cannot easily be described or modelled. In this manner, a possible approach for describing contact morphology has been established in the updated grains contact models. Some initial research [3, 4] of $BaTiO_3$-ceramics intergranular contacts show that they have the great influence on electrical properties of the entire material. Intergranular contacts are formed during sintering process. When two particles of powder are sintered, they form a contact, while the interatomic forces start forming a particle's neck in the contact area. When a powder aggregate is sintered, necks between powder particles are formed, which causes increment in material's density. A common driving force of the transport mechanisms is the reduction in the surface area, and thus the reduction of surface free energy of the system which contributes to densification. In further process, a neck begins to grow and this process is controlled by different diffusion mechanisms (lattice diffusion, grain boundary diffusion etc.) with the rates determined by total flux of atoms coming to the neck.

The aim of this presentation is to review models of three or more spherical grains in contact, as a base for calculating the values of possible contact areas in given geometry configuration. This matter is organized in two directions. First, the simulation of neck growth in time domain is done by combining results for contact surfaces' values with the kinetics of forming three or more contact areas. Second, the model of three or more grains in contact is used for establishing an equivalent electrical model of such grains' association. It is shown that BaTiO3 sample can be modelled as impedance containing two capacitors, an inductor and one resistor [7]. As a ceramics sample consists of numerous grains organized in clusters of different sizes, it could be supposed that each cluster and even each intergranular contact within the cluster, shows similar behaviour. The dominant contribution to the equivalent impedance within a wide frequency range comes from a capacitance [7]. So, any intergranular contact can be observed as an intergranular microcapacitor. On the base of these considerations, equivalent electrical models of three and four grain clusters are presented. All of these models and electrical contact surfaces processes are based on computer modelling and simulation methods application.

An extreme complexity of the sintering process influences the study of this process through different sintering models. Most of the sintering models have used two-sphere model as the simplest model for studying elementary mechanisms responsible for the progress of the sintering process. Such an idealization of the geometry of the sintering particles enables very detailed study of physical processes acting in the contact region. In this paper, Coble's two sphere model [1] is used as initial one for developing a new *two-ellipsoid model*. Ellipsoidal geometry gives a more appropriate representation of an average grain than the spherical one. Namely, the specific energy and curvature of the particle surfaces provide an effective stress on the atoms under the surface defined by the Young-Laplace equation that uses two radii of curvature in a point of grain’s surface. The simplest surface with two different curvature radii is an ellipsoid.

The relations connecting geometric parameters of the ellipsoidal model with consolidation parameters, sintering time and temperature are reformulated. For better understanding of intergranular processes, Coble's model was generalized for other possible geometric shapes (sphere-polyhedron, polyhedron-polyhedron). Then, the results of a new model are compared with those obtained from Coble's two-sphere model.

The sphere-sphere model

In order to explain two grain contact during sintering process and better understanding of electrical properties of $BaTiO_3$-ceramics, we start with the Coble's model [1], Fig. 1. In the process of the diffusion in initial-stage sintering, two grains, approximated by spheres penetrated each other slightly. The volume that fills intersection of spheres (the distance between centres is smaller than a sum of two radii) transforms into a neck (a kind of collar circumscribing the contact area), with the next assumptions: (i) $x << a$, (ii) volume conservation, (iii) centre-to-centre approach, and (iv) a straight line neck geometry. For the model system topology shown on Fig. 1, [24] were the following equations from the volume conservation principle in the contact region are derived:

$$\rho_1 = \frac{X_2^2}{4R_1}, \quad \rho_2 = \frac{X_2^2}{4R_2}, \quad X_2 = \sqrt{2}X_1, \tag{1}$$

24. Chen, J.H. Johnson, P.F., Computer Simulation of Initial Stage Sintering in Two-Dimensional Particulate Systems", P.E. Russell, Ed., Microbeam Analysis- 405-409, 1989,

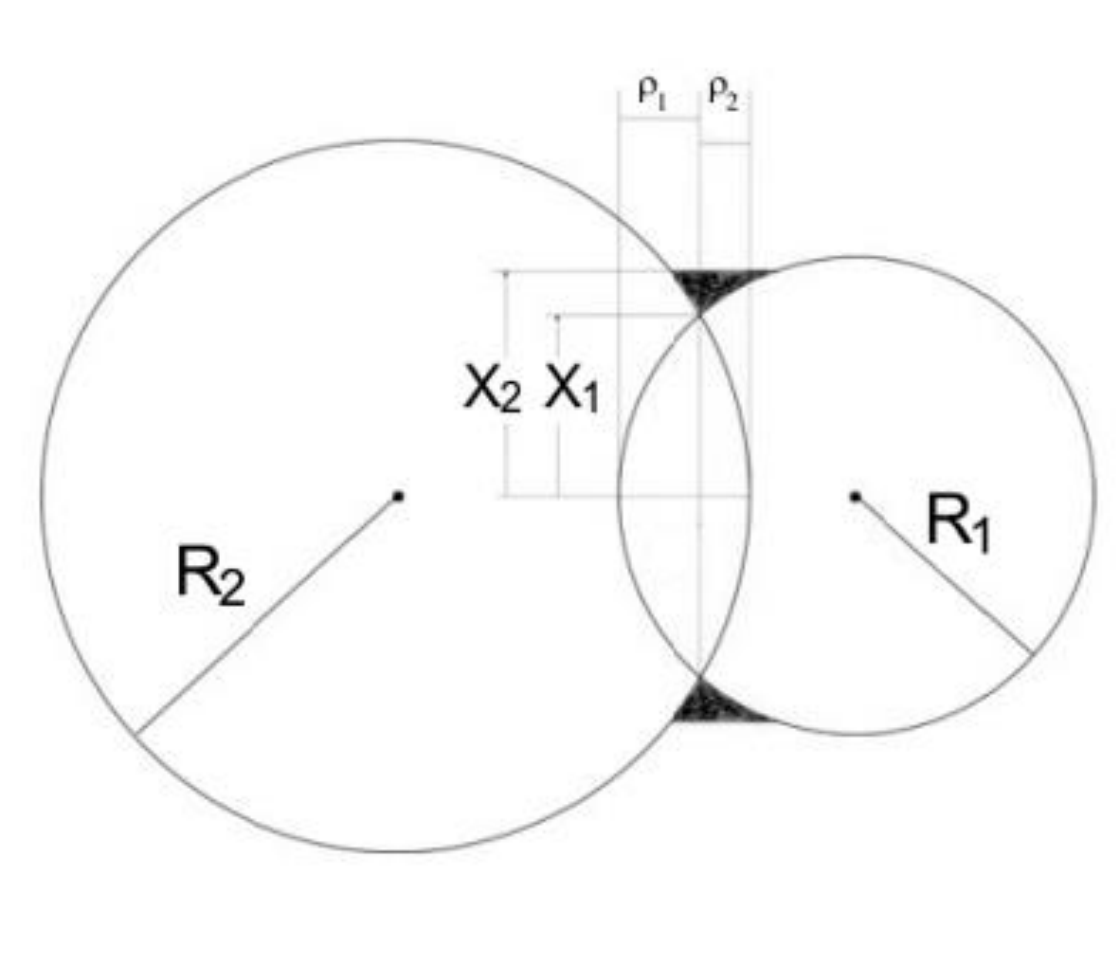

Figure. **1.** The Coble's two sphere model.

where ρ_1, ρ_2 are spherical caps heights (forming the common volume of the spheres intersection), X_1- radius of a common circle, X_2 - the radius of the neck formed by diffusion in initial stage of sintering, R_1 and R_2 - radii of two spheres.

In the general case, the neck radius is time dependent and can be written in the form, $X_2 = g(t; T, \mathbf{A})$ where T is sintering temperature, and $\mathbf{A}$ is system parameters vector

$$\mathbf{A} = \{a, \mathbf{D}, \mathbf{Q}, \gamma, T_m, \Omega, \delta_B\}$$

where a is particle radius, $\mathbf{D}$ and $\mathbf{Q}$ are the vectors of diffusion coefficients and activation energies of transport mechanisms respectively, γ is boundary free energy, T_m - melting temperature, Ω - atom volume, and δ_B -effective grain boundary thickness.

Densification and neck formation is a result of the action of next possible transport mechanisms [6]: lattice diffusion from grain boundary, grain boundary diffusion, viscous flow (from grain's bulk), grain surface diffusion, grain surface evaporation, and gas diffusion.

It is known that a polyhedral crystal in equilibrium with the surroundings would assume a shape with the minimum surface free energy [3].

This principle was transferred into the following extended proportion [4], known as "equilibrium form":

$$\frac{\gamma_i}{r_i} = \frac{kT}{2v_1} \ln \frac{P}{P_\infty}, \quad i = 1, 2, 3, \ldots$$

where γ_i is the specific surface energy of the *i-th* face of the polyhedral crystal, r_i is the central distance to the *i-th* face, v_i is the molecular volume of the solid, P is the vapour pressure of the polyhedral crystal, and P_∞ is the vapour pressure of a crystal of infinite dimensions.

The same authors also gave in their extended model, equations for lattice and boundary diffusion of the following type:

$$Y_1 + Y_2 = \left[B_L t \left(\frac{1}{R_1} + \frac{1}{R_2} \right) \right]^{1/2}, \quad B_L = 8 D_L \frac{\gamma \Omega}{kT}, \tag{2}$$

$$Y_1 + Y_2 = \left[B_B t \left(\frac{1}{R_1} + \frac{1}{R_2} \right) \right]^{1/3}, \quad B_B = 12 D_B \delta_B \frac{\gamma \Omega}{kT}, \tag{3}$$

where D_L and D_B are lattice and grain-boundary diffusion coefficients, respectively.

The equations (2) and (3) are fundamental in modelling the "geometry" of intergrain sintering and the neck formation. Two spheres with radii R_1 and R_2, the common intersection circle area is given by

$$P_c = \pi\left(R_1^2 - \frac{(d^2 + R_1^2 - R_2^2)^2}{4d^2} \right),$$

provided d is the centres' distance. The common volume is

$$V_C = \frac{\pi}{6}\left(3X_1^2\left(R_1 + R_2\right) + R_1^{\,3} + R_2^{\,3}\right).$$

The next step towards a more realistic Coble's model is considering the neck profile update as it is shown in Fig. 2. The cross section with rotation symmetry plane reveals the neck border outwards radius r existence. In the case $R_1 = R_2$, the graphical interpretation of the cross-section of the common lens-like zone, the "neck" and the relative position of both is shown in Figure 3 (left side), while on the right side are shown all mentioned elements in 3D – perspective projection.

On the other hand, the Figure 4 displays the functional dependence of $r(R, h)$, where R is the radius of spheres (which are equal), and h is the thickness of a half of lens.

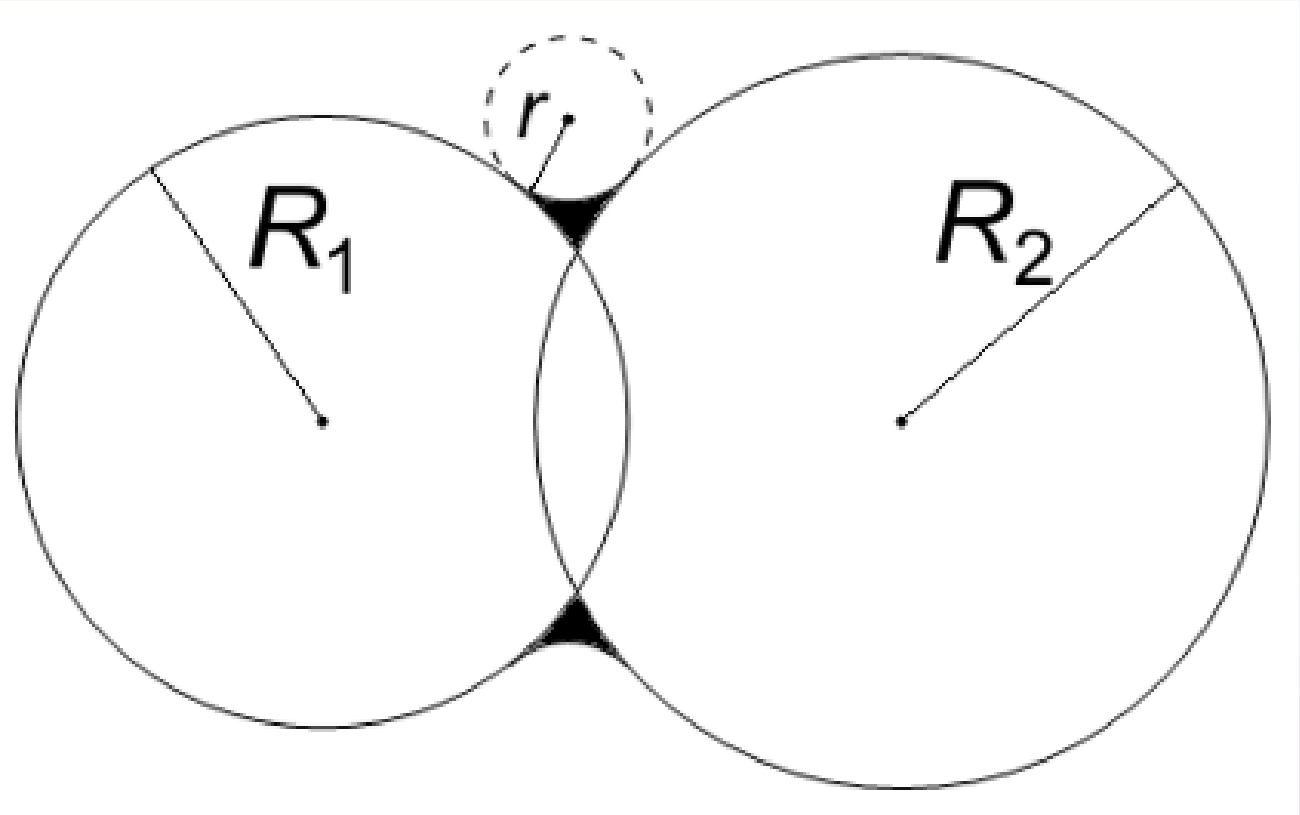

Figure. **2.** The “realistic” two sphere model.

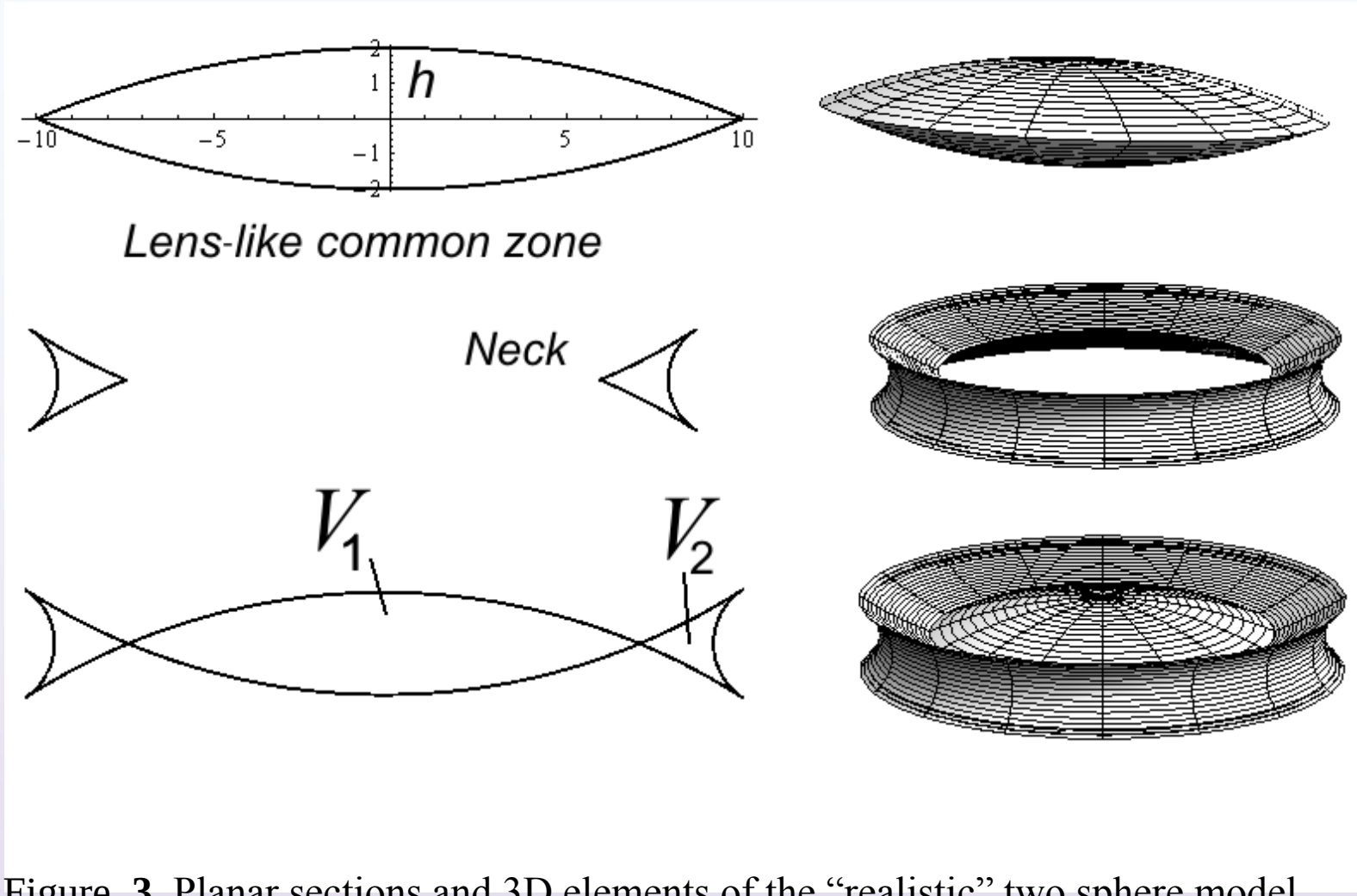

Figure. **3**. Planar sections and 3D elements of the “realistic” two sphere model.

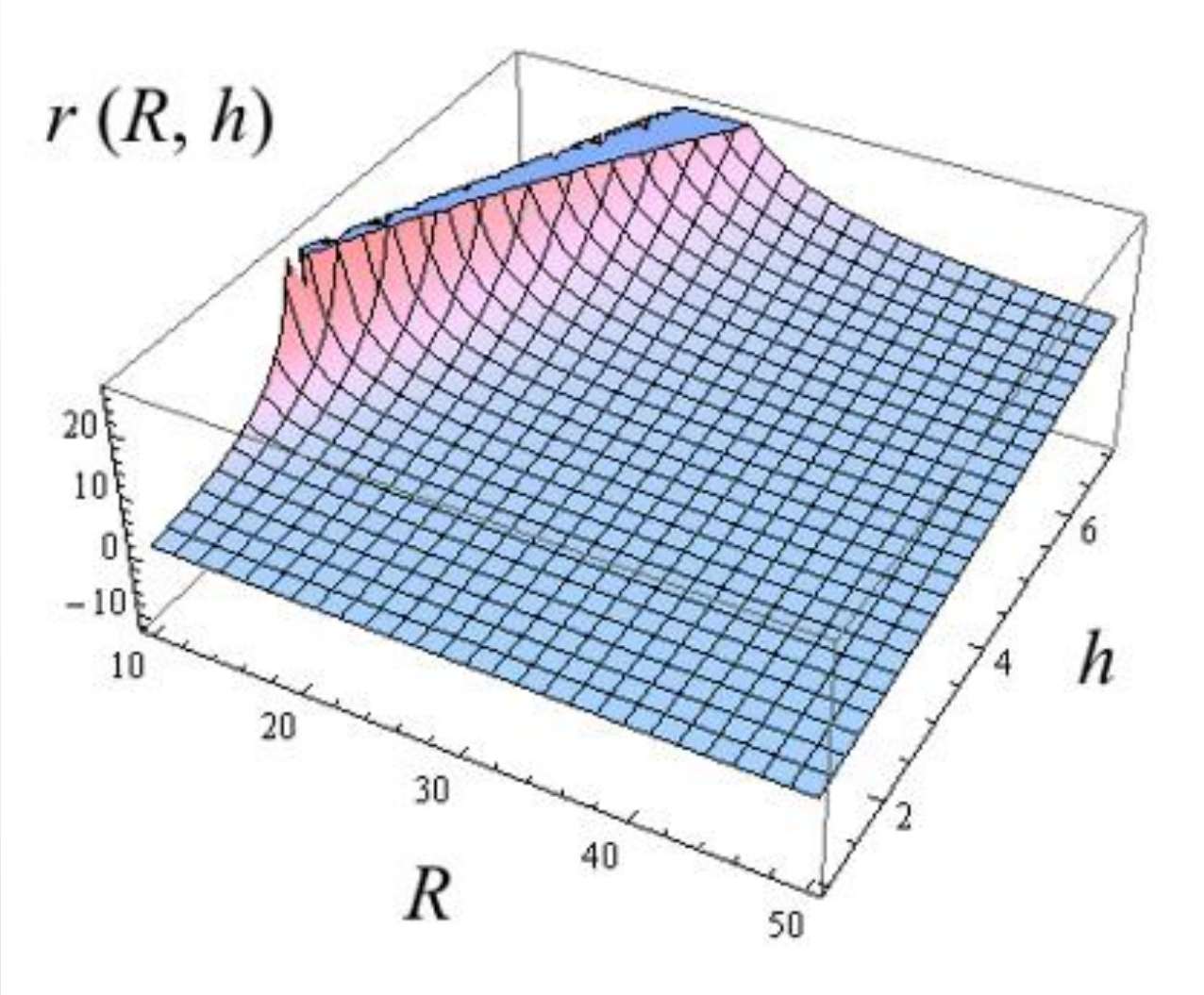

Figure **4.** The radius r from Fig. 3 as function of $R = R_1 = R_2$, and h, the height of a "half length" of lens-like common zone.

In connection with ceramics grains' clusters there is an intriguing concept of Apollonian sphere packing, the 3D equivalent of Apollonian gasket, a fractal construction mentioned by Mandelbrot [30]. Using inversion method, Boyd [31] established criteria for a single sphere to tangent other N unequal spheres touching each other. Based on this result, Borkovec et al. [32] estimated fractal dimension of the Apollonian sphere packing as approx. 2.473394, which is on the lower limit of the dimensions estimated using SEM photos of ceramics material, ranging from 2.4 to 2.85 (roughly).

---

30. Mandelbrot, B. B., The fractal geometry of nature, W. H. Freeman, New York 1983.

31. Boyd D. W., The osculatory packing of a three dimensional sphere, Canad. J. Math. 25, 303-322 (1973).

32. Borkovec M. et al., The Fractal Dimension of the Apollonian Sphere Packing, Fractals, Vol. 2, No. 4, 521-526 (1994).

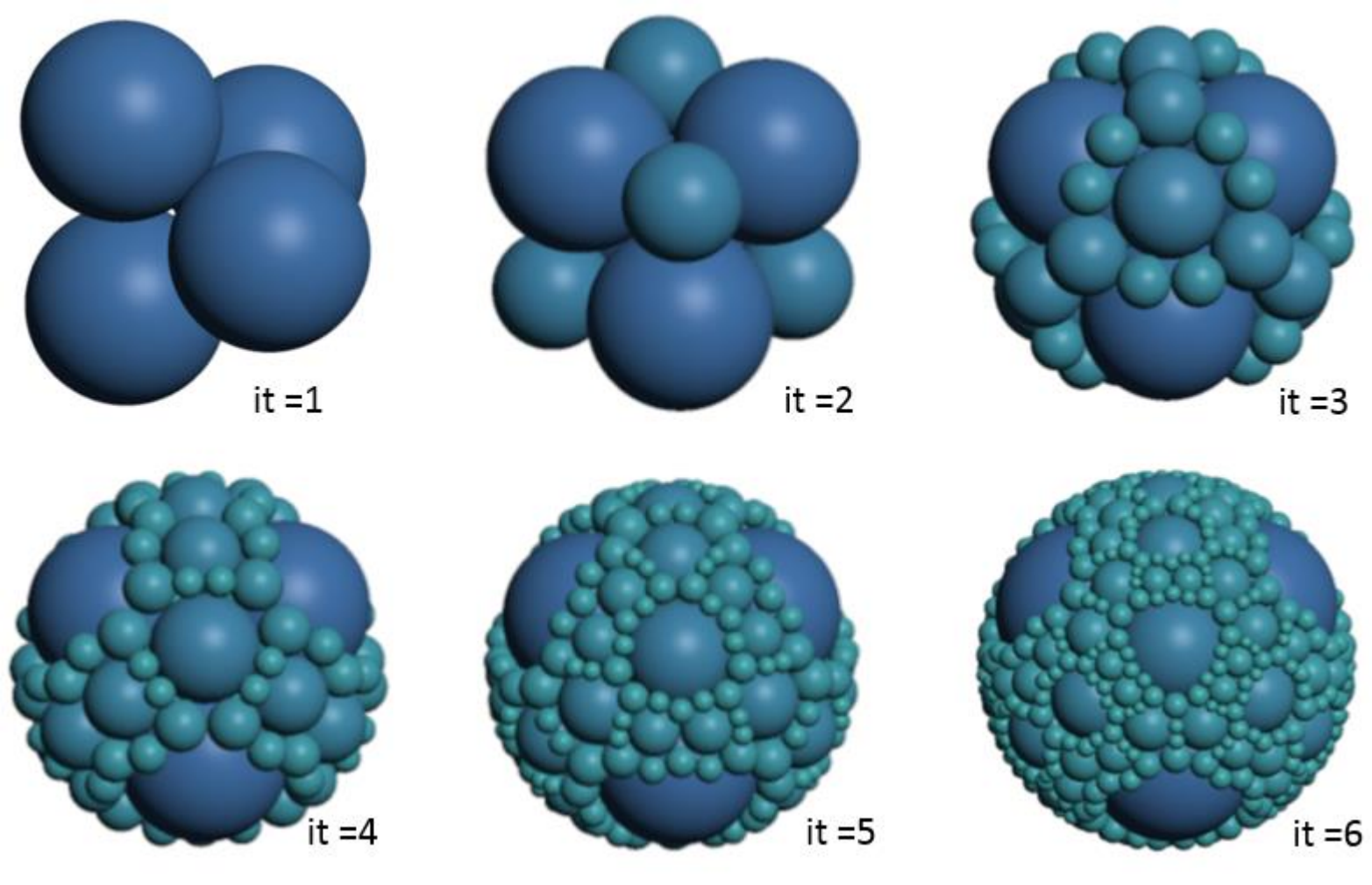

Figure **4a.** The 3D Apollonian sphere fractal generated by AploFrac 1.0 (freeware by Th. Bonner, 2011). No of iterations 1 – 6. According to [Borkovec et al.], DH_f = 2.4739465 is fractal dimension of the limiting figure (iteration tends to + oo)

Spherical to Ellipsoidal Model Transformation

Spherical model (S) can be successfully converted into ellipsoidal one (E) by applying an affine transformation $\Phi: \mathrm{S} \to \mathrm{E}$ of the form

$$\Phi: \begin{bmatrix} x \\ y \\ z \end{bmatrix} \to \begin{bmatrix} x/a \\ y/b \\ z/c \end{bmatrix}, \qquad (a, b, c > 0) \ , \tag{4}$$

where a, b and c are scaling parameters introduced for generation of ellipsoidal semi axes a_i, b_i and c_i ($i = 1, 2$), and x, y and z are local variables. The main properties of this transformation are its *non-singularity* ($a, b, c \neq 0$) and *continuity* which induces *topological invariance*. This means that the ratio conserving property of the transformation (4) is of essential importance for derivation of the ellipsoidal model.

Ellipsoid-ellipsoid model

The grains of $BaTiO_3$-ceramics sample can be approximated by ellipsoids scattered throughout the material's volume. These ellipsoids can be seen as a model of grains in mutual contact. Actually, due to sintering pressure and sintering process, one grain partly penetrates into another, forming a small contact area that can be pretty accurately approximated by intersection of ellipsoids E_1 and E_2. Our aim is to determine the value of this area as the function of grains' centres distance δ_E^o (Fig. 5).

Assumed that the ellipsoidal axes are pairwise parallel and lengths of the axes are proportional by the factor k, two ellipsoids E_1 and E_2, having centres at $C_1 = (x_1, y_1, z_1)$ and $C_2 = (x_2, y_2, z_2)$ from $\mathbb{R}^3$, being coaxial (having parallel axes) with semi-axes a_i, b_i, c_i ($i = 1, 2$) provided that $a_i > b_i > c_i$, and $a_2/a_1 = b_2/b_1 = c_2/c_1 = k$ ($k > 0$), are considered (Fig. 5a). Suppose that E_1 and E_2 approximate two neighbour grains in sintered $BaTiO_3$-ceramics (Fig. 5b). Straightforward calculation gives that the distance between C_1 and C_2 in the beginning of sintering (sintering time = 0) is given by

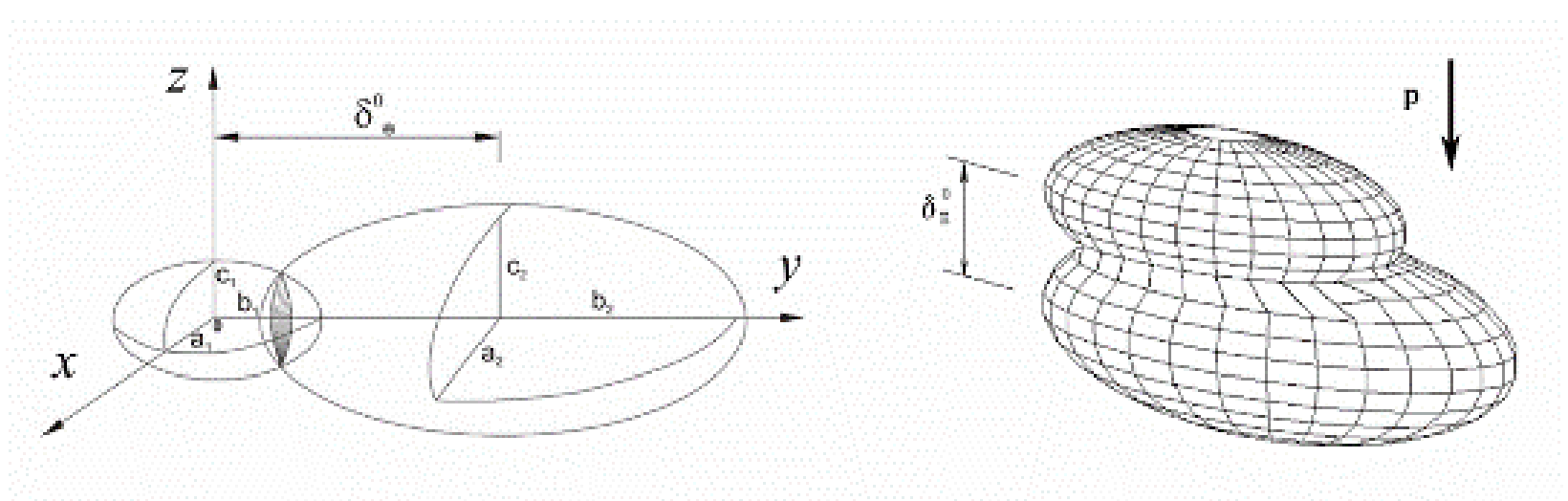

Figure **5**. a) Ellipsoidal grain approximation, b) neck growth of two ellipsoidal grains in sintering process.

$$\delta_E^o = \frac{1+k}{\sqrt{\dfrac{\cos^2\alpha}{a_1^2} + \dfrac{\cos^2\beta}{b_1^2} + \dfrac{\cos^2\gamma}{c_1^2}}},$$

where $(\cos\alpha, \cos\beta, \cos\gamma)$ is the unit vector of C_1C_2-segment. The difference between grain center distances at the beginning and at the end of sintering process during the elapsed time $\delta(\tau)$ is given by

$$\delta(\tau) = \delta_E^o - \delta_E(\tau) = \left[1 + \frac{X_2^2}{4k\,R_1^2}\right]\delta_E^o$$

The value of $\delta(\tau)$ contains information about dynamics of the inter-grains' neck formation. From this formula we can express the neck radius via the proportionality factor k as

$$X_2 = \sqrt{4 \cdot R_1^{\,2} \cdot k \cdot \left(\frac{\delta_E \cdot \sqrt{\frac{\cos^2 \alpha}{a^2} + \frac{\cos^2 \beta}{b^2} + \frac{\cos^2 \gamma}{c^2}}}{1+k} - 1 \right)}$$

where R_1-the radius of spherical grain corresponding to ellipsoidal grain E_1.

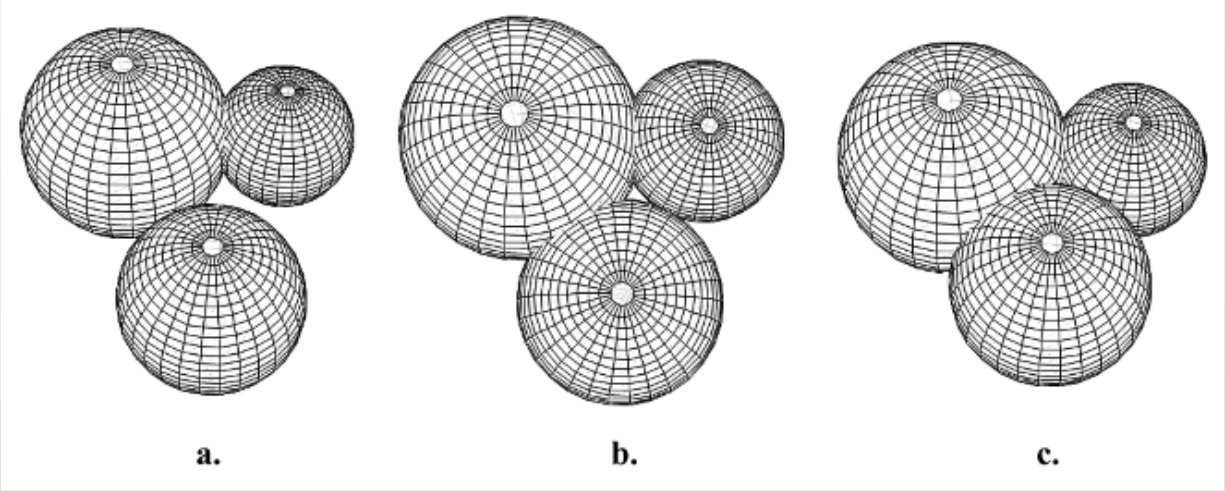

Figure **6**. 3D model of contacting three spherical grains during **a.** initial, **b.** middle and **c.** final moment of simulation.

The modelling procedure

- For modelling of spherical grains, the polyhedron-polyhedron model system is used.
- The approximated ellipsoidal surface of a grain is represented by series of polygons connected to each other side by side with C^0 continuity [13] (Fig. 6).
- Also, the real function $f(x, y, z)$ representing the grain's volume as follows: an arbitrary point $M(x_1, y_1, z_1)$ belongs to the interior of grain if $f(x_1, y_1, z_1) \geq 0$, and it is outside of the grain if $f(x_1, y_1, z_1) < 0$.
- Two grains are fixed in space so that they can touch or intersect themselves, and the third one is approached along the determined direction. We have observed the process from the moment of contacting mobile grain with one of the static grains until the moment of grains assimilation, then pores between them a vanished.
- During simulation, the area size of each contact surface, the distance between each pair of grains as well as the length of the pore formed between grains, has been calculated.
- The edge polygons are not treated due to their small influence on the value of total area (less than 10^{-4} for the approximation of grain with 10^6 polygons) as well as considerable influence on the simulation rate.

Ellipsoidal contact model

According to the author's knowledge all known inter-grain contact models of sintered ceramics use spherical approximation of grains. Contrary to this, observations of SEM photographs lead to the conclusion that majority of $BaTiO_3$-ceramic grains can be better approximated by ellipsoids than by spheres. So, there is an interest to consider two grains in contact as two ellipsoids partly penetrating each other. In this way, we can extend those elements of Coble's model that concern area of a contact zone [14].

Consider two coaxial ellipsoids E_1 and E_2, having centres at C_1 and C_2, such that $E_1 \cap E_2 = (x_p, y_p, z_p)$. Straightforward calculation gives that the distance $\delta_E^{\,0}$, between C_1 and C_2 in the beginning of sintering (sintering time $\tau = 0$) is given above.

By the formula (1) $X_2 = \sqrt{2}X_1$, where X_1 is given by

$$X_1 = \sqrt{\frac{R_1^{\,2} + R_2^{\,2}}{2} - \frac{d^2}{4} - \frac{\left(R_1^{\,2} - R_2^{\,2}\right)^2}{4d^2}}, \qquad R_2 \le d \le R_1 + R_2,$$

where d is a distance between spheres' centres and $R_2 > R_1$.

Denoting $q = R_1/R_2$, the neck radius will be given by

$$X_2(s) = R_2\sqrt{1+q^2-\frac{(s-1)^2}{2q^2}-\frac{q^2(q^2-1)}{2(s-1)^2}}, \qquad (5)$$

where $s = (d - R_2)/R_1$. Formula (5) gives the relationship between the neck radius X_2 and ellipsoid centres' distance d , normalized on the unit interval. The corresponding diagram is given in Fig. 7.

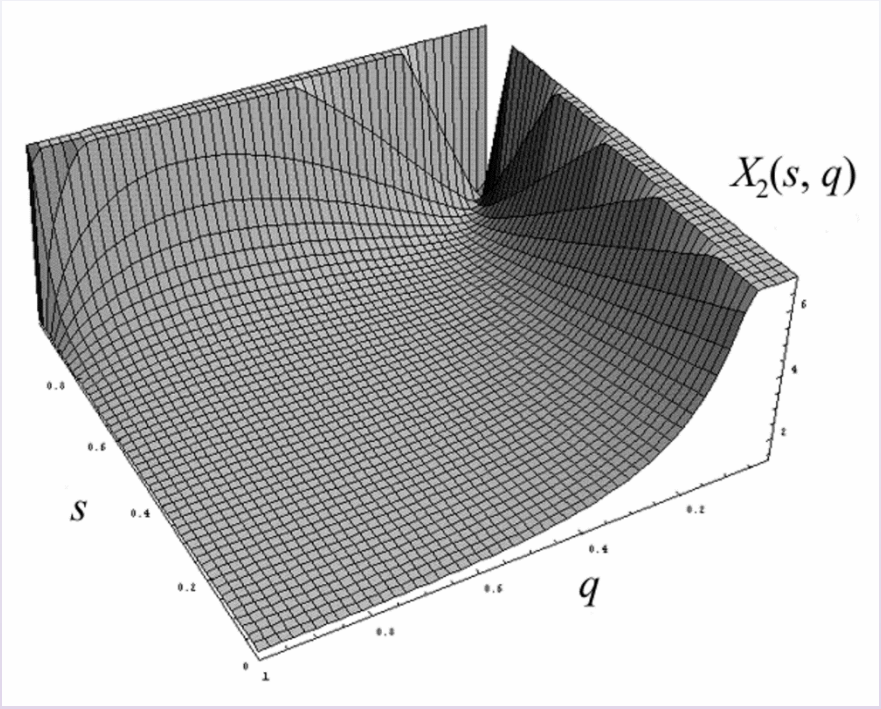

Figure **7**. Diagram of X_2 via $(d - R_2)/R_1$ and q.

Sphere-polyhedron model

Suppose that a ceramic grain has approximately spherical shape but the roughness of the surface approves replacing spherical model by a polyhedral one. For describing a constructive way of obtaining such a polyhedron we will consider a specific subdivision procedure illustrated in Fig. 8. Replace a sphere by a regular polyhedron inscribed in the sphere. Among the five regular polyhedra, icosahedron is a good choice by two reasons. First, it is the best approximation of the sphere; second, all its faces are triangles which simplifies subdivision procedure [6, 17].

Consider two grains, one approximated by an n-stage polyhedron (inscribed into a sphere having radius R_1), another by a sphere (radius = R_2). Suppose that these two spheres penetrate each other as in Fig. 2, for the same spacing $\rho_1 = \rho_2 = \rho$, and consequently the same common circle radius $X_1 = X_2 = X$. Now, we need to evaluate the volume of the "cap" of n-stage polyhedron that contains into the R_2 - sphere. For this purpose we will use the cubic function that shows increasing the volume of the cap with the height ρ and cap circle radius X: $V_{\text{cap}} = \pi\rho\left(3X^2 + \rho^2\right)/6$. After n subdivision iterations, an approximate formula for the common volume value reads [17]

17. Mitić, V.V., Kocić, Lj.M., Ristić, M.M. The Fractals and $BaTiO_3$-Ceramics Structure, Extended Abstracts of the 5th Conference and Exhibition of the European Ceramic Society, Euro Ceramics V, Part 2, Versailles, France,. 1060-1063, 1997.

$$(V_n)_{cap} = \frac{3 \cdot V_n}{R_1^3} \cdot \rho^2 \cdot \left(R_1 - \frac{\rho}{3} \right) \qquad (6)$$

where $V_n = V_0 \left[1 + k + k\beta \cdot \frac{1 - (k\beta)^{n-1}}{1 - k\beta} \right]$ is a polyhedron volume after n-steps,

$\beta = \frac{\alpha}{1 + k\alpha}$ and $\alpha = \frac{4 \cdot \pi \cdot \left(3 - \sqrt{5}\right) - 5}{5 \cdot k} - 1$.

During the initial sintering process stage, two grains penetrate each other and form a neck. Diameter of the neck is determined by the volume conservation law.

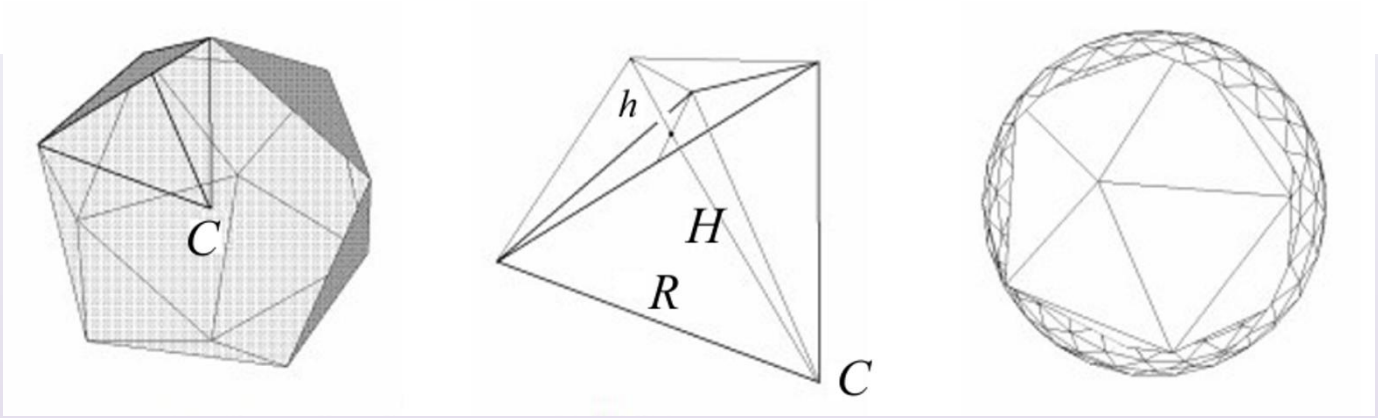

Figure **8**. Icosahedron subdivision geometry.

Polyhedron - polyhedron model

Except by the sphere, a ceramics grain can be approximated by polyhedron. Typical approach uses intersection of an *octahedron* O, and a *cube* C (Figure 9) in a way that octahedron's vertices are the cube side centres. In this case, the octahedron is fully inscribed into the cube (Fig. 9, leftmost), and $O \cap C = O$. In this case, octahedron O can be considered as having its original size, or $\lambda \times O$, with $\lambda = 1$. If the multiplication factor increases to 1.35, the intersection becomes a *truncated octahedron* (Fig. 9, middle). For $\lambda = 1.5$, the *cuboctahedron* is obtained as intersection (Fig. 9, right). Further increasing of λ yields *truncated cube* and finally the *cube*.

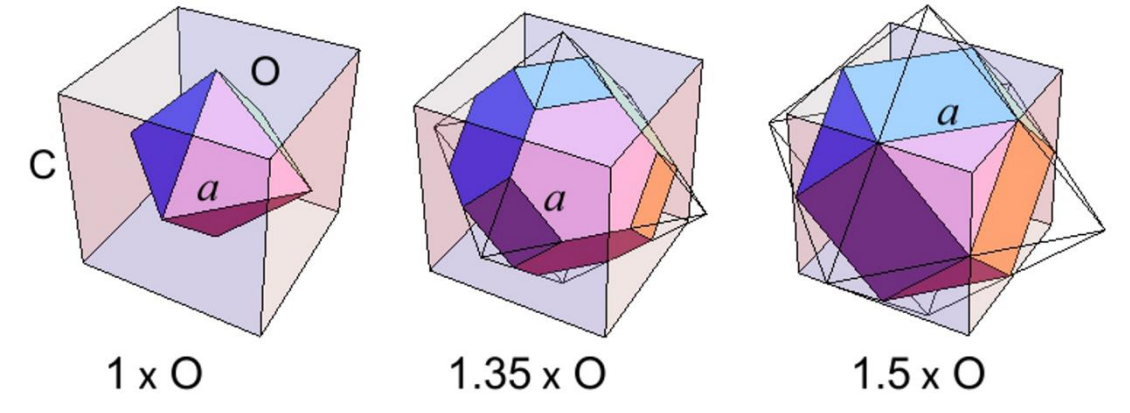

Figure **9.** Grain's approximations by the octahedron-cube intersection.

The main geometric parameter that influences energetic behaviour of the grain is the area-volume ratio, A/V. Providing the side length of each polyhedron is a, the A/V ratio is given in the Table 1.

Table 1	A	V	A/V	$\approx A/V$ for $a=1$
octahedron	$\sqrt{3}\,a^2$	$\sqrt{2}\,a^3/12$	$6\sqrt{6}/a$	14.6969
truncated octahedron	$\left(6+12\sqrt{3}\right)a^2$	$8\sqrt{2}a^3$	$\frac{3\sqrt{2}\left(1+2\sqrt{3}\right)}{8a}$	2.36745
cuboctahedron	$\left(6+2\sqrt{3}\right)a^2$	$\frac{5}{3}\sqrt{2}a^3$	$\frac{3\sqrt{2}\left(3+\sqrt{3}\right)}{5a}$	4.01528
truncated cube	$2\left(6+6\sqrt{2}+\sqrt{3}\right)a^2$	$\frac{1}{3}\left(21+14\sqrt{2}\right)a^3$	$\frac{6}{7}\left(3-2\sqrt{2}\right)\left(6+6\sqrt{2}+\sqrt{3}\right)$	2.38496
cube	$6a^2$	a^3	6	6

The diagram that integrates the data from Table 1 is given in Figure 10. The importance of this model is in having a simple tool for manipulating and fast evaluating in the situation when we have a huge number of grains to process. Also, it can be used as a starting point for developing fractal model of intergrain configuration. Here, we start with two polyhedrons, P_m and P_n obtained as an m - stage or n - stage output of the procedure described above (Fig. 10). So, we can use formula (5) with R_1 and R_2 as the corresponding radii of circumscribed spheres.

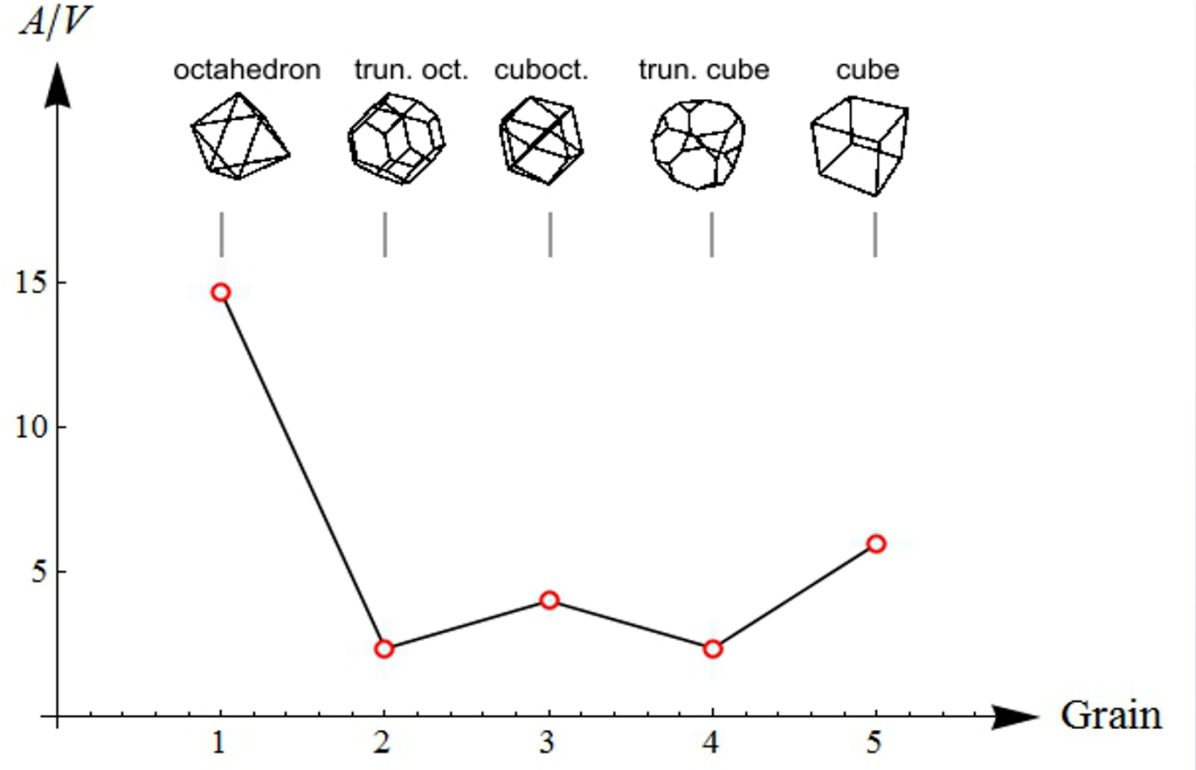

Figure **10.** Different grain's approxi-mations.

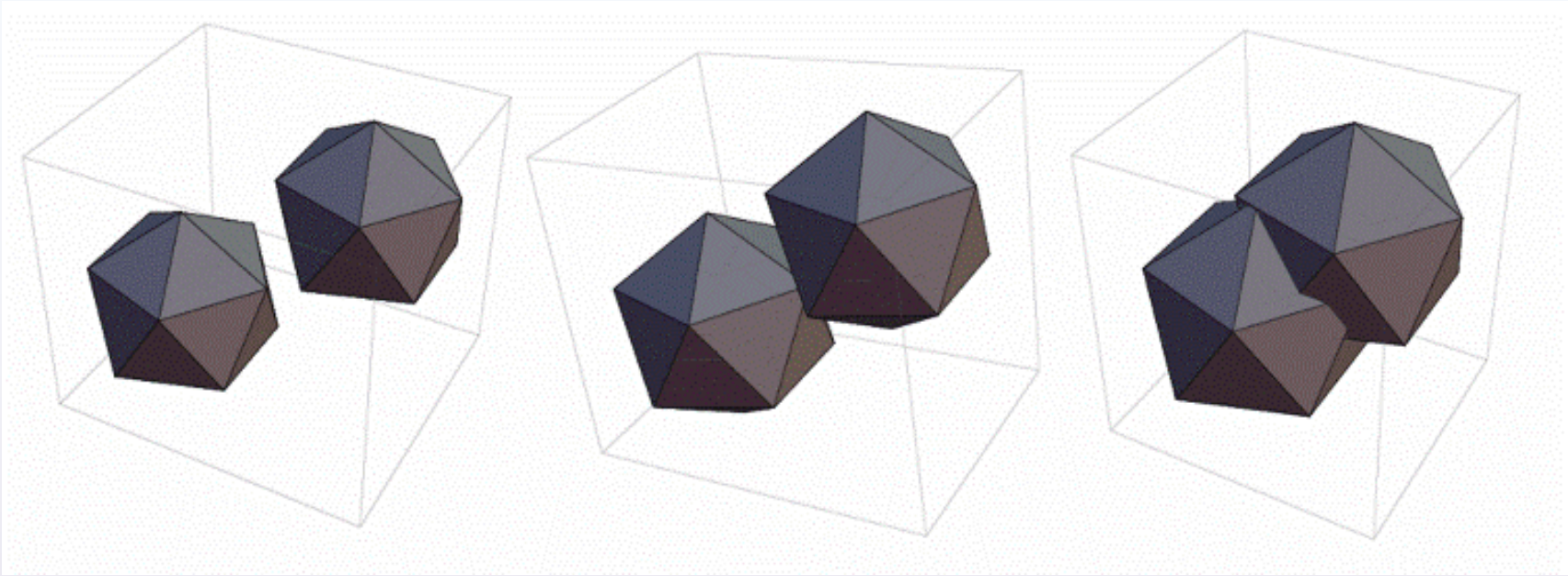

Figure **11**. Ceramic grains approximated by polyhedra in sintering process of joining two grains, forming a capacitor-like contact zone.

Heywang Model and the Curie-Weiss Law

The most widely accepted model to explain PTCR effect is the Heywang model [25] which describes the resistance-temperature behaviour based on a double Schottky barrier. This barrier is caused by deep acceptor states trapped at the surface of grains. The height of the barrier at the grain boundaries is described as:

$$\phi_0(T) = \frac{e n_S^2}{8\varepsilon_0 \varepsilon_{gb}(T) N_D} \tag{7}$$

where n_s is the acceptor stale density, N_D is the charge carrier density, T is the temperature, ε_o is the permittivity of free space ($\varepsilon_0 = 8.85 \times 10^{-12}$ F/m), and ε_{gb} is the relative permittivity of the grain boundary region. Thus, the resistivity ρ is given by:

$$\rho_S = R_0 \exp \frac{e\phi_0}{kT} \tag{8}$$

where R_0 is a constant, k is the Boltzmann constant, and e is the electron charge. According to the Curie-Weiss Law [26]:

$$\varepsilon_r = C / (T - T_c) \tag{9}$$

where C is the Curie constant, T is the temperature, and T_c is the Curie temperature. Above the T_c, the resistivity increases quickly, because of the variation of ε_r. Thus, PTCR effect directly relates to grain boundary. From eq. (7), n_s, N_D, and ε_r can greatly affect the height of the barrier. As it will be pointed in the further text, all above formulas (7), (8) and (9) are amenable to corrections due fractal nature component, present in ceramics microstructure.

---

25. W. Heywang, H. Thomann, Electronic Ceramics, London and New York, 1991.

26. Pontes, F.M., Pontes, D.S.L., Leite, E.R., Longo, E., Chiquito, A. J., Pizani, P. S., Varela, J.A., Electrical conduction mechanism and phase transition studies using dielectric properties and Raman spectroscopy in ferroelectric Pb0.76Ca0.24TiO3 thin films, *J. App. Phy.*, 94, 11, 7256. (2003).

Temperature impact

Arguing about the crystal surface „natural roughness “ as macroscopic steps collection on the arbitrary section surface of the crystal plane section, an observation Frenkel [27] had come forward with, that this roughness does not coincide with the crystal faces atomic roughness, with small surface energy, which can occur as a thermal fluctuations consequence at high temperatures. This temperature consideration illustrates the impact on dynamical processes inside the ceramics body. Such impact generates a motion inside the ceramics crystals in the Fermi gas form, containing different particles such as electrons (Bloch wave), atoms, atomic nuclei etc. [28]. In essence, this motion has a Brownian character and imposes necessity of introducing the third fractality factor–factor of movements,

$$\alpha_M \ (0 < \alpha_M < 1).$$

25. Frenkel', Ya. I. On the surface crawling particles in crystals and the natural roughness of natural faces, JETP 16 (1), 1948.
26. Mitić, V.V., Fecht,H.J., Kocić,Lj., Materials Science And Energy Fractal Nature New Frontiers, Contemporary Materials (Renewable energy sources), VI, 2 (2015) Page 190-203.

Our hypothesis ([29]) is that $BaTiO_3$-ceramics working temperature must be influenced by these three fractality factors, making correction of „theoretic" temperature to T_f, where the index "f" stands for "fractal",

$$T_f = \alpha T, \tag{10}$$

where α is a fractal corrective factor. As it will be shown below, α is composed out of three "sub-factors", already mentioned α_M as well as two more, designed by α_S and α_P, (being also reals from (0, 1) interval) which role will be closer explained in the last section. The functional relationship will be expressed as

$$\alpha = \Phi(\alpha_s, \alpha_P, \alpha_M) \ . \tag{11}$$

The argument for this expectation hides in the fact that geometrically irregular motion of huge particles number has to unleash an extra energy to the system. In other words, fractality of the system represented by three factors α_S, α_P, and α_M should increase overall free energy of the system, and this increment must be subtracted from input energy which is in fact, an input thermal energy denoted by T. In other words, $T_f = T - \triangle T$, and since it from (10) follows

$$a = \frac{T_f}{T} = \frac{T - \mathrm{V}T}{T}$$

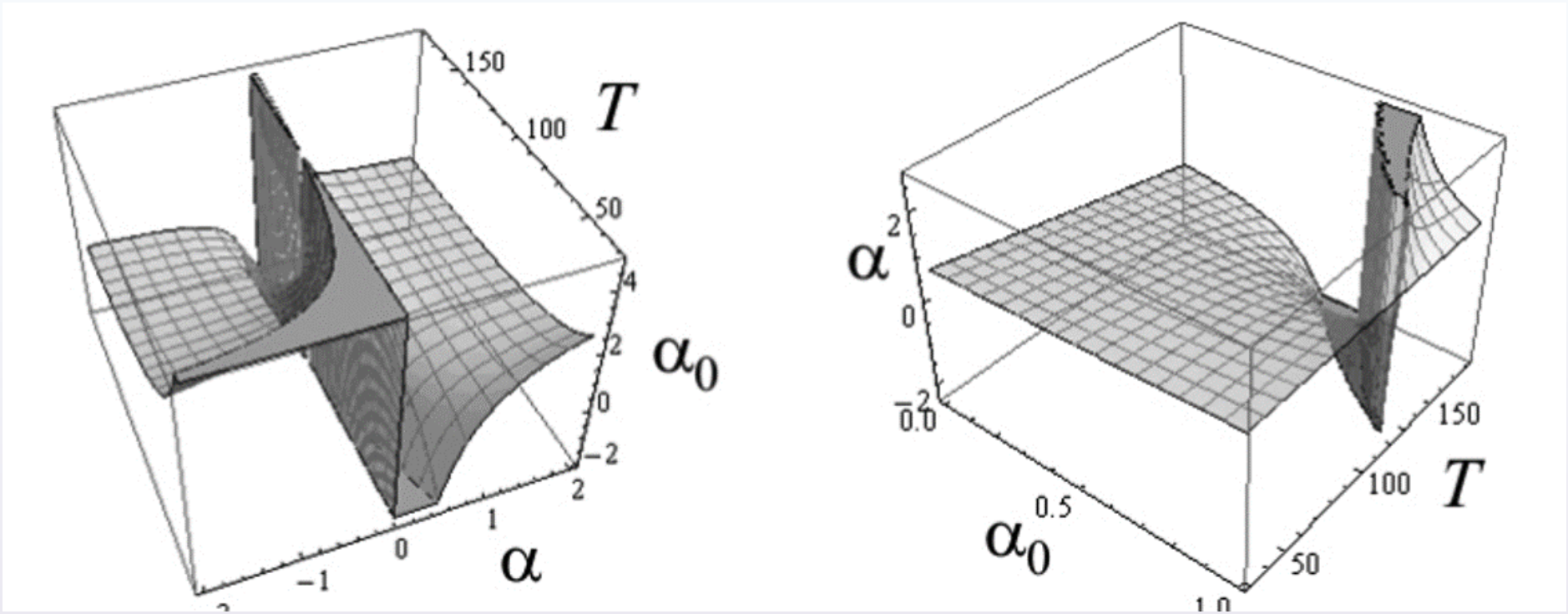

Figure **12**. The dependence of α on T and α_0 according to (13).

it should be $0 < \alpha = 1 - \Delta T / T < 1$.

The nature of the function in (11) is unknown by now, but at the first moment, the linear approximation will suffice,

$$\Phi(\alpha_s, \alpha_P, \alpha_M) = u\alpha_s + v\alpha_P + w\alpha_M,$$

where $u, v, w > 0$ are real coefficients satisfying $u + v + w = 1$.

Back to grain contacts, we see that two grains (Fig.13) partly penetrating each into another, and the corresponding microcapacitor model, formed by the contact area is shown in. This area has a fractal structure, which means that an effective size of A is greater than if is smooth one. (A striking example of Le Méhauté et al. concerning lithium batteries is given in Mandelbrot [10, p.462]). Thus, a contact zone between two ceramic grains is shown to contain the serial link of micro-capacitors C_i ($i >> 1$), so that the total capacity of the contact is $C_{contact} = \sum_i C_i$, and since $C_i = \varepsilon_0 \varepsilon_r \frac{A_i}{d_i}$, one has

$$C_{contact} = \sum_i \varepsilon_0 \varepsilon_r \frac{A_i}{d_i} = \varepsilon_0 \varepsilon_r \sum_i \frac{A_i}{d_i} = \varepsilon_0 \varepsilon_r \frac{\alpha_0 A}{d}, \qquad (12)$$

where α_0 is a corrective factor that embodies fractality of the intergrain contact zone (see [29]). On the other hand, in formula (10) another corrective coefficient α is used to correct the temperature. Using the Curie-Weiss law (9), and having in mind that ε_r is corrected to the value $\alpha_0\varepsilon_r$, it follows $\alpha_0\varepsilon_r = C/(\alpha T - T_C)$. After elimination of Currie constant C using (9), one gets

$$\alpha = \frac{1}{\alpha_0} + \left(1 - \frac{1}{\alpha_0}\right)\frac{T_C}{T}\ , \text{ and reversely, } \alpha_0 = \frac{T - T_C}{\alpha T - Tc}\ , \qquad (13)$$

which gives functional dependency of α_0 via temperature T. The Figure 12 visualizes the relationship between α and α_0, where the natural range for both α and α_0, are deliberately extended for better insight.

More generally, every expression that contains a function of temperature, say $F(T)$, if it is differentiable, may be expand to the Taylor series as

$$F(\alpha T) = F(T - \Delta T) = \sum_{k=0}^{+\infty} \frac{1}{k!} F^{(k)}(T)(-1)^k \Delta T^k.$$

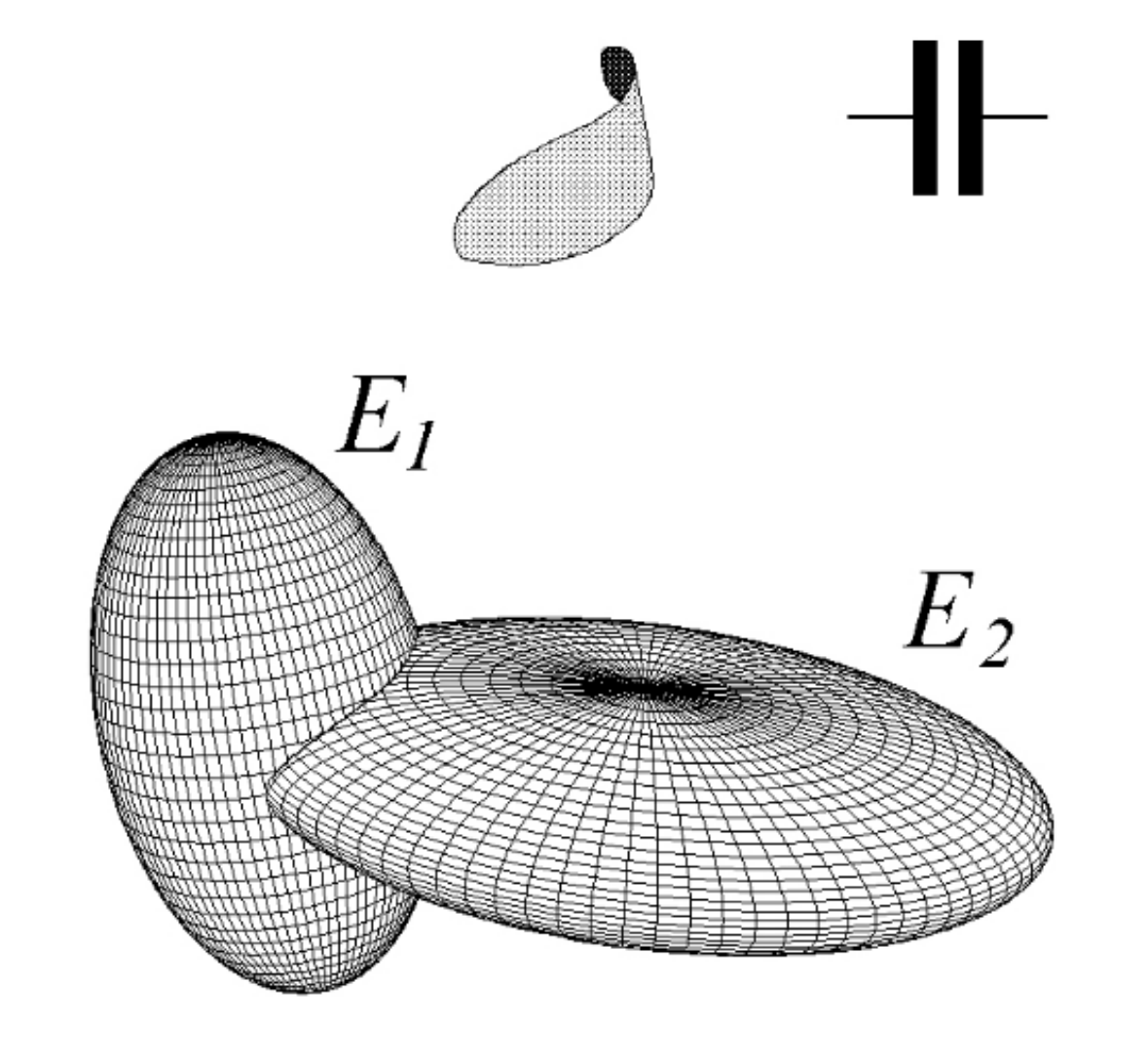

Figure **13**. Equivalent electrical model of contacted grains.

Intergranular impedance model

Taking into account that intergrain contact surface, is a region, where processes occur on the electronic level in the electro-ceramic material structural complex grain-contact-grain, can be represented by an electrical equivalent network consisting of three *RC* branches as it has been noticed in introduction (Fig. 14).

All this allowed us to consider $BaTiO_3$-ceramics sample, as a system with a huge number of mutually contacted grains, which form clusters. For each of them, it is possible to establish the equivalent electrical model and, for defined set of input parameters, using symbolic analysis, obtain the frequency diagram. However, the simple *RC* circuit is not sufficient to explain resonant behaviour of a ceramic sample. In order to calculate equivalent impedance for a wide frequency range, the equivalent electrical circuit for a ceramic material can be introduced as an equivalent impedance Z_e, containing two capacitances C and C_e, an inductance L and a resistance R.

Therefore, it is more likely that equivalent circuit model of contacted grains has parallel and series branches as presented in Fig. 14.

Consider now, an intergranular contact impedance as shown in Figure 14. Here, C_e is the main capacity component while C, R and L are parasite capacity, resistivity and inductivity resp., without α-correction, which means that intergranular geometry is considered as being flat and smooth. It is not difficult to see that the equivalent impedance, with α-correction included should be

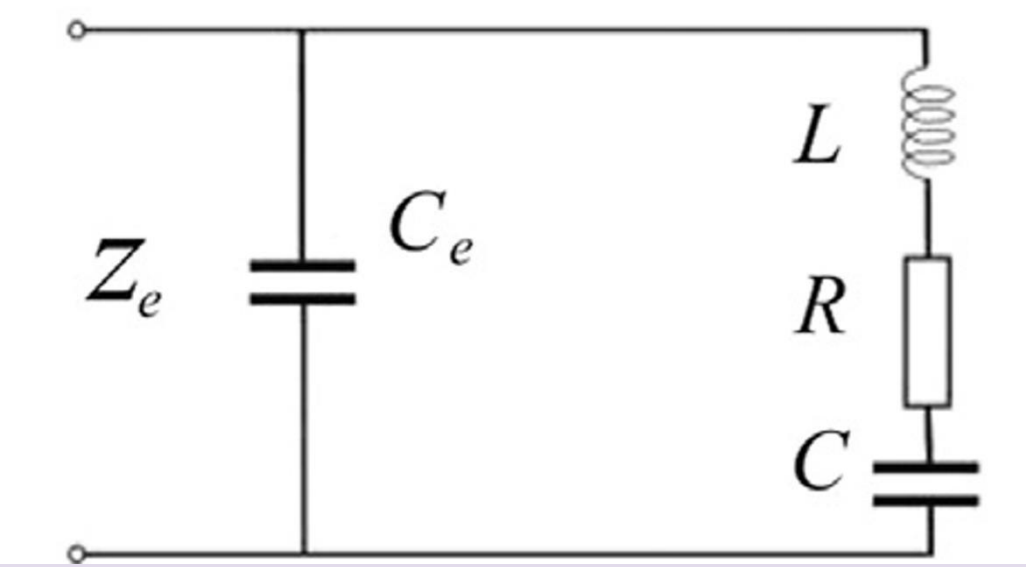

Figure **14**. Two ceramics grains in contact form a micro-capacitor with resistive and inductive component.

$$Z_e = \frac{1+\alpha_0\left(CRs+CLs^2\right)}{\alpha_0(C_e+C)s+\alpha_0{}^2C_eC\left(R+Ls\right)s^2}, \quad s = j\omega = j2\pi f,$$

or, expressed via frequency

$$Z_e = \sqrt{\frac{A^2}{4\pi f^2 B^2} + \frac{\alpha_0{}^4C^4R^2}{D^2}}$$

where

$$A = 4\pi^2\alpha_0{}^2C^2f^2(4\pi^2\alpha_0C_ef^2L^2+\alpha_0C_eR^2-L)-8\pi^2\alpha_0{}^2CC_ef^2L+\alpha_0vC+\alpha_0C_e\ ,$$

$$B = \alpha_0C^2(4\pi^2\alpha_0C_e{}^2f^2(4\pi^2f^2L^2+R^2)-8\pi^2\alpha_0C_ef^2L+1)+2\alpha^2CC_e(1-4\pi^2\alpha_0C_ef^2L)+\alpha^2C_e{}^2\ ,$$

$$D = 4\ \pi^2\alpha_0{}^4C^2C_e{}^2f^2R^2+(\alpha_0C(4\ \pi^2\alpha_0C_ef^2L-1)-\alpha_0C_e)^2\ .$$

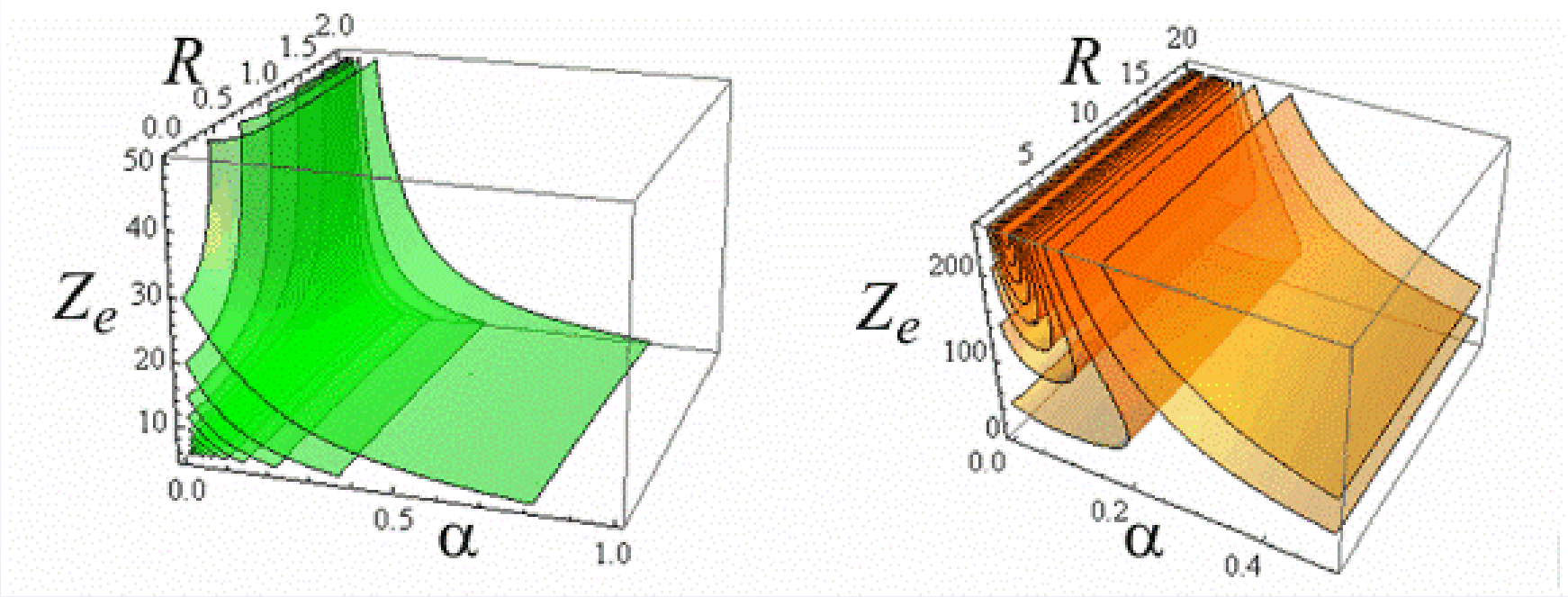

Figure 15. The level surfaces of intergranular impendence Z_e given by (9) as a function of $0 < \alpha < 1$, $0 < R < 2$, T=80°C and f = 1(8)80 and for c_e=0.1; c=0.01; L=0.001 (left); c_e=0.01; R=1; L=0.001 (right); Physical units are neglected.

In this manner, Z_e includes, except C_e, C, L, R and f, also the corrective factor α_0 and since it also depends on α as it is shown by the graphs as in Figure 15.

If more than two grains are in contact, and this is the most common case in ceramics bulk, the situation becomes much more complicated. Let the simple case of four grains in contact be considered (Figure 16a). If these grains have four contacts, then the configuration of intergranular impedances will have form of a tetrahedron (Fig. 16b). The equivalent impedance between the grains G_1 and G_2, is the same as between points A and B on tetrahedral scheme. The triangles $Z_2Z_3Z_4$ and $Z_3Z_5Z_6$ can be transform in the corresponding "stars" $Z_aZ_bZ_c$ and $Z_pZ_qZ_r$ (Fig. 16c) with

$$Z_a = \frac{Z_2Z_4}{\Sigma'},\ Z_b = \frac{Z_2Z_3}{\Sigma'},\ Z_c = \frac{Z_3Z_4}{\Sigma'},$$
$$Z_p = \frac{Z_3Z_5}{\Sigma''},\ Z_q = \frac{Z_3Z_6}{\Sigma''},\ Z_r = \frac{Z_5Z_6}{\Sigma''}, \qquad (14)$$

where $\Sigma' = Z_1 + Z_2 + Z_3$ and $\Sigma'' = Z_3 + Z_5 + Z_6$.

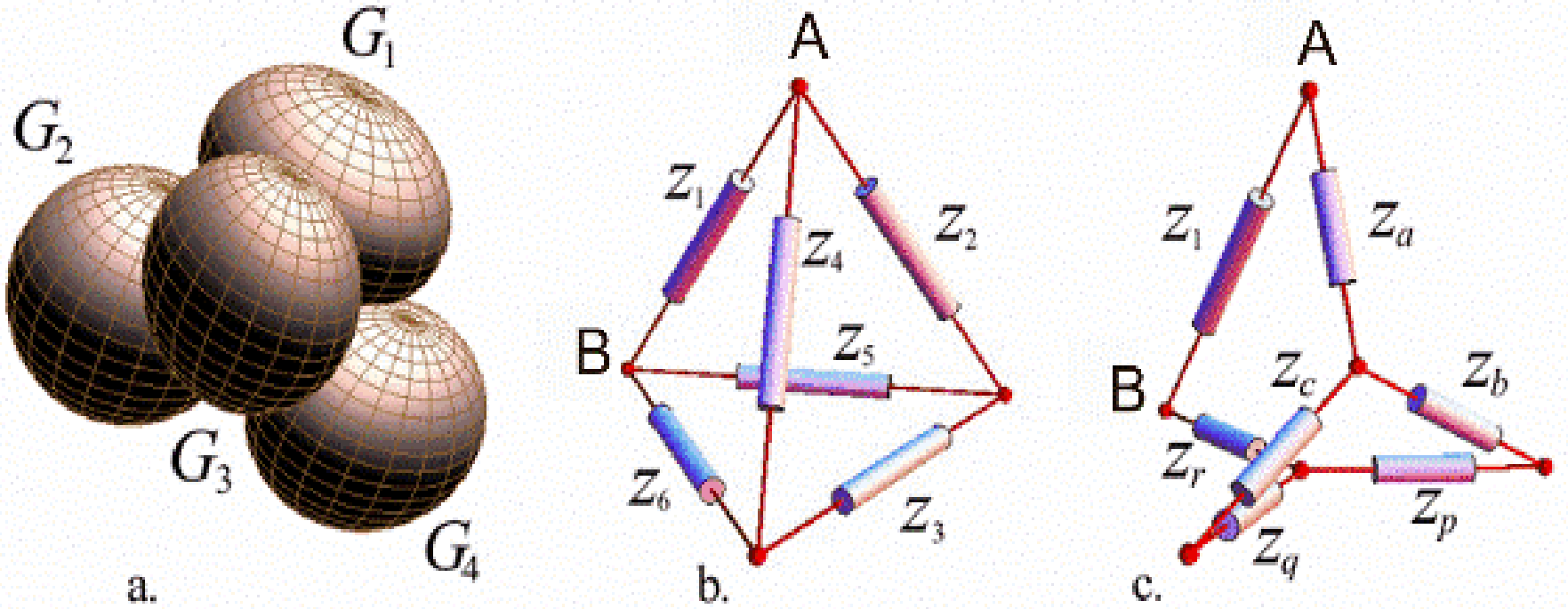

Figure 16. a. Four grains of BaTiO3-ceramics approximated by ellipsoids. b. Tetrahedral configuration of associated intergranular impedances. c. After triangle-to-star transformation.

The equivalent circuit is shown in Fig. 17, and the final calculation gives

$$Z_{AB} = \frac{Z_1 (Z_a + Z_b)}{Z_1 + Z_a + Z_b} + \frac{(Z_b + Z_p)(Z_c + Z_q)}{Z_b + Z_c + Z_p + Z_q},$$

or, by taking into account (14),

$$Z_{AB} = \frac{Z_1 Z_2 (Z_3 + Z_4)}{Z_1 (Z_1 + Z_2 + Z_3) + Z_2 (Z_3 + Z_4)} + \frac{Z_3 (Z_6 (Z_1 + Z_2) + Z_3 (Z_4 + Z_6) + Z_4 (Z_5 + Z_6))(Z_5 (Z_1 + Z_3) + Z_2 (Z_3 + 2Z_5 + Z_6))}{(Z_1 + Z_2 + Z_3)(Z_3 + Z_5 + Z_6)((Z_1 + Z_4)(Z_5 + Z_6) + Z_3 (Z_4 + Z_5 + Z_6) + Z_2 (Z_3 + 2(Z_5 + Z_6)))}. \quad (15)$$

Suppose the all the impedances are equal $Z_k = Z$. Then, according to (15), $Z_{AB} = \frac{5}{3} Z$. If the parasite components L, R and C are neglected, and if $1 / Z_i = j\omega\alpha_0 C_e = j 2\pi f \ \alpha_0 C_e$, all i, then

$$Z_{AB} = \frac{5}{3} \frac{1}{j \omega \alpha_0 C_e} = \frac{1}{j \omega (3\alpha_0 C_e / 5)}.$$

Similar calculations in the case of eight grains in contact, arranged in cubic manner (Fig. 17, right), gives

$$Z_{AB(\mathrm{CUBE})} = \frac{5}{6}\frac{1}{j\,\omega\,\alpha_0 C_e} = \frac{1}{j\,\omega\left(6\,\alpha_0 C_e / 5\right)},$$

and therefore, $C_{AB} = (6/5)\ \alpha_0\, C_e$, so the capacity of the cubic cluster is bigger than the capacity of a single contact.

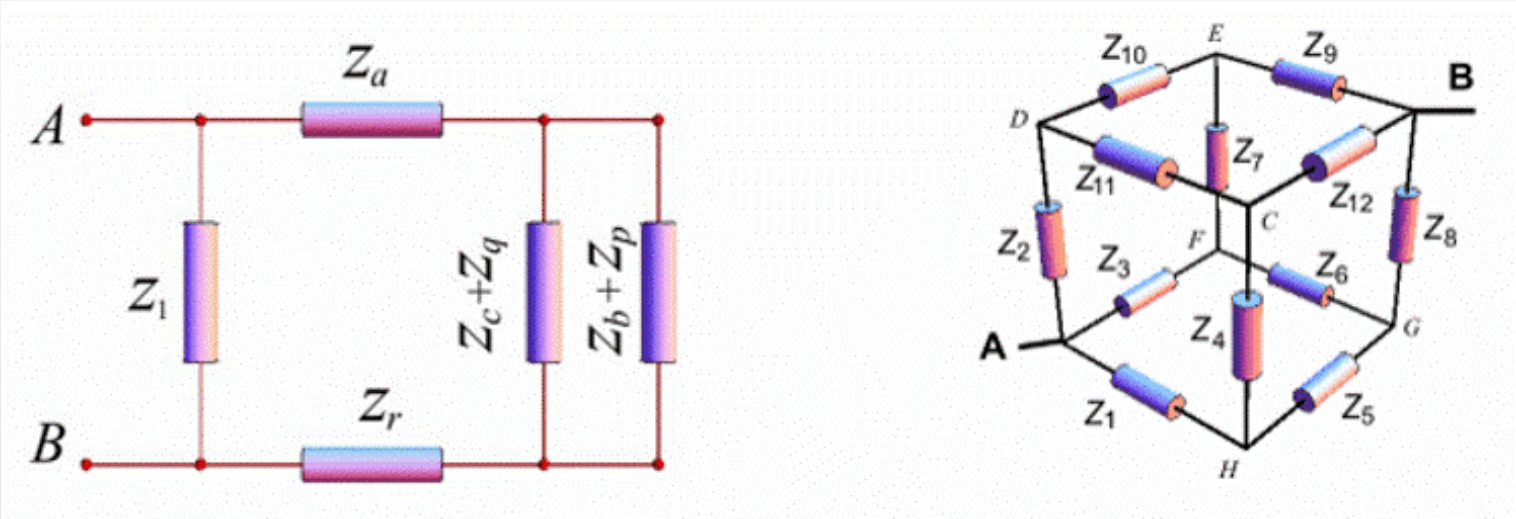

Figure **17**. Left. The equivalent circuit for the four grains contacts. Right. Cube of impedances.

Combined grain approximations

In some cases, polyhedral grain's approximation is acceptable, as well. In this case a polyhedron can be constructed as a 3D graph which nodes are points on the ellipsoidal surface. So, we can consider an approximate model of two grains' group in three ways: 1. ellipsoid - ellipsoid (EE) contact; 2. ellipsoid - polyhedron (EP) and 3. ellipsoid - grain (EG) contact (Figure 18).

Here is interesting to determine what the distribution of the intergranular contacts looks like. secondly, what is a more general formula for evaluating the size of all contact patches in the volume unit of $BaTiO_3$-ceramics. And last, but the most complex is the question of the nature of intergrain layers and their relationship with microcapacitor distribution. of course, it must be keep in mind that all parameters mentioned are functions of sintering process parameters (t, p and τ).

In the light of the geometric method explained above we can extend this approach from the case of EE intersections to the case of EP and EG intersections.

In fact, the value of two grains' contact area is given by

$$A = \int_S d\sigma$$

where *S* is a mathematical surface that will be described soon and dσ is a usual differential element of the surface. For all three models a surface *S* can be characterized in the unique way by intersection of the ellipsoidal surface with: 1. Another ellipsoidal surface, 2. a polyhedron surface and 3. real grain surface that can be expressed in terms of fractal functions. Even in the case the analytical method can be applied (EE) there is no use for this because the method of evaluation of the above integral must be a numerical method. Consequently, the method of two surface intersection is reasonable to be numerical, as well. In all cases it is enough to find a discrete points laying in the intersection line. In the case of EE intersection, the analytical solution of the intersection is to be discretized which reduces the problem on the case of EP intersection. The method is, as follows.

A polyhedron P can be regarded as union of vertices V and sides σ. The set of vertices is divided by ellipsoidal surface E in two groups: V_1 - vertices inside of E including the surface; V_2 - vertices lay outside of E. These two groups of vertices divide the set of sides in three groups:

$$\sigma = \sigma_1 \cup \sigma_2 \cup \sigma_3 ,$$

where σ_1 are sides whose both end points are in E, σ_3 are sides outside of E and σ_2 contains all sides that connect vertices from V_1 and vertices from V_2. Each side from σ_2 contains a unique point being characterized by the unique parameter t, $t \in (0, 1)$, so that $(1 - t)\mathbf{p_1} + t\ \mathbf{p_2}$ is a point on the ellipsoid. If the ellipsoid has semi - axes **a**, **b**, **c** and $\mathbf{p_1} = (x_1, y_1, z_1)$, $\mathbf{p_2} = (x_2, y_2, z_2)$, parameter t must obey a quadratic equation $A\, t^2 + B\, t + C = 0$, where

$$A = (x_1 - x_2)^2 / a^2 + (y_1 - y_2)^2 / b^2 + (z_1 - z_2)^2 / c^2,$$

$$B = 2 \times \left[(x_1 x_2 - x_1^2) / a^2 + (y_1 y_2 - y_1^2) / b^2 + (z_1 z_2 - z_1^2) / c^2 \right],$$

$$C = x_1^2 / a^2 + y_1^2 / b^2 + z_1^2 / c^2 - 1.$$

What we want to get is the value of size of a part of surface of *P* which is immersed into ellipsoid [10]. Let this surface be denote by π, then $|\pi|$ - the value we want, can be approximate by the union of triangular elements. The size of each triangle is given by 1/2 of the modulus of vector product of its sides.

As far as the EG contact is concerned, the calculation is a little bit complex mainly due to the fact that a fractal grain is defined by recursive functions (a fractal structure of such contact is shown on magnified detail in the scope of Figure 18). But using the binary tree algorithm and a convex hull property of fractal algorithms the intersection of one meridian line in fractal grain with an ellipsoid is not difficult to find. Actually, let S_0 be a starting set in 3D space for the recursive procedure of making auto composition of the Hutchinson contractive operator. Then, a sequence of sets has been produced.

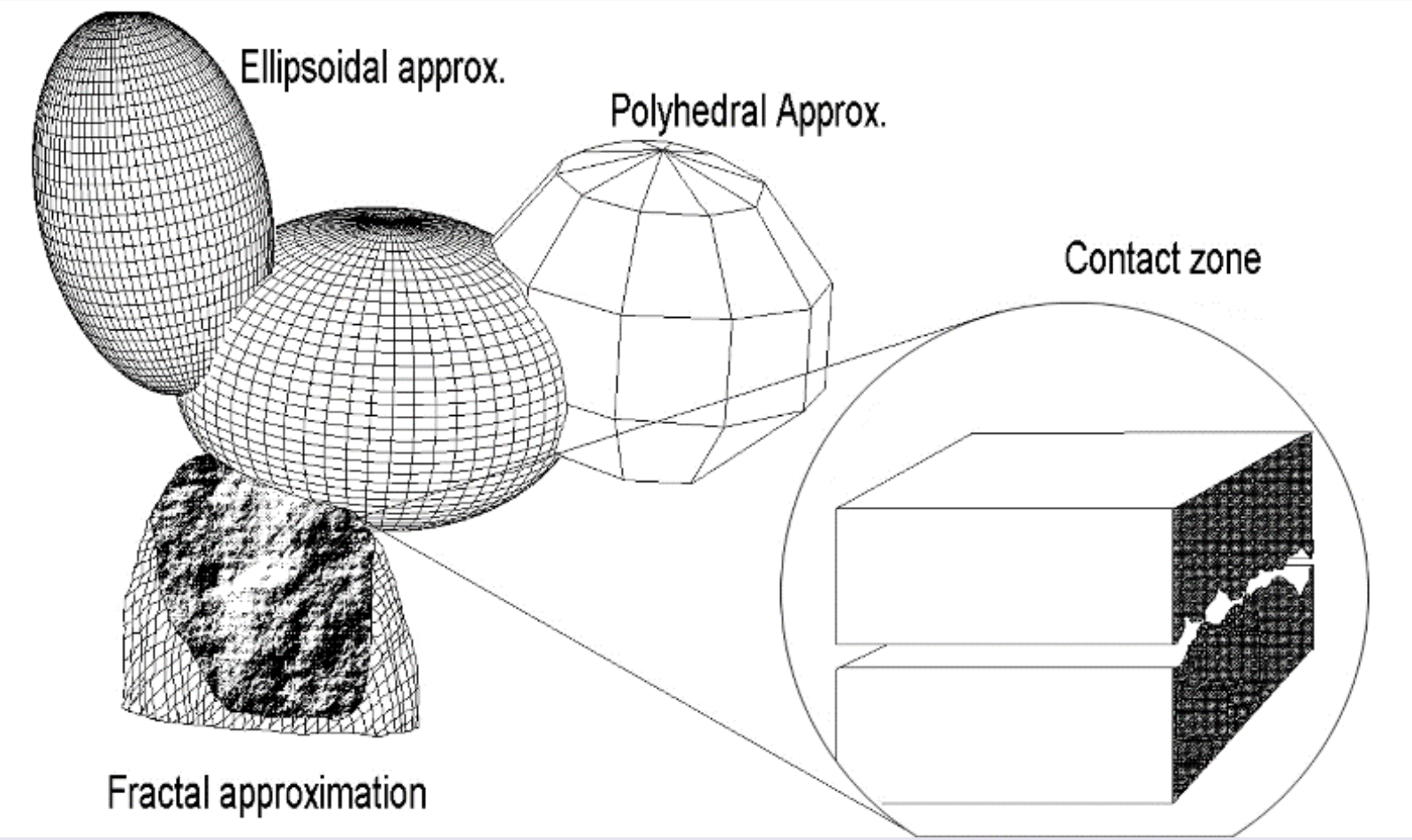

Figure **18**. EE-EP-EG-group of $BaTiO_3$-ceramics grains and a fractal structure of the contact zone.

Being a union of smaller copies of the attractorlet from previous stage the new attractorlet obeys the convex hull property which allowed to find its intersection in any compact set in 3D. After the fractal intersection contour is determined its area can be estimated by the using of suitable numerical method.

A surface S that appears in the integral formula is union of all intergrain contact surfaces in a prescribed volume V of $BaTiO_3$-ceramic sample. This surface can be defined by using characteristic function of some set A

$$\chi_A(x) = \begin{cases} 1, & x \in A, \\ 0, & \text{otherwise.} \end{cases}$$

Let G be a contact zone between any two grains. Define the following function

$$F(x, y, z) = \chi_G(\mathbf{r}),\ \mathbf{r} = \begin{bmatrix} x & y & z \end{bmatrix}^T \in \mathrm{R}^3.$$

It is clear that F is a discontinued function defined over the volume of the sample being considering. Let ∇F be the usual gradient of the function F with convention that in the point of discontinuity $\mathbf{r}_0$, where the limes of pre-gradient fraction goes to infinity, it will be taken $\nabla F(\mathbf{r}_0) = +\infty$. It is easy to see that the set defined by

$$\partial G = \left\{ \mathbf{r} : \left| \nabla F\left(\mathbf{r}_0\right) \right| > 1 \right\}$$

represents the surface of A contact zone (see [10]). In order to extend ΔG on all contact surfaces it is enough to replace the function F defined above by F_1

$$F_1(x, y, z) = \prod_{i \in I} \chi_{G_i}(\mathbf{r})$$

where I is a subset of a natural numbers broad enough to number all contact zones. The corresponding surface is $S = \partial G_1$. Therefore, the total contact area is given by

$$A = \int_S d\sigma = \int_V \prod_{i \in I} \chi_{G_i}(\mathbf{r})\, d\sigma .$$

Non-contact intergranular capacities

If two grains are close to each other but not in a direct contact, then neighbour crystal surfaces pairwise form micro-capacitors. The polarization effect makes two close grains to have opposite electric charges (Fig.19). Each flat facet of one grain's surface S_1 corresponds to the neighbour facet S_2 of the second grain. Since each facet (S_1 or S_2) belongs to a single plane (no plane contains both facets since if it does, then the capacitor does not exist), then there exists a pair of planes intersecting each other making an acute angle, say φ ($\varphi < \pi/2$). Let d be the distance between centres of the facets. In this way, a kind of "slanted" capacitor is formed. In a cross section, such a capacitor is shown in Figure 20 (left). Note that the edge effect caused by fringing electric field is neglected. The most appropriate model thou is the model of two planes situated as in Fig. 20 (right) in a cylindrical coordinate system (ϕ, r, z), where the intersection of planes coincide with z-axes.

Consider the Poisson's equation for electrostatic field in cylindrical coordinates

$$\frac{1}{r}\frac{\partial}{\partial r}\left(r\frac{\partial V}{\partial r}\right)+\frac{1}{r^2}\frac{\partial^2 V}{\partial \phi^2}+\frac{\partial^2 V}{\partial z^2}=-\frac{\rho_V}{\varepsilon}\ , \qquad (16)$$

with boundary conditions $\phi = 0,\ V = 0;\quad \phi = \varphi,\ V = V_0;$

Assuming the geometry of two nonparallel planes we see that potential V has to be constant along radial and axial coordinates r and z, which implies $\frac{\partial V}{\partial r} = \frac{\partial V}{\partial z} = 0$. That simplifies (16) to the partial differential equation (17)

$$\frac{1}{r^2}\frac{\partial^2 V}{\partial \phi^2} = -\frac{\rho_V}{\varepsilon} \quad , \tag{17}$$

with solution

$$V = -\frac{1}{2}\frac{\rho_V}{\varepsilon} r^2 \phi^2 + c_1 \phi + c_2 \, , \tag{18}$$

where c_1 and c_2 are constants regarding the angular coordinate ϕ and $\varepsilon = \varepsilon_0 \varepsilon_r$. From the boundary conditions, one gets $c_2 = 0$, and $c_1 = \frac{V_0}{\alpha} + \frac{1}{2}\frac{\rho_V}{\varepsilon}\varphi r^2$, which, being substituted in (18) gives

$$V = \frac{1}{\varphi} V_0 \phi + \frac{1}{2}\frac{\rho_V}{\varepsilon} r^2 \phi \left(\varphi - \phi\right) . \tag{19}$$

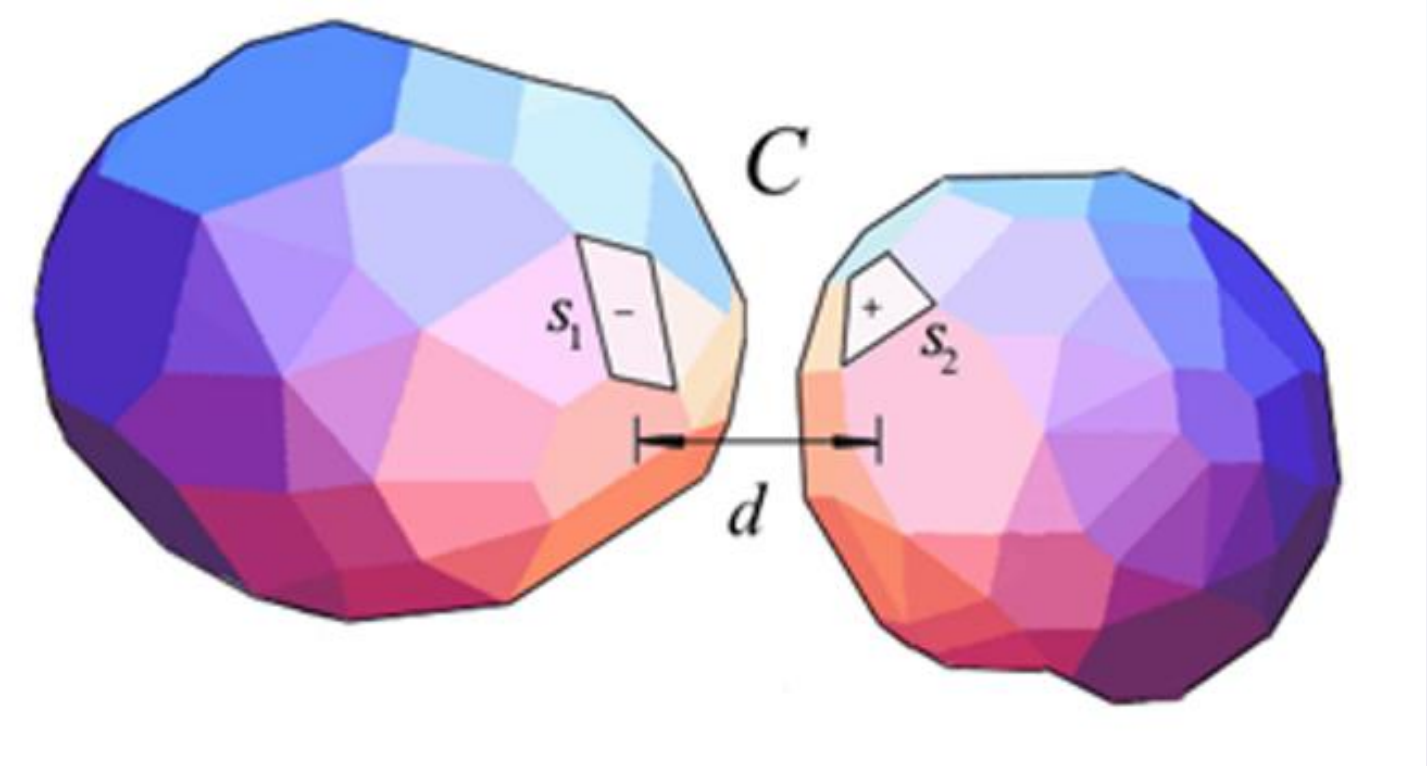

Figure **19**. Two neighbor grains and a micro-capacitor.

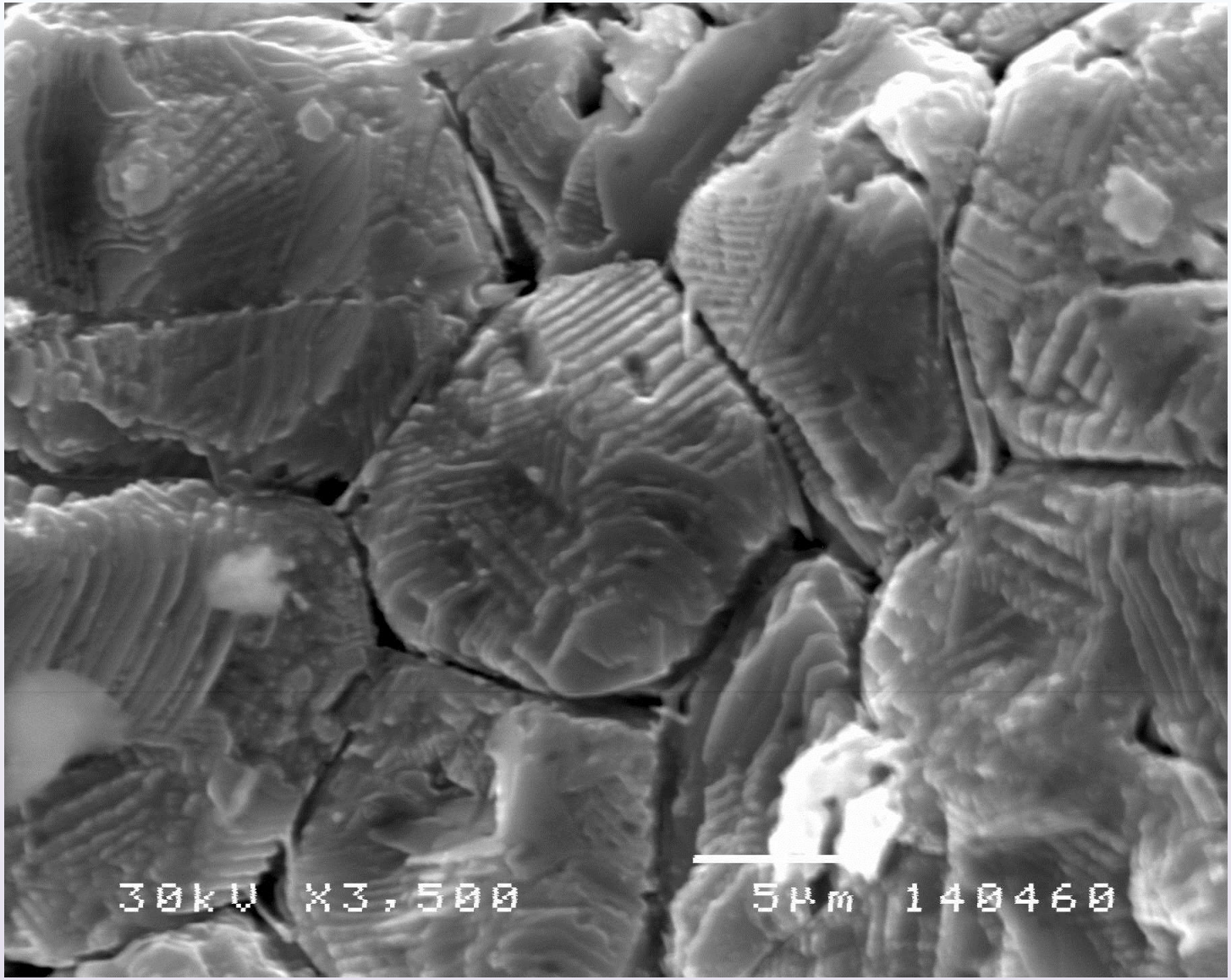

Figure **19a**. The neighbor grains in the BaTiO3 + 0.1Ho ceramics specimen, sintered in 1320^{o}C.

The level surfaces $V = 5(5)40$ are displayed in Fig. 21, for $0 \le \phi \le \varphi$, $0 \le r \le 15$, and $1 \le V_0 \le 20$.

Since $\mathbf{E} = -\Delta V$, and since the gradient in cylindrical coordinates evaluates as

$$\operatorname{grad} V(\phi, r, z) = \frac{1}{r}\frac{\partial V}{\partial \phi}\mathbf{e}_\phi + \frac{\partial V}{\partial r}\mathbf{e}_r + \frac{\partial V}{\partial z}\mathbf{e}_z ,$$

wherefrom one has

$$\mathbf{E} = \frac{1}{r}\frac{\partial V}{\partial \phi}\mathbf{e}_\phi + \frac{\partial V}{\partial r}\mathbf{e}_r = \left(\frac{V_0}{\alpha}\frac{1}{r} + \frac{1}{2}\frac{\rho_V}{\varepsilon} r(\varphi - 2\phi)\right)\mathbf{e}_\phi + \frac{\rho_V}{\varepsilon} r(\varphi - \phi)\phi\, \mathbf{e}_r ,$$

and the electric flux density $\mathbf{D} = \varepsilon \mathbf{E}$ is

$$\mathbf{D} = \left(\varepsilon\frac{V_0}{\alpha}\frac{1}{r} + \frac{\rho_V}{2} r(\varphi - 2\phi)\right)\mathbf{e}_\phi + \rho_V r(\varphi - \phi)\phi\, \mathbf{e}_r ,$$

where

$$Q = \iint_S D_\phi \, ds = \int_0^{\Delta z} dz \int_R^{R+\Delta r} \left(\varepsilon\frac{V_0}{\alpha}\frac{1}{r} + \frac{\rho_V}{2} r(\varphi - 2\phi)\Big|_{\phi=0}\right) r\, dr =$$

$$= \Delta z \left(\varepsilon\frac{V_0}{\alpha}\Delta r + \frac{1}{6}\rho_V \varphi\, \Delta r\, R\,(2R + \Delta r)\right);$$

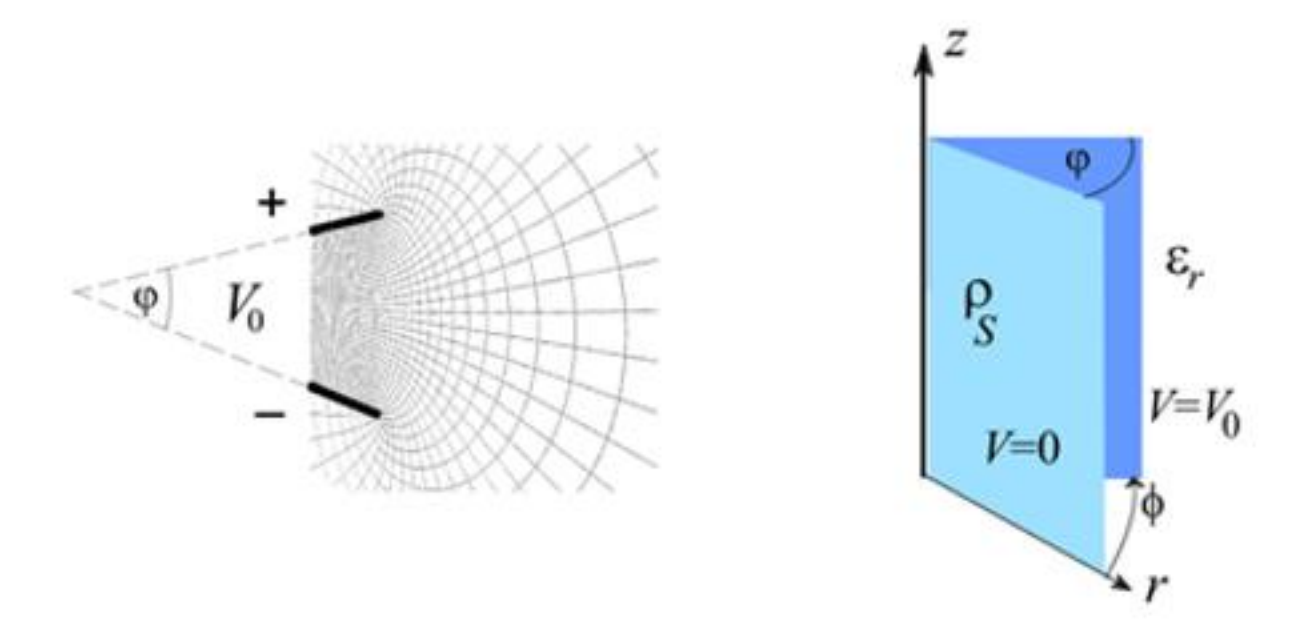

Figure **20**. Electrostatic field configuration for two slanted micro-surfaces and an approximating mathematical model in cylindrical coordinates.

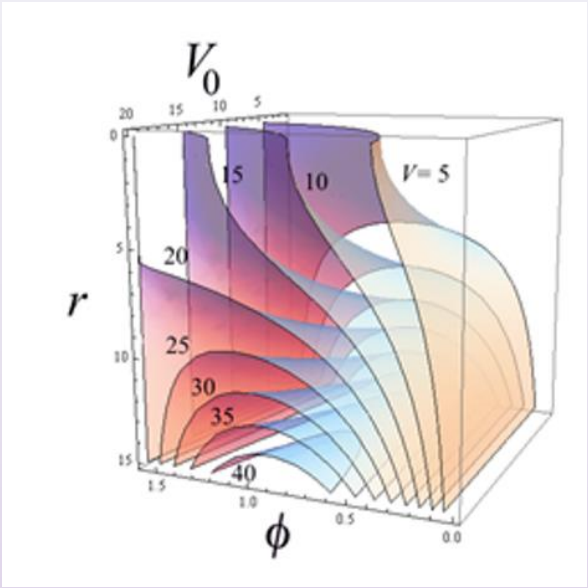

Figure **21**. Solutions (19) of Poisson's equation (2) for voltages 5 to 40 V.

The choice of limits for z is made to simplify the expression without loss of generality. Otherwise, the radial coordinate r depends on the distance of the facet element from the intersection line, and it is taken to be R. Thou, the surface of the facet is approximated by a rectangular element of the area $\Delta s = \Delta z\, \Delta r$, it follows from the familiar formula

$$C = \frac{Q}{|V_a - V_b|} = \frac{Q}{V_0},$$

and

$$C = \frac{\Delta z\, \Delta r}{V_0}\left(\varepsilon \frac{V_0}{\varphi} + \frac{1}{6}\rho_V \varphi\, R(2R + \Delta r)\right), \qquad (20)$$

which suggested a minimum capacitance for the angle

$$\varphi_{\min} = \left(\frac{6V_0}{\varepsilon \rho_V R(2R + \Delta r)}\right)^{1/2}.$$

Contact intergranular capacities

If two grains are in firm contact, they may form a capacitance zones having fractal shaped electrodes. In fact, the fractal dimension of grains' surfaces will be reproduced on contact zones forming capacitor plates with identical fractal dimensions. This situation is shown in the Fig. 22.

The contact zone can be approximated by classic parallel-plates capacitor with distance d and surface area A so to have capacity $C_0 = \varepsilon \frac{A}{d}$, where ε is the local permittivity constant ($\varepsilon = \varepsilon_0 \varepsilon_r$). Such a capacitor undergoes the fractal transformation using iterated procedure driven by Iterated Function System $\{w_1, w_2, w_3, ..., w_n\}$, where

$$w_k\left(\begin{bmatrix} x \\ y \end{bmatrix}\right) = \begin{bmatrix} a_k & 0 \\ c_k & d_k \end{bmatrix}\begin{bmatrix} x \\ y \end{bmatrix} + \begin{bmatrix} e_k \\ f_k \end{bmatrix} = \mathbf{A}_k \begin{bmatrix} x \\ y \end{bmatrix} + \mathbf{b}_k \ , \qquad (21)$$

is a contractive affine transformation in the plane of the cross-orthogonal section of the capacitor.

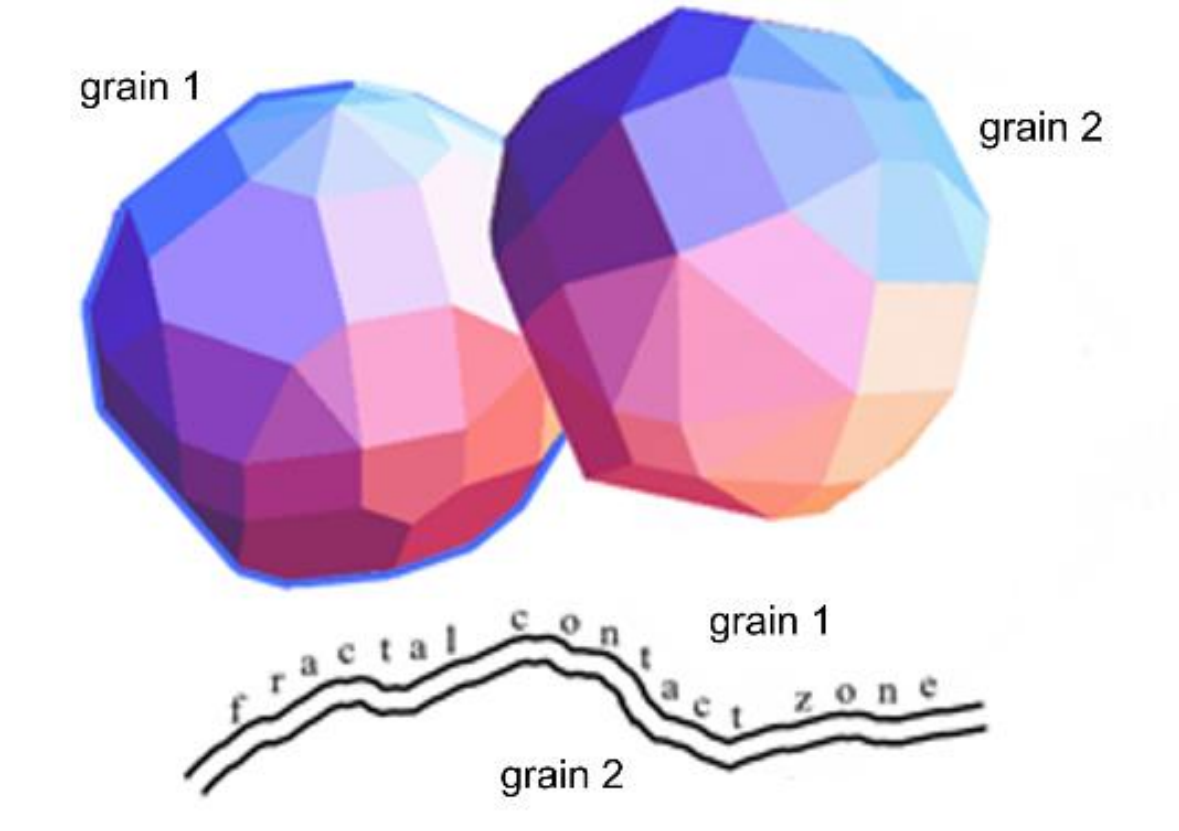

Figure **22**. Contact capacitor zone has fractal morphology.

The values a_k, c_k, d_k, e_k, f_k are determined in such a way that an adequate form of fractal initiator-generator pair. In the example at picture, initiator is the double line, parallel to each at a distance d, and of length L. The parallel lines are plates of a capacitor seen from the side. Suppose that the area of the surface is $A = L \times a$, where a is the width of the plates, and that a keeps constant. Then the capacity C_0 has the value

$$C_0 = \varepsilon a \frac{L}{d} .$$

Let the simplified case, for $n = 3$ be considered, which means that the IFS has only 3 contractive mappings. Consequently, there exists three matrices $\mathbf{A}_1, \mathbf{A}_2, \mathbf{A}_3$, defined by (21) and corresponding mappings that map the continuous double line of length L and separated by the thickness d ($d << L$, Fig. 23, left and up) into the three double segments shown underneath.

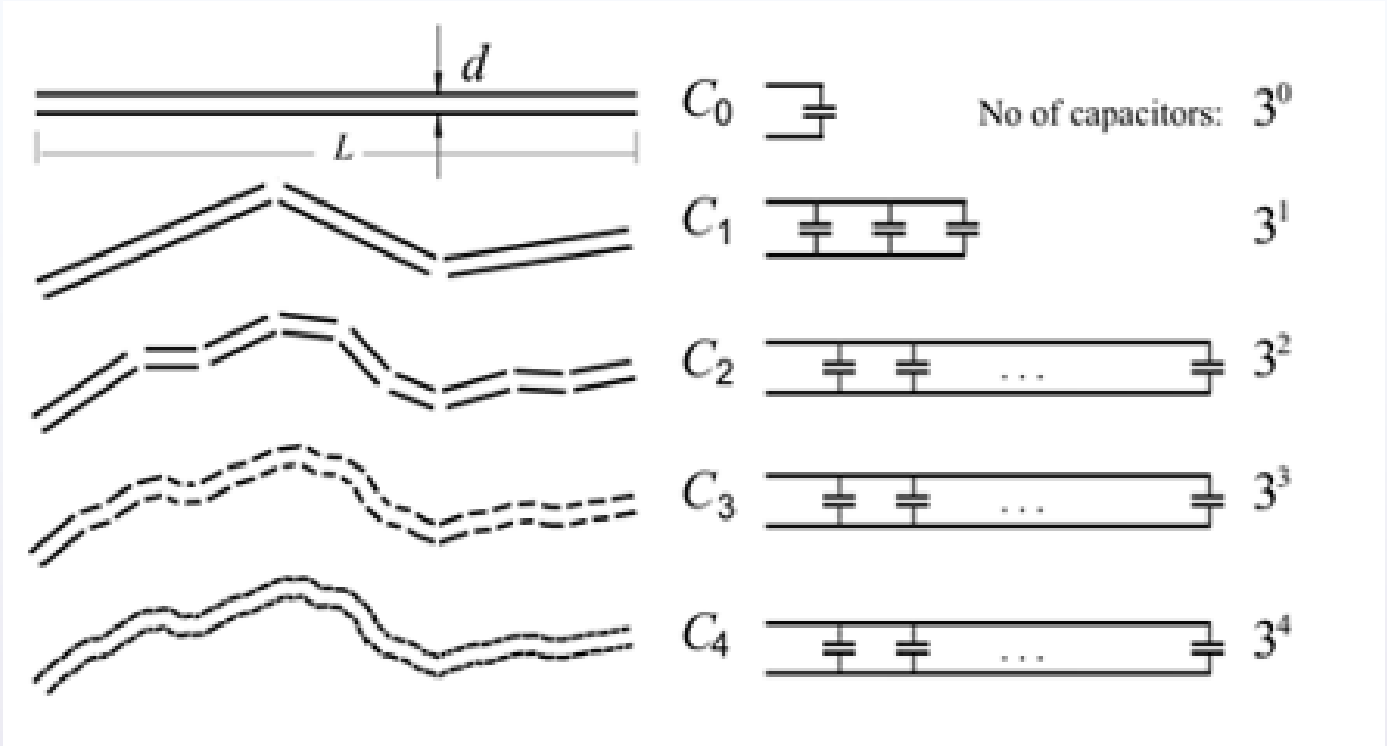

Figure **23**. Modeling intergranular capacitor by Iterated Function Systems and equivalent capacity schemes.

The values a_k, c_k, d_k, e_k, f_k are determined in such a way that an adequate form of fractal initiator-generator pair. In the example at picture, initiator is the double line, parallel to each at a distance d, and of length L. The parallel lines are plates of a capacitor seen from the side. Suppose that the area of the surface is $A = L \times a$, where a is the width of the plates, and that a keeps constant. Then the capacity C_0 has the value

$$C_0 = \varepsilon a \frac{L}{d} .$$

Let the simplified case, for $n = 3$ be considered, which means that the IFS has only 3 contractive mappings. Consequently, there exists three matrices $\mathbf{A}_1, \mathbf{A}_2, \mathbf{A}_3$, defined by (21) and corresponding mappings that map the continuous double line of length L and separated by the thickness d ($d << L$, Fig. 23, left and up) into the three double segments shown underneath.

Being contractions, these mappings transform each longitude into new, smaller values, bounded by the factors of matrix norms

$$\|\mathbf{A}_k\|^2 = \frac{1}{2}\left(a_k^{\,2} + c_k^{\,2} + d_k^{\,2} + \sqrt{\left(a_k^{\,2} + c_k^{\,2} + d_k^{\,2}\right)^2 - 4\, a_k^{\,2} d_k^{\,2}} \right).$$

In other words, the length L of the capacitor will transform into three new lengths: $\|\mathbf{A}_1\|L$, $\|\mathbf{A}_2\|L$, and $\|\mathbf{A}_3\|L$. At the same time, the distance d undergoes the same transformation.

The capacities of the new three capacitors will be

$$C_1 = \varepsilon a \frac{\|\mathbf{A}_1\|L}{\|\mathbf{A}_1\|d},\ C_2 = \varepsilon a \frac{\|\mathbf{A}_2\|L}{\|\mathbf{A}_2\|d},\ C_3 = \varepsilon a \frac{\|\mathbf{A}_3\|L}{\|\mathbf{A}_3\|d},$$

and, due to cancellation, the new capacitors will (theoretically) retain the same capacities as the initial one, i.e., $C_1 = C_0,\ C_2 = C_0,\ C_3 = C_0$. Since these capacitors are connected in parallel scheme, the total capacity after the first iteration will be $C^{(1)} = 3C_0$. Continuing the iteration will yield 3^2 new capacitors so that we will get $C^{(2)} = 3^2 C_0$. Consequently, after N iterations the approximate value of capacity will be $C^{(N)} = 3^N C_0$. Note that these are theoretical results. In reality, due to fringing effect, more plausible formula will be $C^{(N)} \cong 3^N C_0$.

To the local fractality embodied in intergranular contacts it should be added the stereological distribution of the contacts throughout the ceramics bulk. Although these may seem stochastic, it is not so. Some amount of regularity, inherited from crystallite structures with fractal configuration appears. Some possible basic models are shown in the Figure 24.

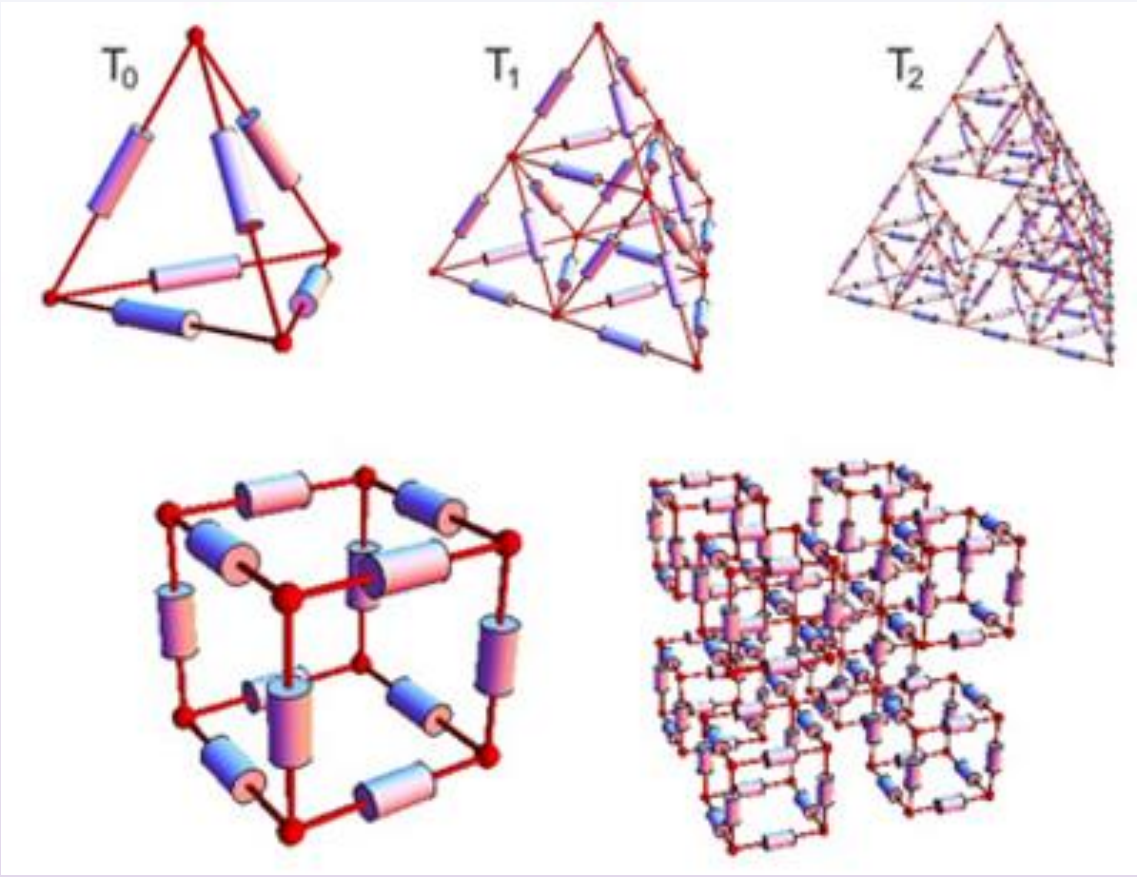

Figure **24.** Possible 3D model of intergranular capacities organized according the Sierpinski pyramid (top) and Menger sponge (below).

Inner fractality and α-corrections

Note that fractal dimension of typical grain's surface, let it be denoted by Σ, is just slightly above surface's topological dimension, $D_T = 2$. The difference $DH_f - D_T = DH_f - 2$, is thereby supposed to be responsible for affection to a part of ferroelectric phenomena in barium titanate ceramics that cannot be explain by purely grain surfaces Euclidean geometry. It is suitable to introduce a normalized surface fractality parameter α_s satisfying the inequality

$$(1-\varphi)\min\{DH_f - 2\} < \alpha_S < \varphi \max\{DH_f - 2\}, \quad 0 < \varphi < 1,$$

which ensures the unit range $0 < \alpha_S < 1$.

Also, $BaTiO_3$-ceramics is a porous material that corresponds to lacunar fractal models. It brings in a new phenomenon. Namely, solidification of porous and "spongy" materials increases overall fractal dimension from (theoretically) 2 to full solid 3.

In other words, fractal dimension of a porous material, DH_p satisfies $2 < DH_p < 3$. It causes another correction factor $\alpha_P = D_T - DH_P$, where $D_T = 3$ is dimension of the space and DH_p is corresponding fractal dimension of a porous configuration. Therefore, $0 < \alpha_P < 1$.

The dimensionless quantities α_S and α_P will be called geometric fractality factors. We suggest the existence of the third factor α_M caused by influence of disorder movement of ferroelectric particles that is factor of fractal movements.

As it is known, there is a "cloud" of moving particles in semiconductors (and metals as well) consists of electrons in atoms with large atomic numbers, nucleons in heavy atomic nuclei, and gases consisting of quasi particles with half-integral spin. This is called Fermi gas and obeys Fermi-Dirac statistics.

The classic theory of Fermi gas assumes that

(i) the interactions between the electrons are irrelevant and can be ignored;

(ii) the electrons move in a constant potential and we can ignore everything about the structure of the material;

(iii) (The crystal comprises a fixed background of N identical positively charge nuclei and N electrons, which can move freely inside the crystal without seeing any of the nuclei (monovalent case); and (vi) Coulomb interactions are negligible because the system is neutral overall.

Now, real dynamics of Fermi gas impose necessity of inclusion of factor of fractal movements α_M, that makes third factor, next to geometric ones α_S and α_P (see Section IX). The (0, 1) normalization comes from the following reasoning. Since Fermi gas particles have dynamics similar to 3D Brownian one, α_M should be derivate of Hausdorff fractal dimension DH_M of a Brownian 3D space-filling curve. It is obvious that $1 \leq DH_M \leq 3$.

The lower limit, $\min DH_M = 1$, is imposed by continuity of trajectory of a particle. The upper limit $\max DH_M = 3$, in turn is the maximum of trajectory complexity in 3D space. It is reasonable to normalize quantity α_M, by taking

$$\alpha_M = \frac{1}{2}\left(DH_M - 1\right),$$

which gives $0 < \alpha_M < 1$. The similar reasoning brings to limitations for other two factors α_S and α_P to belong to (0, 1).

Now by the Curie-Weiss law, by (10) and (11), the relative permittivity will be given by

$$\varepsilon_{r,\alpha} = \frac{C_c}{T_f - T_S} = \frac{C_c}{\alpha T - T_S} = \frac{C_c}{\Phi\left(\alpha_s, \alpha_P, \alpha_M\right) T - T_S},$$

where C_c is the Curie constant.

So, formula (20) can be modified as follows

$$C = \frac{\Delta z\, \Delta r}{V_0}\left(\varepsilon_{r,\alpha}\frac{V_0}{\varphi} + \frac{1}{6}\rho_V \varphi\, R\left(2R + \Delta r\right)\right).$$

Fractal structure of grains

Since seminal works of Mandelbrot [*], [**], have appear, fractals keep finding applications in many technological domains. Powder metallurgy is not an exception. Some earlier works have been devoted to this topic. The core of this point of view is fractal geometry of the grains of powder components and dynamics of sintering.

In fact, dynamics of motion inside the BaTiO3-ceramics is very similar to Brownian motion. The only quantifier that is inherent in such irregular object like graph of B-motion is Hausdorf or fractal dimension. In other words, Brownian path is a fractal in its nature.

Note that the graph of D1-Brownian motion is neither “self-similar” nor “self-affine”. For the graph above, $DH_f = 1.5$, and this is characterization of any part of this graph.

---

[*] B. Mandelbrot: Les objets fractals, forme, hasard et dimension, *Flammarion*, Paris,1975.

[**] B. Mandelbrot: The Fractal Geometry of Nature (3ed.), *W. H. Freeman*, San Francisco, 1983

Fractals have been “discovered” relatively lately, much latter than other very fundamental secrets of the Nature.

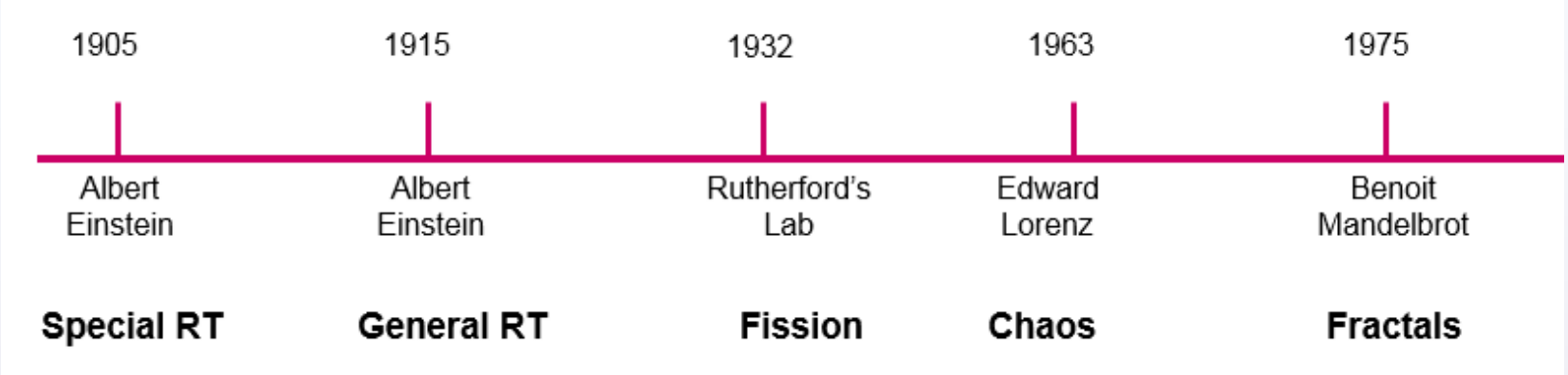

Figure **25.** Timeline of important discoveries in the first ¾ of 20-th Century

In the papers [Mitić, Kocić et al., 33, 34, 35] fractal analysis was first time applied in investigating ceramics materials properties. In fact, even before they become ceramics, many powder materials have fractal structure, as noted Kaye [36]. This “fractality property” remains during the sintering process. Still, the fractal dimension of grains’ contours, surfaces as well as pores changes during sintering phases.

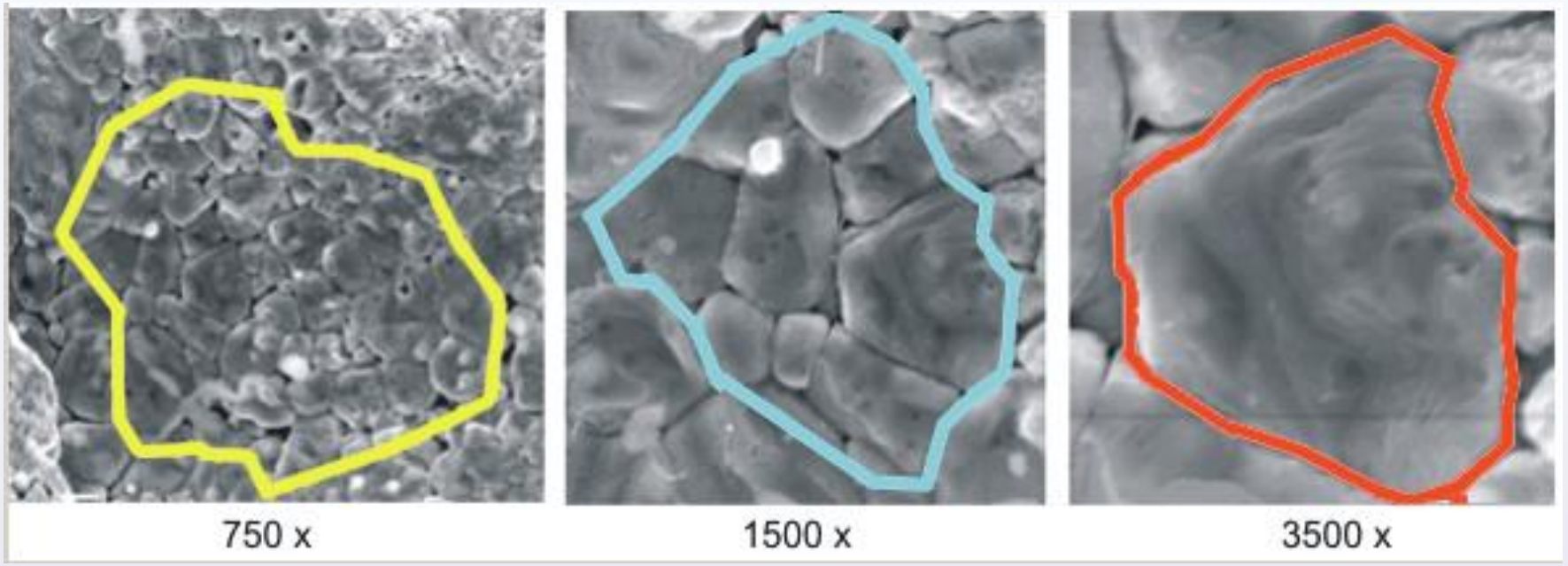

Figure **26.** Self-similarity in grains configuration.

Electronics ceramics, especially $BaTiO_3$-ceramics which we were focus on in [33, 34, 35], are made out of very fine powder particles having about 2μm as their maximum Ferret diameter. These particles have high enough surface energy to fuse together and to made sintered ceramics. After the sintering process being finished, SEM micro-photographs reveal a lot starting powder fractal-like morphology remains. The above figure shows three SEM's with magnifications of 750, 1500 and 3500. The form of a grain contour is 'self-similar' to the perimeter of a group of grains or of the larger bunch of grains. Here, the word similar is under quotations since it does not represent notion of mathematical similarity. This kind of self-similarity is called *statistical self-similarity*. It is used in looser sense of associative feeling of The Curie-Weis law defined by the approximate relation (9). showing that relative dielectric permittivity depends on temperature hyperbolic changing rate. The spontaneous polarization of barium titanate is about 0.15 C/m2 at room temperature. It is also piezoelectric material. Polycrystalline barium titanate displays positive temperature coefficient, making it a useful material for thermistors and self-regulating electric heating systems.

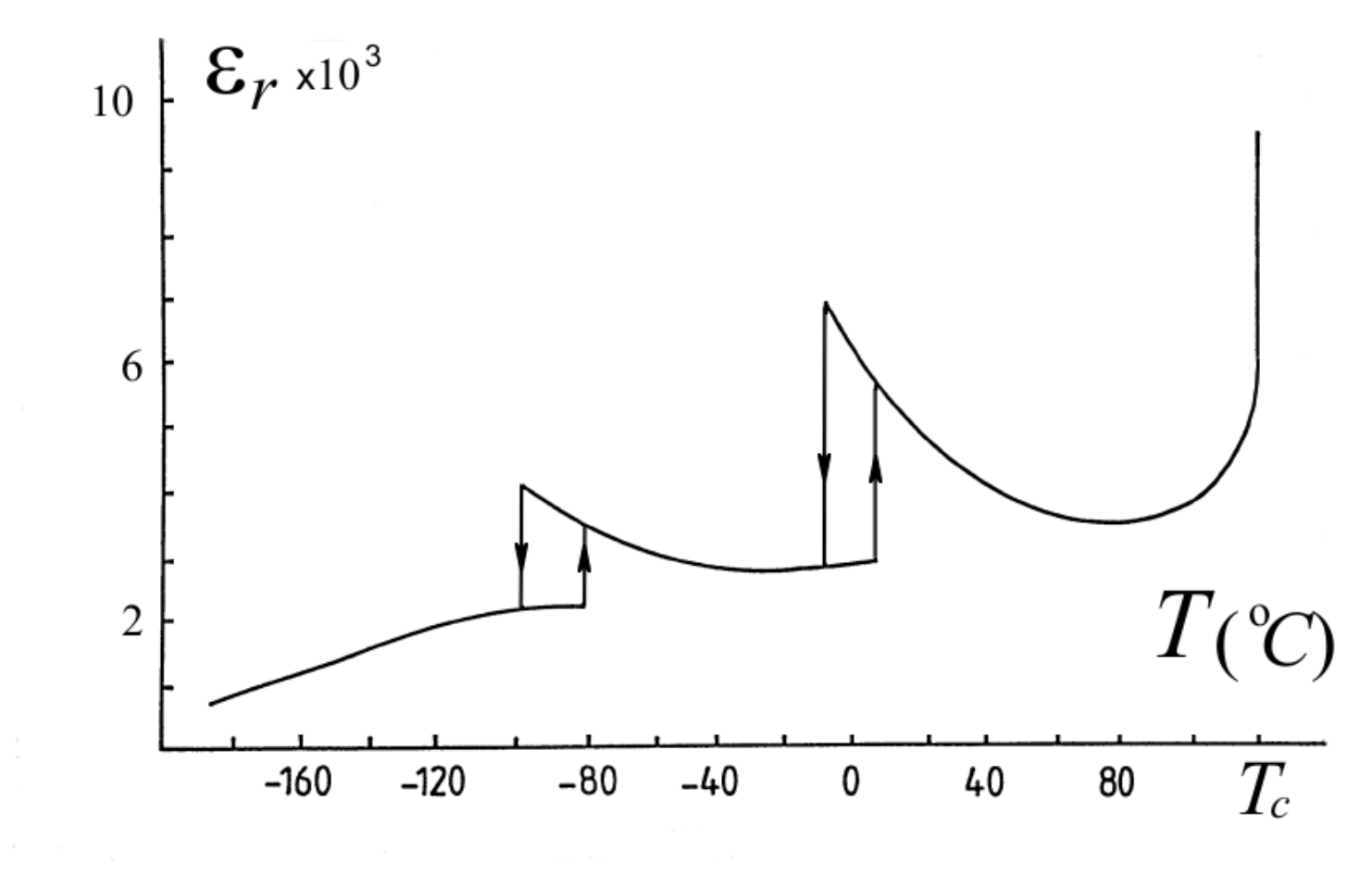

Figure **27.** Relative permittivity of BaTiO3 vs. temperature below the Curie point. Histeresis loops indicate nonlinar dynamics

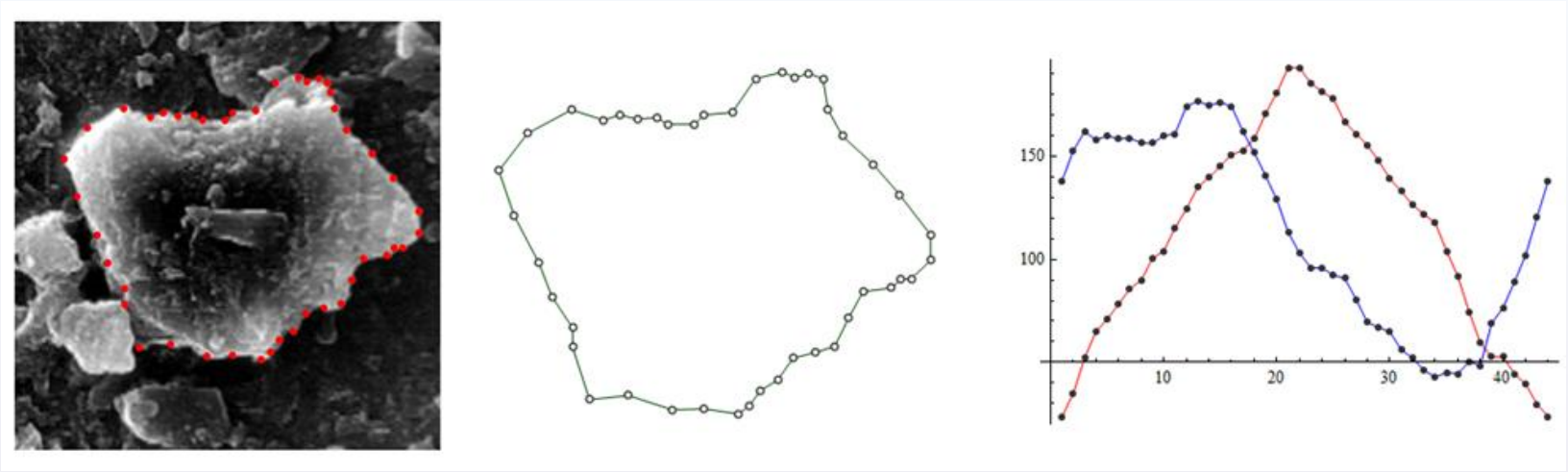

Figure **28.** $BaTiO_3$-ceramics grain (left), extracting contour data (middle) and their parametric form (right).

The slight geometric analysis reveal high complexity of the outline of a ceramics grain. Fractal analysis it the most suitable tool to measure, store and operate with this complexity.

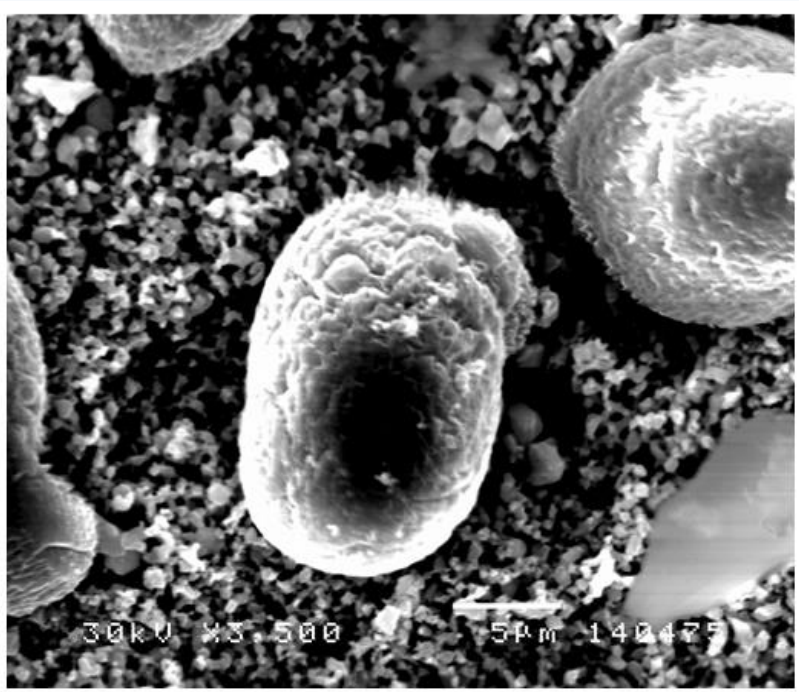

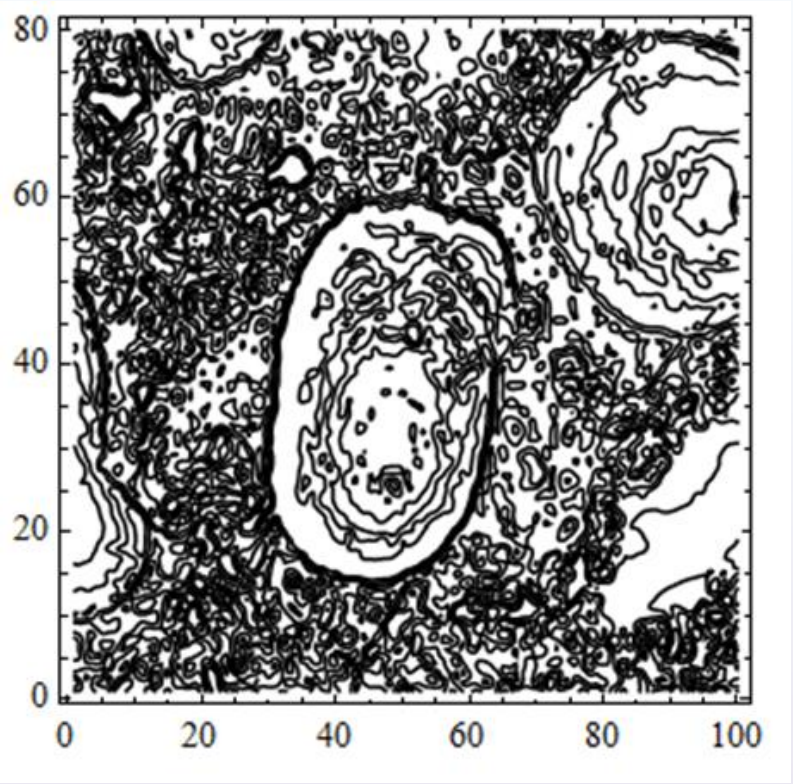

Figure **29.** SEM of Holmium doped (0.5 wt%, sintered at 1320^{o}C) $BaTiO_3$-ceramics grains and its isarithmic map (level lines) diagram. The intricacy of surface leaves impression of chaos and disorder.

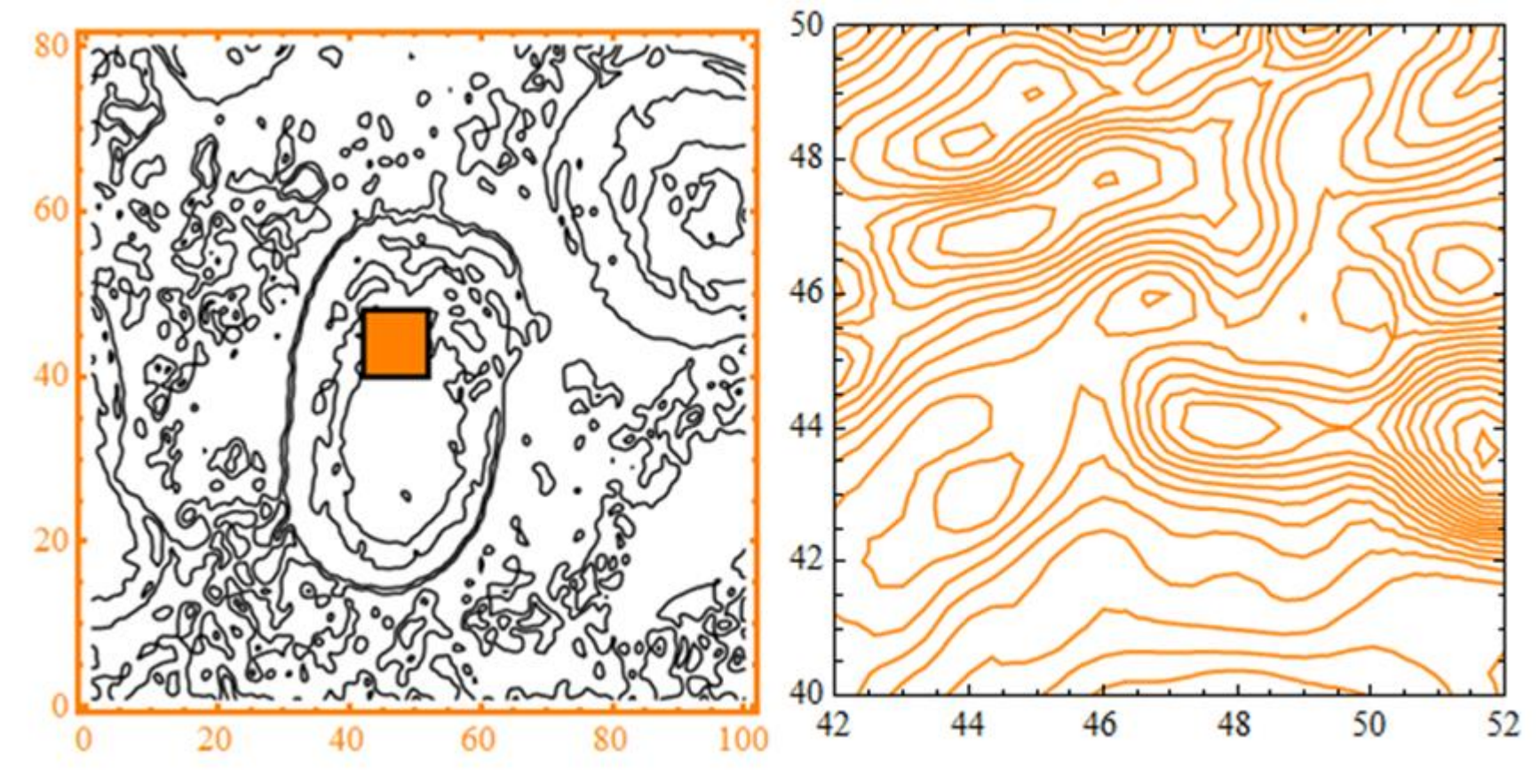

Figure **30.** Enlarged fragment of $BaTiO_3$-ceramics grain SEM and its isarithmic map about 35x35 microns.

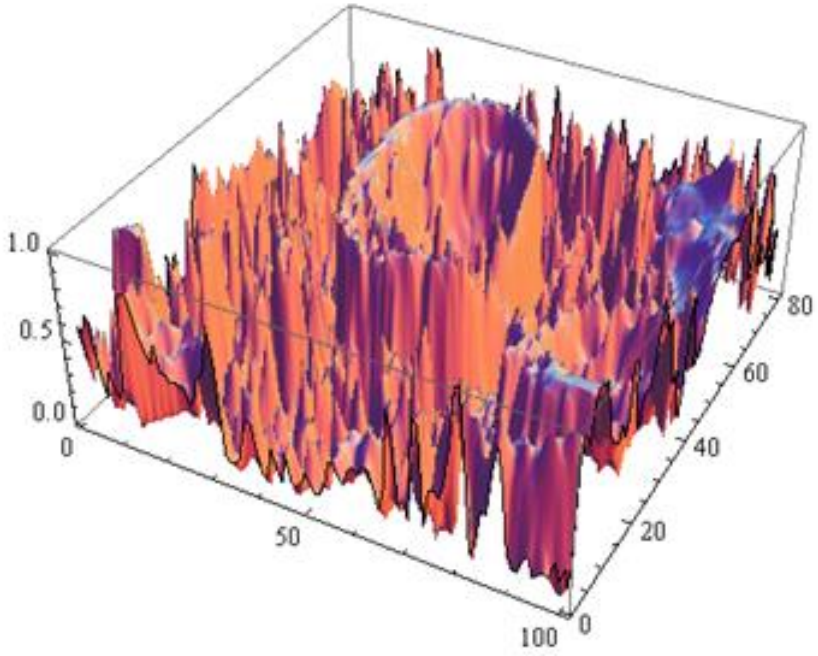

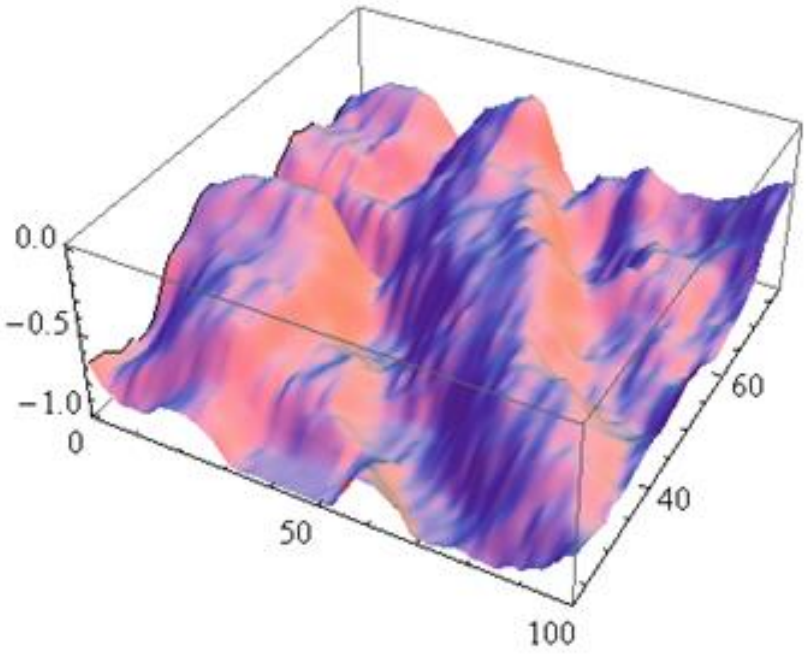

Figure **31.** $BaTiO_3$-ceramics grain from previous SEM represented as numerical 3D surfaces in two resolutions.

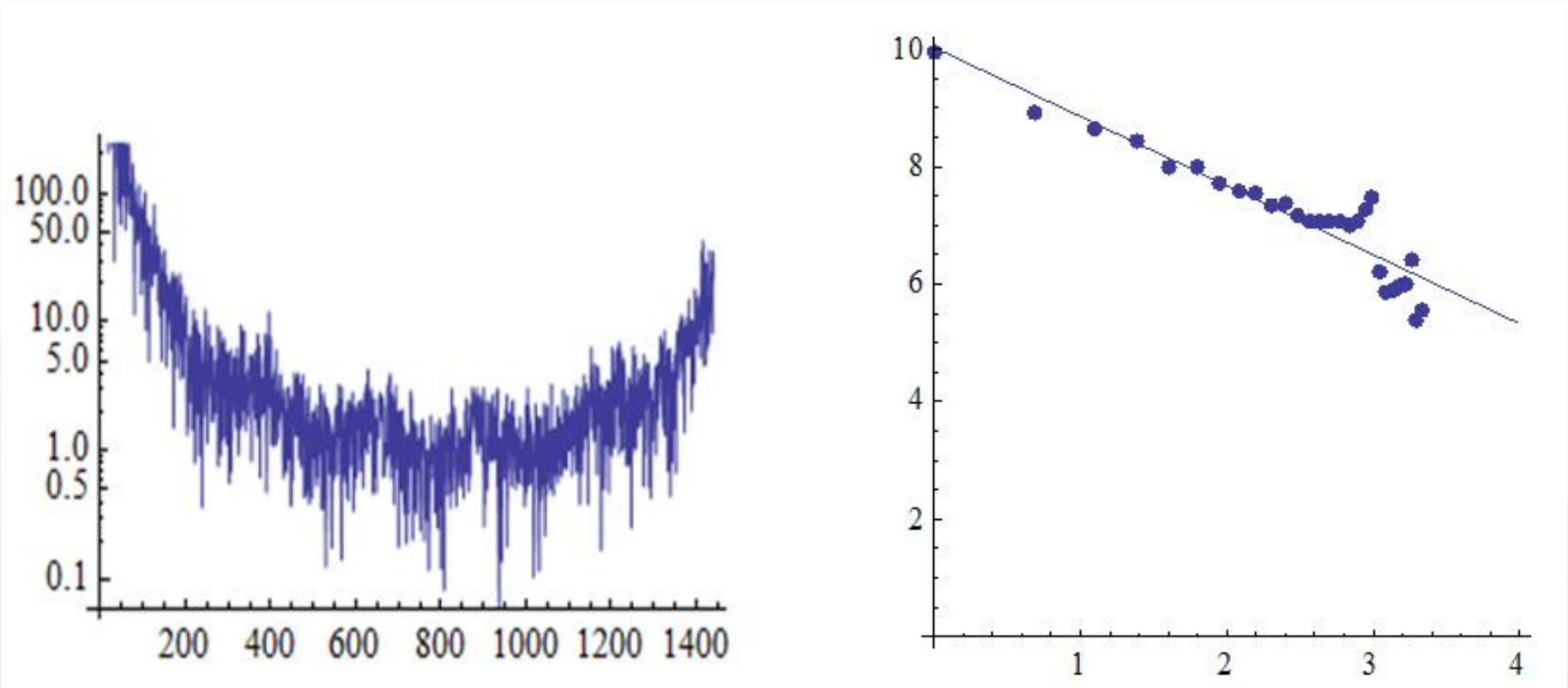

Figure **31.** Left: Discrete Fourier Transform and log-log diagram given by the Herzfeld−Overbeck algorithm. It estimates the fractal dimension of the fragment to 1.91214 with an error of $\delta = \pm 0.085172$.

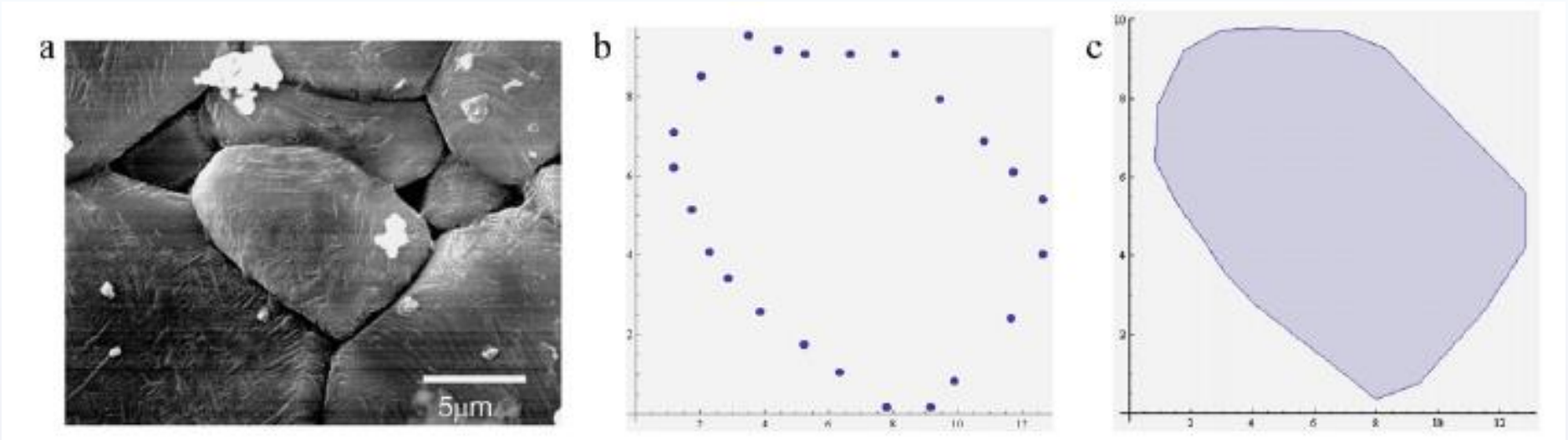

Figure **32.** SEM of $BaTiO_3$-ceramics sample, extracting interpolation points and convex hull of these data

The method used for this first attempt is the box-counting method based on the famous formula

$$DH_f = \lim_{r \to 0} \frac{\ln N(r)}{\ln (1/r)}$$

where $N(r)$ denotes the number of boxes (square boxes in 2D space or cubits in 3D space). Ceramics grains are so called “slim” fractal, i.e. the fractal that is pretty close to the smooth contour.

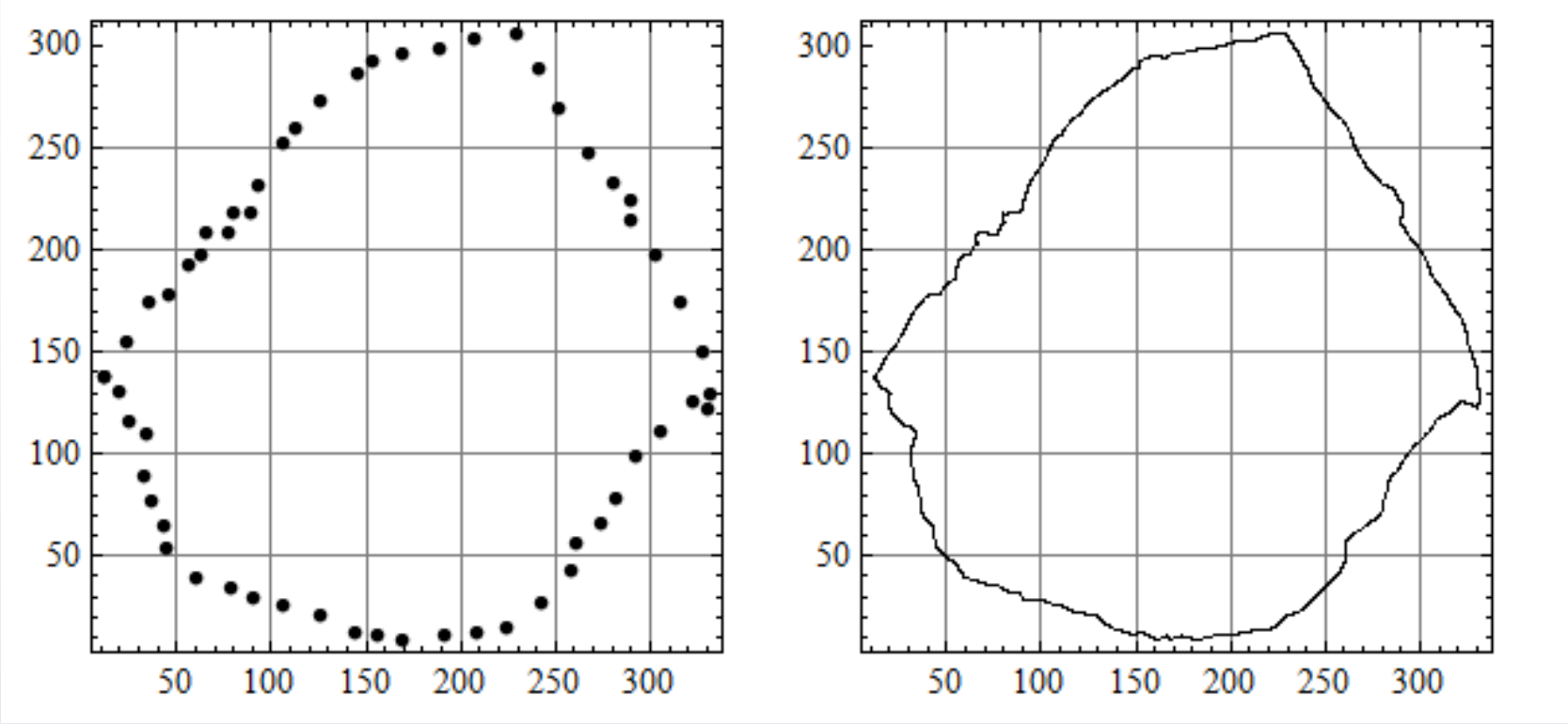

Figure **33.** Once having interpolation points (left), the "hidden variable" fractal interpolation is applied to get the fractal reconstruction of the grain's contour.

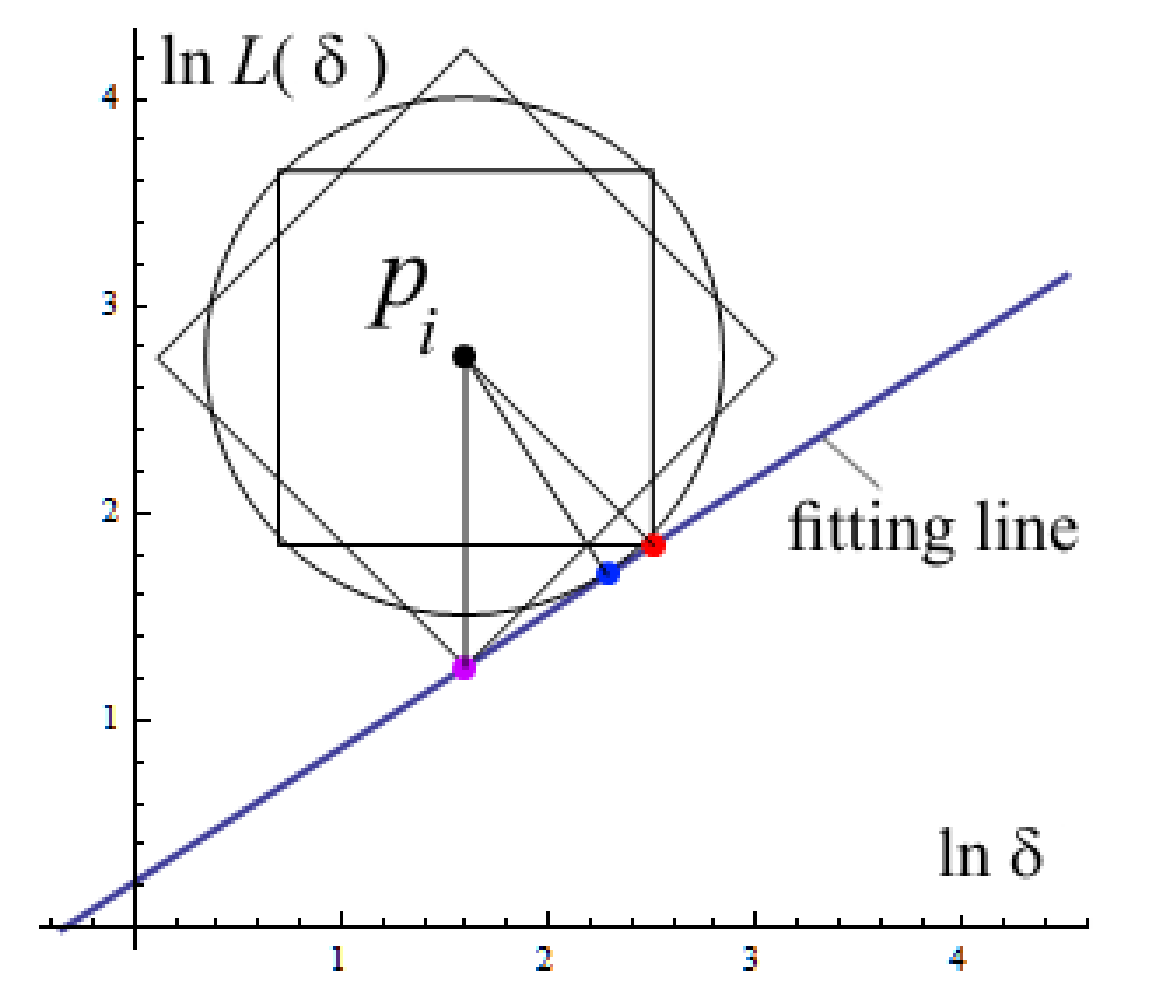

Figure **34.** The {ln *d*, ln *L*(*d*)} data least-square fitting by linear function reveals the slope coefficient *a*, which is equivalent to fractal dimension DH_f of the contour. Two squares and the circle around the point p_i represents the geometric sets of points which distance from is constant in three different metrics.

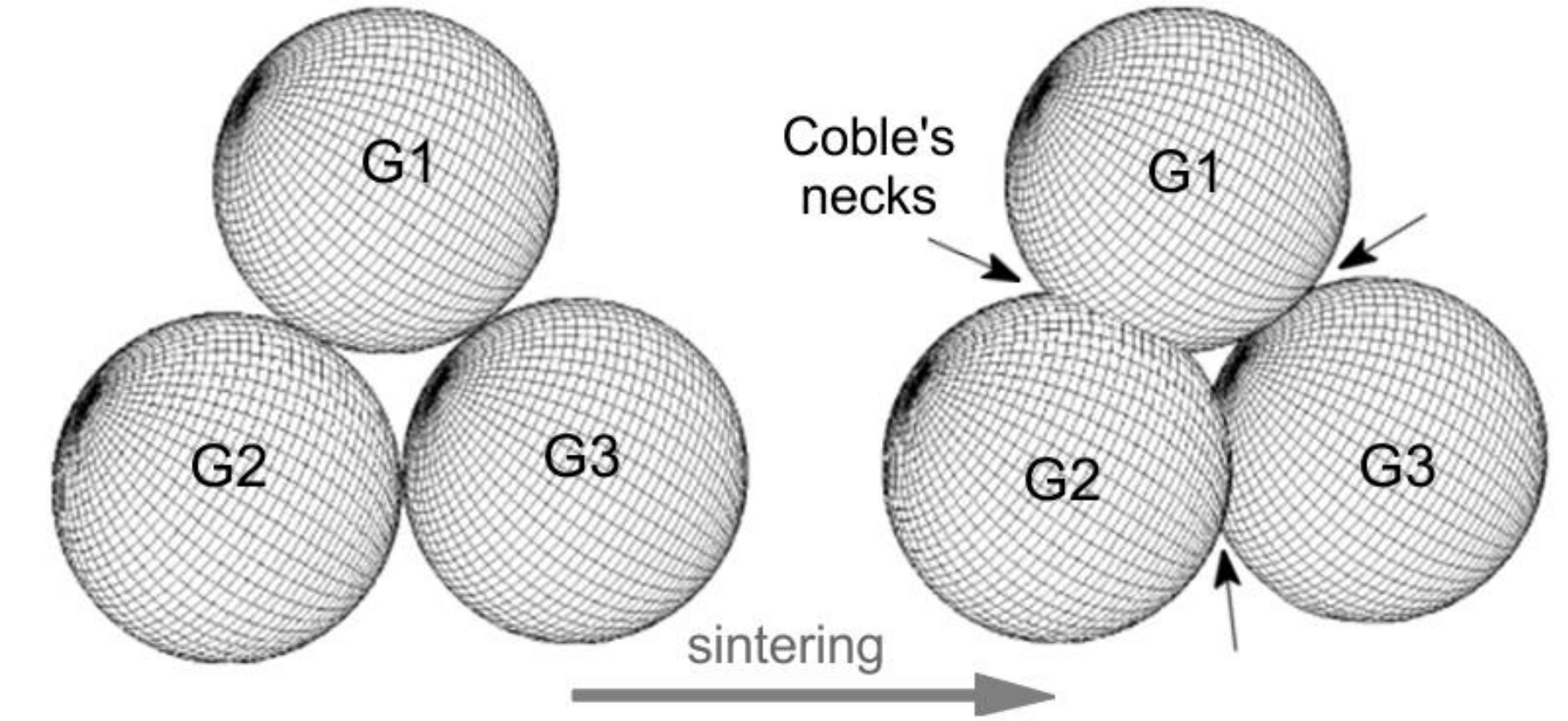

Figure **35.** Three grains approximated by spheres (left) and Coble's neck formed during sintering process (right). This is the mechanism of creating intergranular micro-capacitors, the energy storage units.

Once having the method of retrieving the fractal dimension, gives the chance to go deeper into the nature of grain's micro contacts. At this point the concept of *Minkowski hull* came forward.

A structural pattern of three sphere-shaped ceramic grains: contacting only in one point (left) and making contacts (right). The lower picture explains the construction of the ***generalized Minkowski hull***, as a surface having the distance of the grain's surface defined by the convex body rolling over the surface. Minkowski hull can be used to evaluate fractal dimension of an object. The hull itself is defined as

$$MH(d_{Fmin}, d_{Fmax}) = \left\{ x \in \mathsf{R}^3 : d(x, GS) = d_{cb}(t),\ 0 < t < t_{\max} \right\}$$

Where *GS* is the grain surface and d_{cb} is Feret diameter of a convex body rolling over the surface *GS*. The fractal dimension is then

$$DH_f = \lim_{\delta \to 0} \sup \left\{ 3 - \frac{\ln Vol\left[MH(d_{Fmin}, d_{Fmax}) \right]}{\ln \delta} \right\},\ \delta = d_{Fmax} - d_{Fmin}.$$

The maximum Feret's diameter, d_{Fmax}, also called the maximum distance in some references, is defined as the furthest distance between any two parallel tangents on the particle. Likewise, the minimum Feret's diameter, d_{Fmin}, also called the minimum distance in some references, is defined as the shortest distance between any two parallel tangents on the particle.

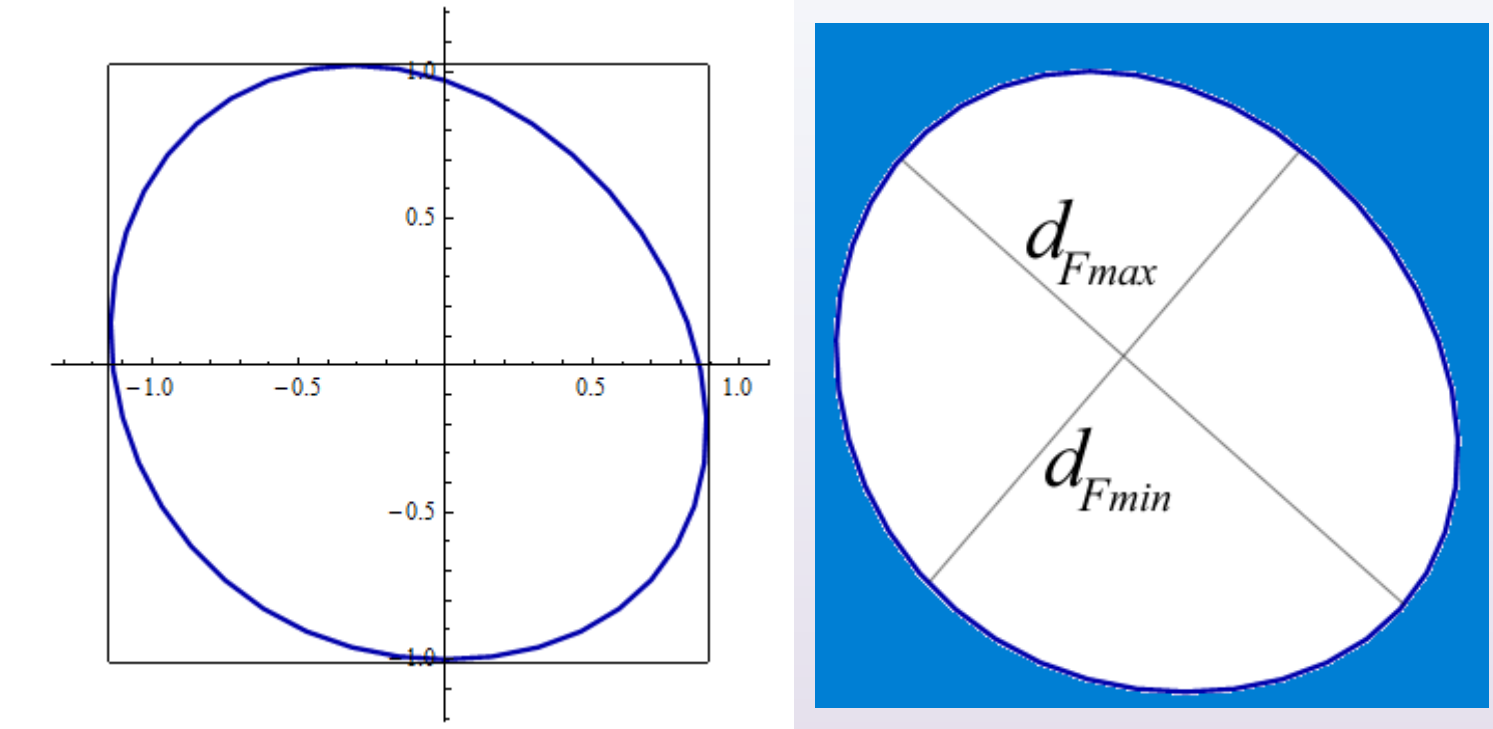

Figure **36.** Construction of the convex planar figure with orthogonal Ferret diameters.

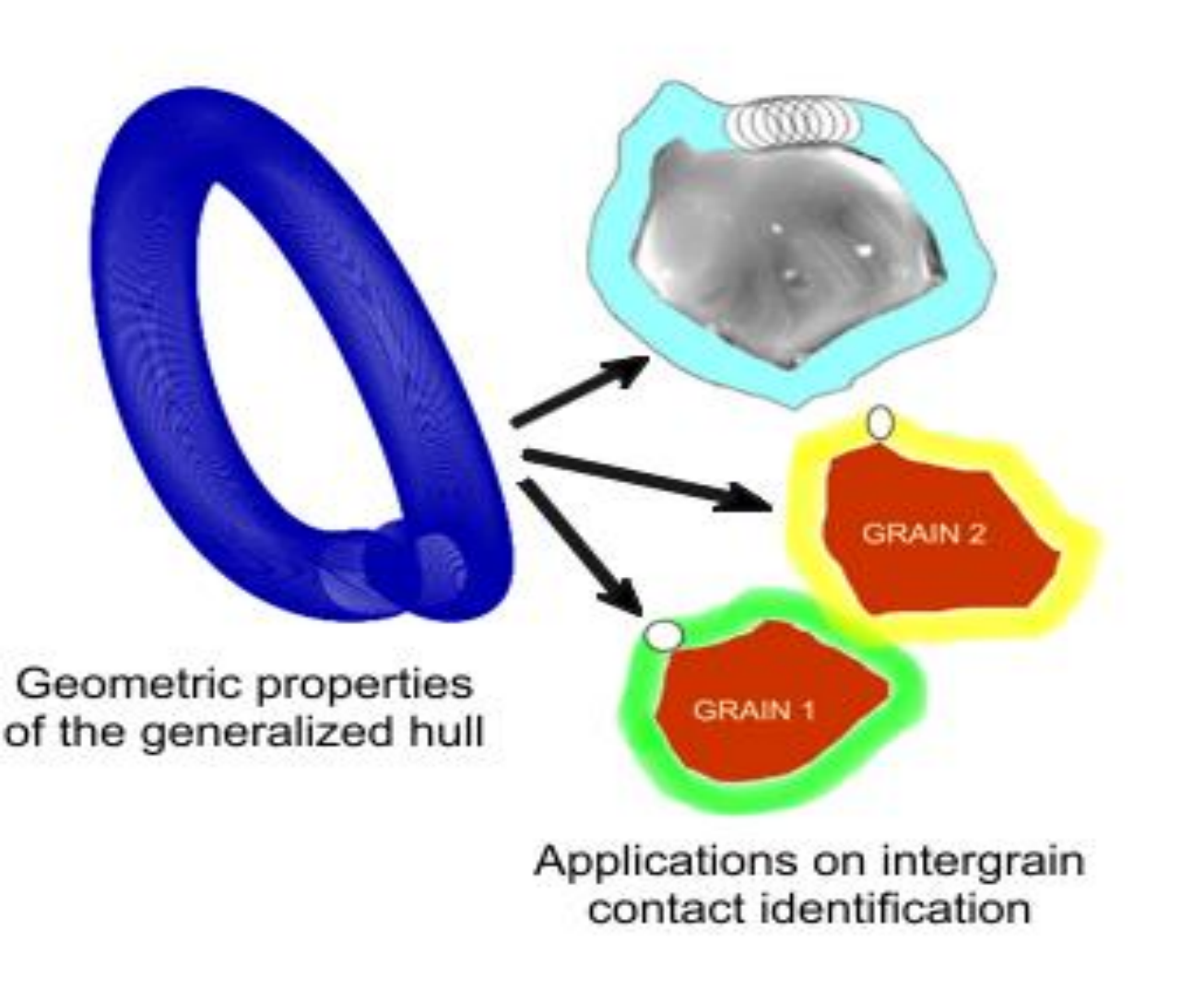

Figure **37.** Construction of Minkowski hull using predefine convex planar figure with orthogonal Ferret diameters (*generalized Minkowski hull* $MH(d_{Fmin}, d_{Fmax})$).

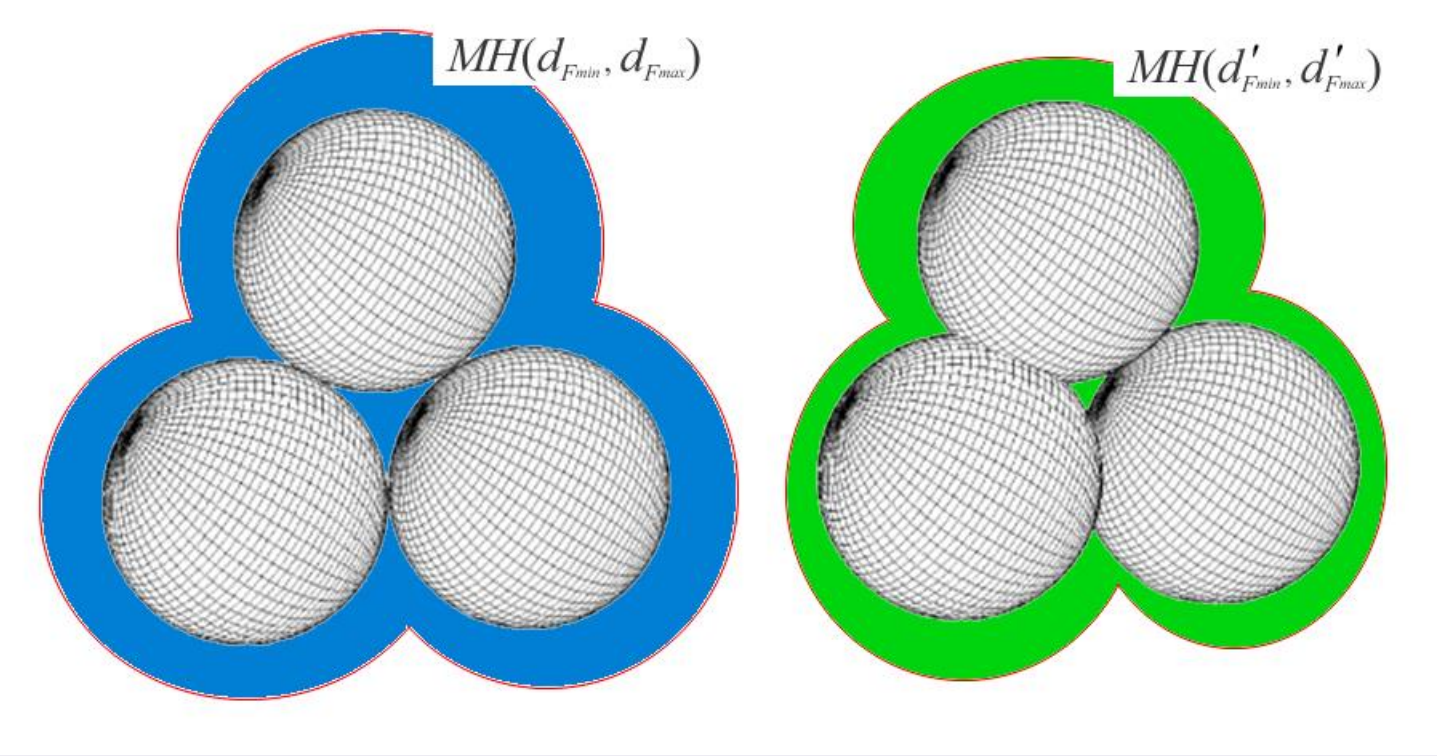

Figure **38.** If $d_{F\min}$, $d_{F\max}$, are two extremal Feret diameters of the 2D convex body used to generate generalized Minkowski hull, $MH(d_{F\min}, d_{F\max})$ is uniquely defined by these diameters and the starting point of rolling motion on the perimeter of 2D grain. This concept extends in natural way on 3D grains and 3D convex bodies. In the case of grains' cluster (as it is in the case of the above picture), the neck formation in the liquid phase of sintering cause overlapping of associated GM hulls. The degree of overlapping define properties of intergrain zones.

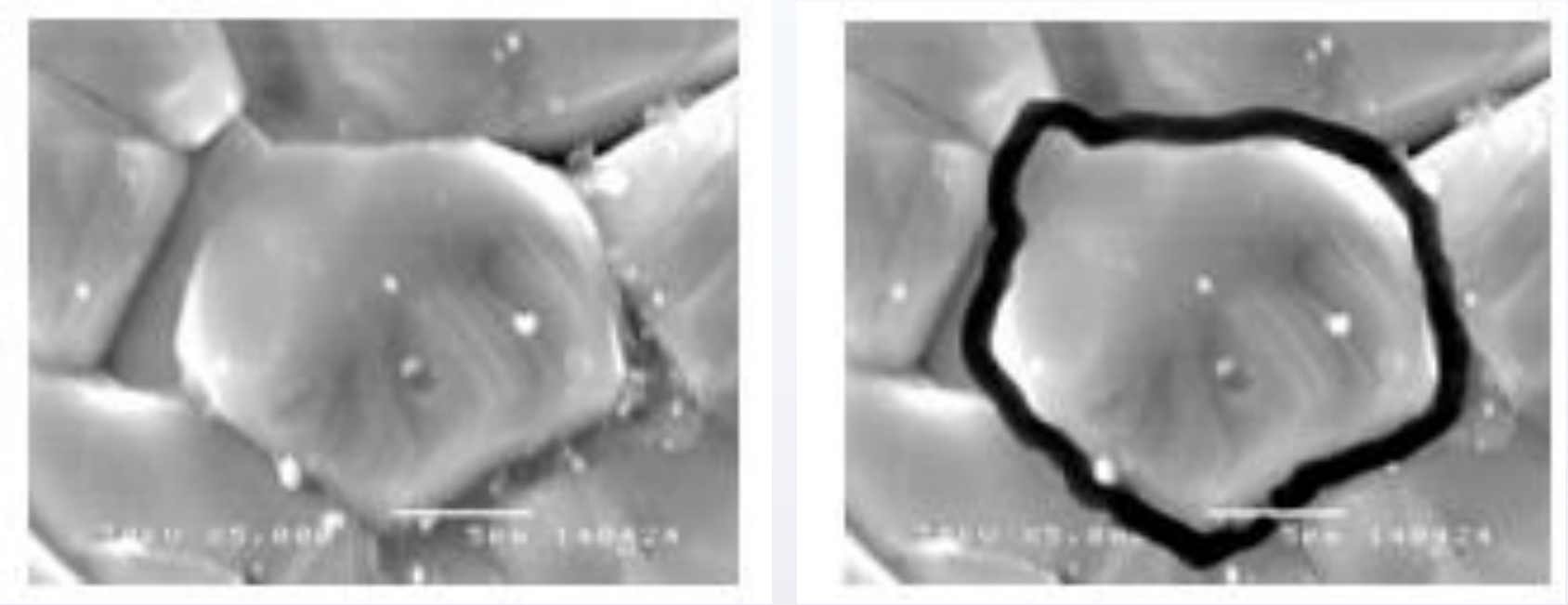

Figure **39.** The generalized Minkowski hull (the black ring on the right photo) of a ceramic grain from the SEM photo (left photo).

Construction of 2D Minkowski hulls $MH(d_{F\min}, d_{F\max})$ using predefine convex planar figure with orthogonal Ferret diameters $d_{F\min}$ and $d_{F\max}$ anticipate quality of the intergrain zone. Diameter changing suites the geometry of ceramics grains since the intergrain space is not constant in thickness, which is visible in the microphotographs.

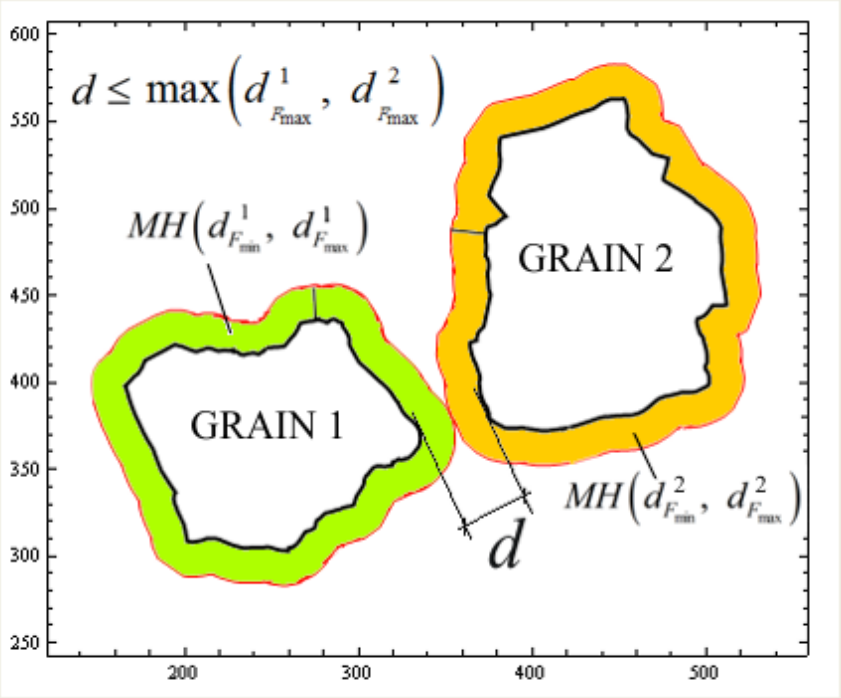

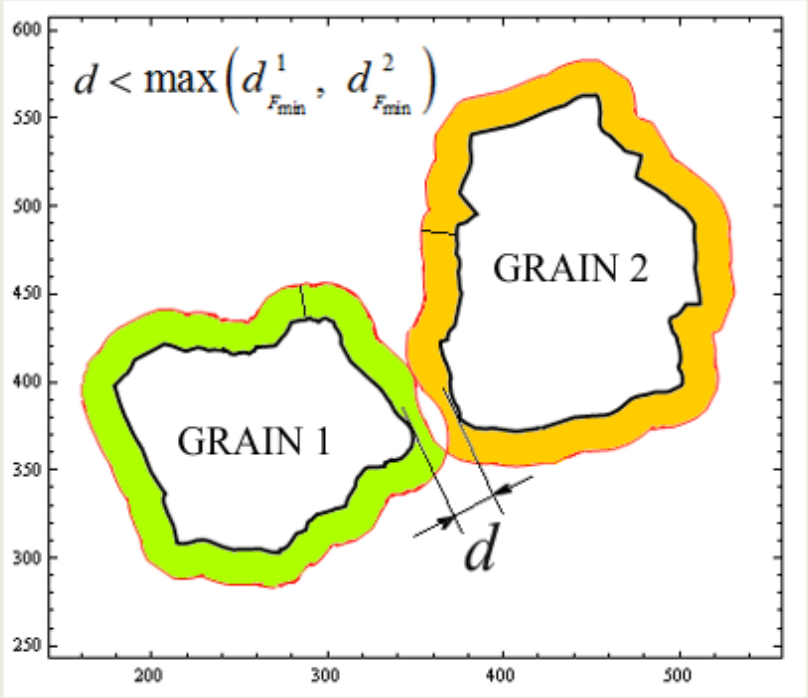

The Minkowski hull is characterized only by its distance from the grain. Consider two grains with hulls $MH\left(d^{2}_{F_{min}}, d^{2}_{F_{max}}\right)$ and $MH\left(d^{1}_{F_{max}}, d^{2}_{F_{max}}\right)$. The meaning of these distances and the Minkowski hulls is that the grains' coarseness stays inside the hull. It means that no micro relief hills overtop the hull boundary. If two grains are in the position when their distance is not bigger than $MH\left(d^{1}_{F_{max}}, d^{2}_{F_{max}}\right)$ the grains are in the *position of the first touch*.

If d becomes smaller than $MH\left(d^{1}_{F_{max}}, d^{2}_{F_{max}}\right)$, the intergranular zone begins to form.

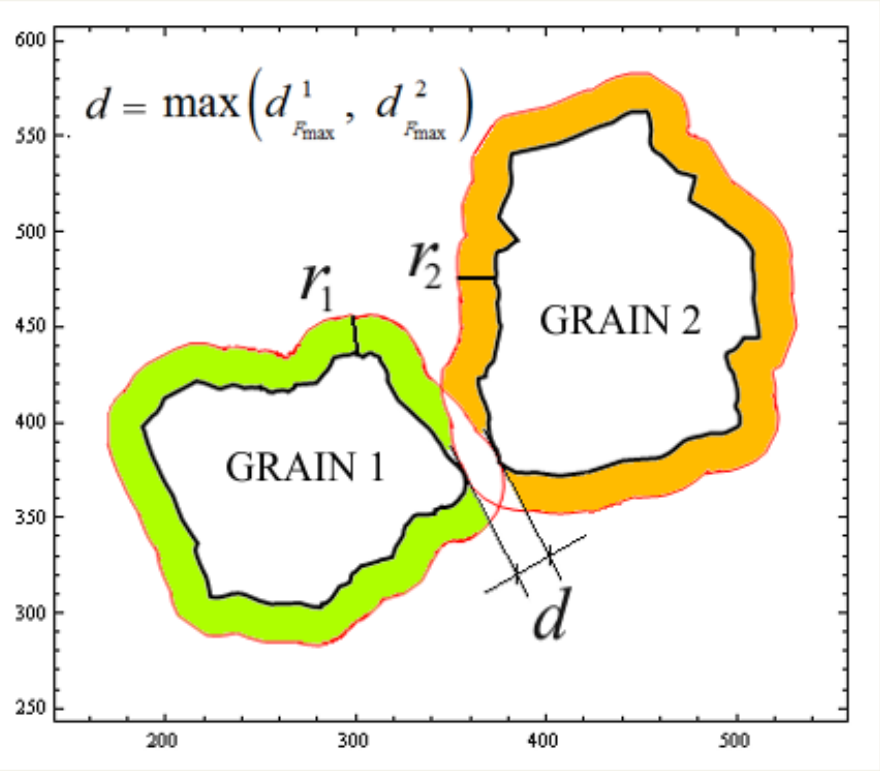

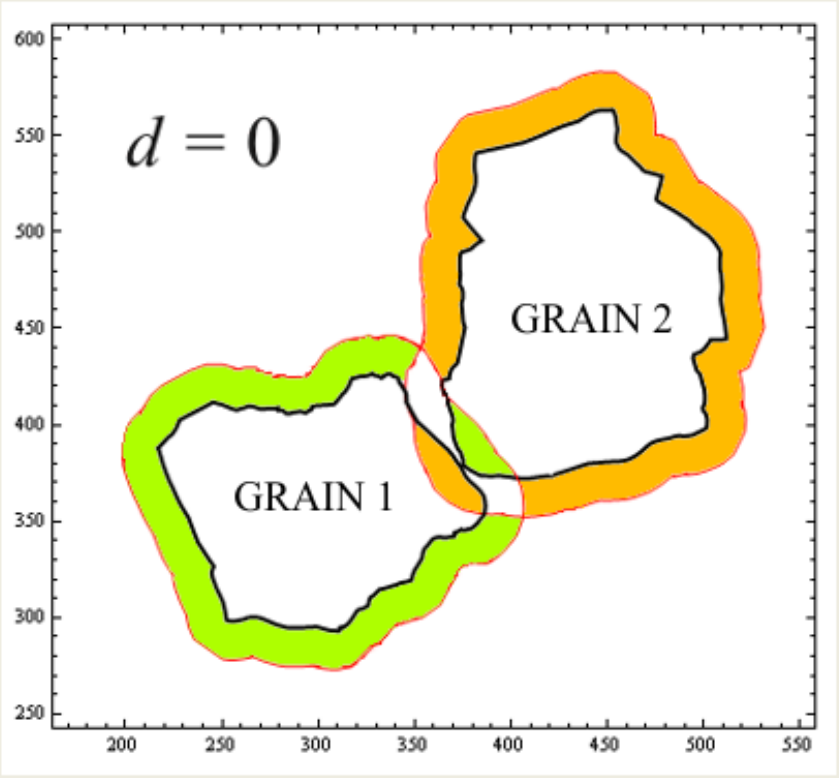

The second characteristic position is when the either hull's contour touches the other grain's body, i.e., when $d = \max\{ r_1 , r_2 \}$, the *second contact* is encountered. The *third contact* comes when $d = \min\{ r_1 , r_2 \}$. Contact of two grains in only one point is the fourth contact, in two points is the *fifth contact* and, finally if 3 points is common, it is the sixth contact. Without the concept of fractal surface, the above considerations will be pointless.

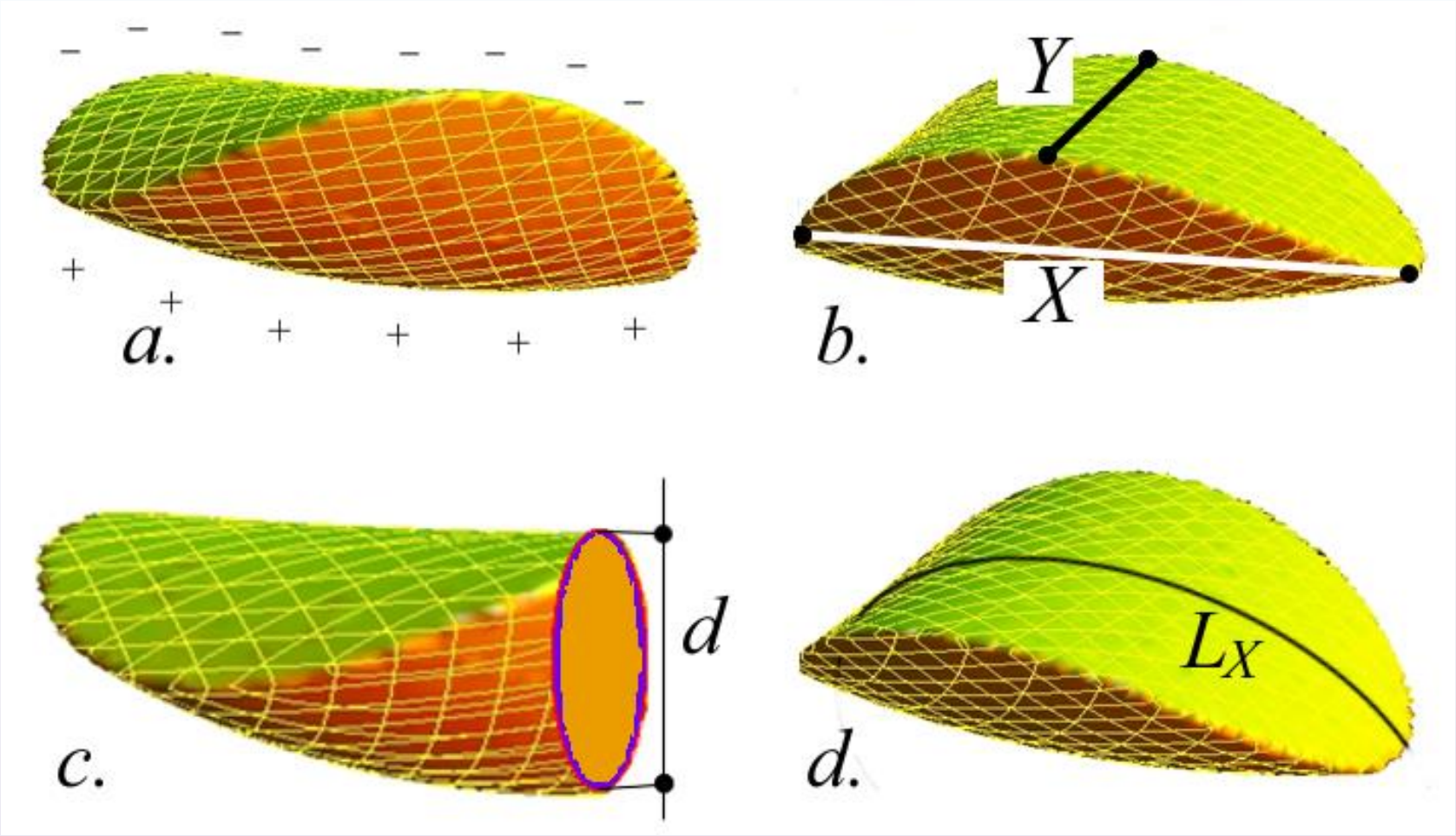

Figure **40.** ***a.*** The lens-shaped contact zones between grains as micro-capacitors formed by Minkowski hulls *MH*(d_{Fmin}, d_{Fmax}) intersection;

b.-c. The amount of integral capacity depends on the volume of caps that is determined by the Feret diameters *X* and *Y* and "lens" thickness *d* ;

d. The curvature, characterized by L_X/X or L_Y/X ratio influences electricity distribution on "lens" surface;

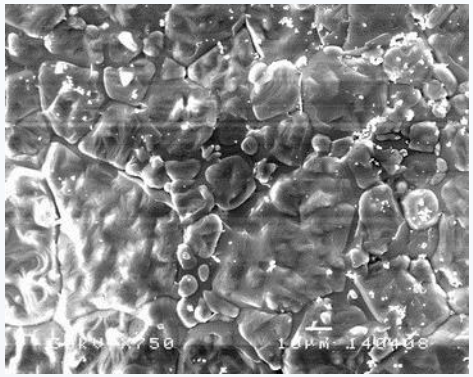

SEM sample and 3D fractal reconstruction

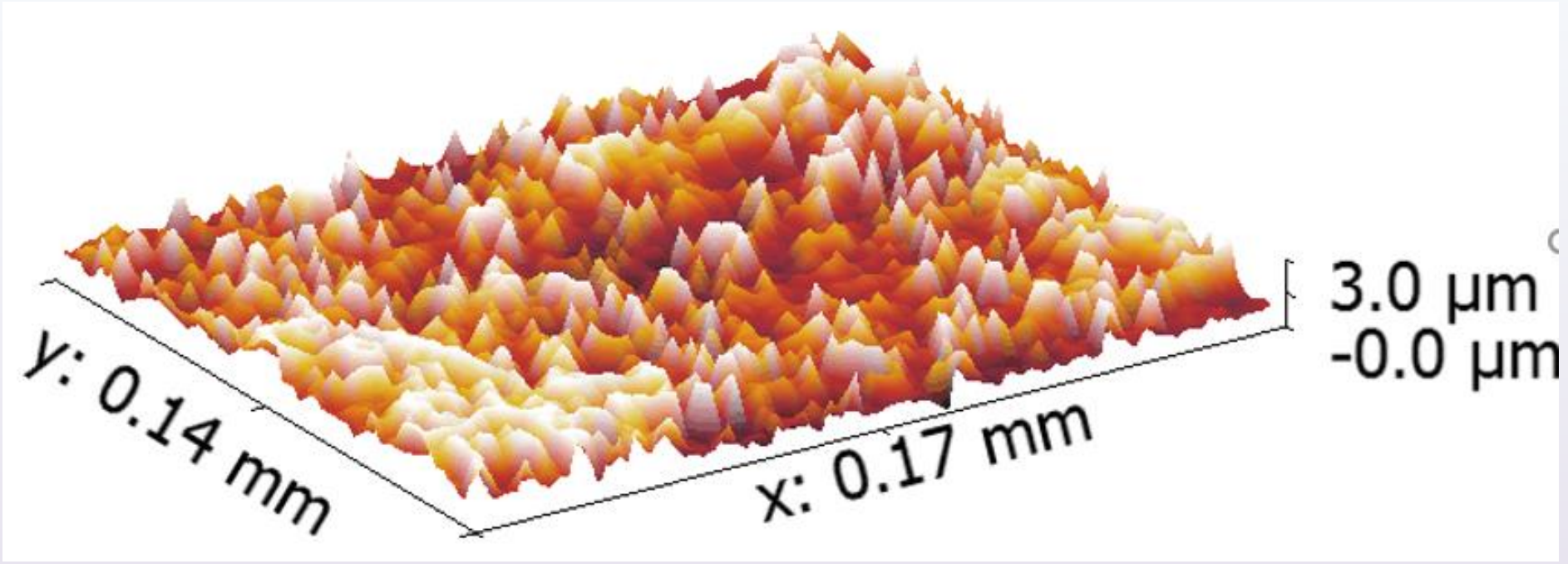

Figure **41.** Reconstruction that emulates TEM microphotograph.

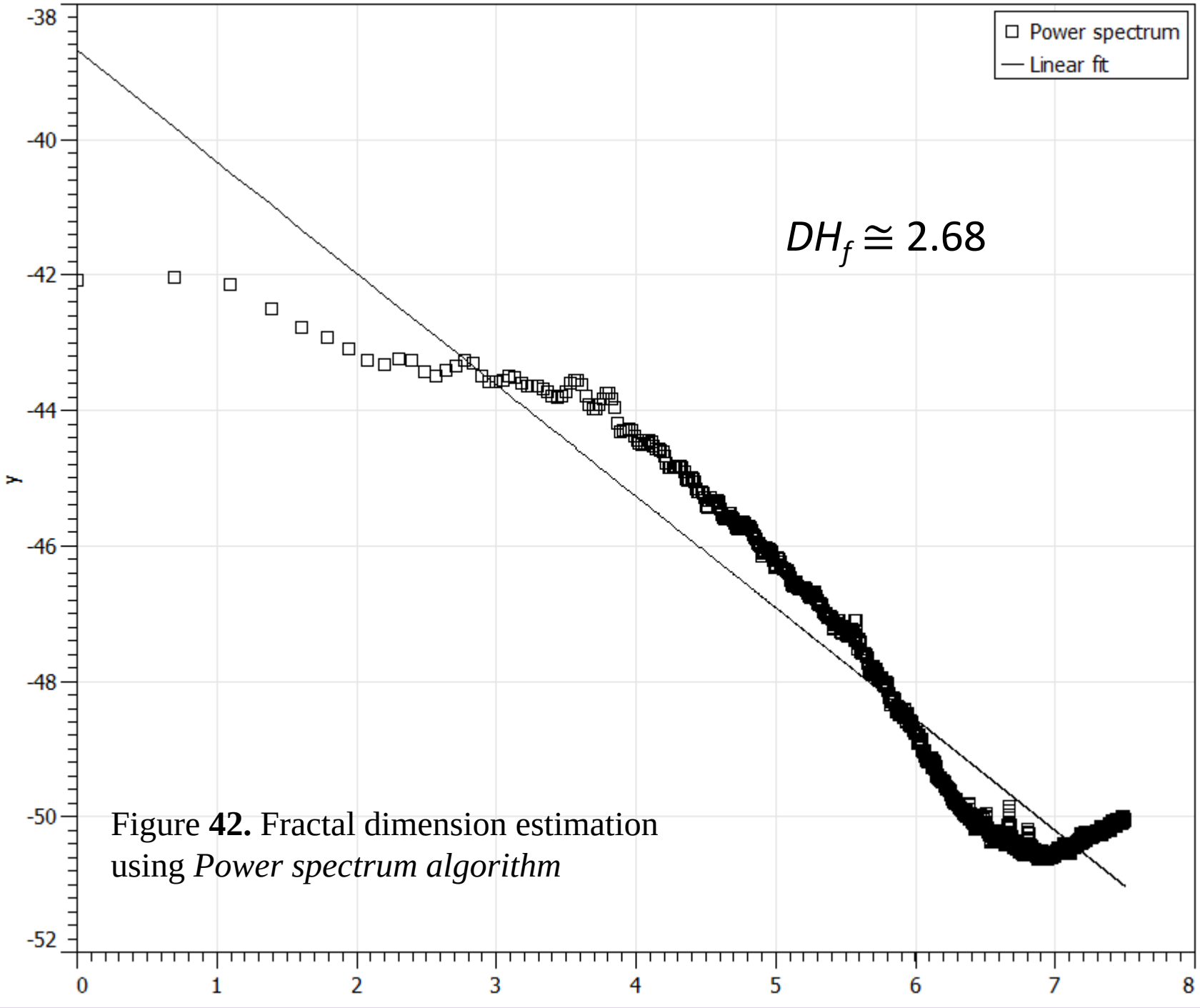

Figure **42.** Fractal dimension estimation using *Power spectrum algorithm*

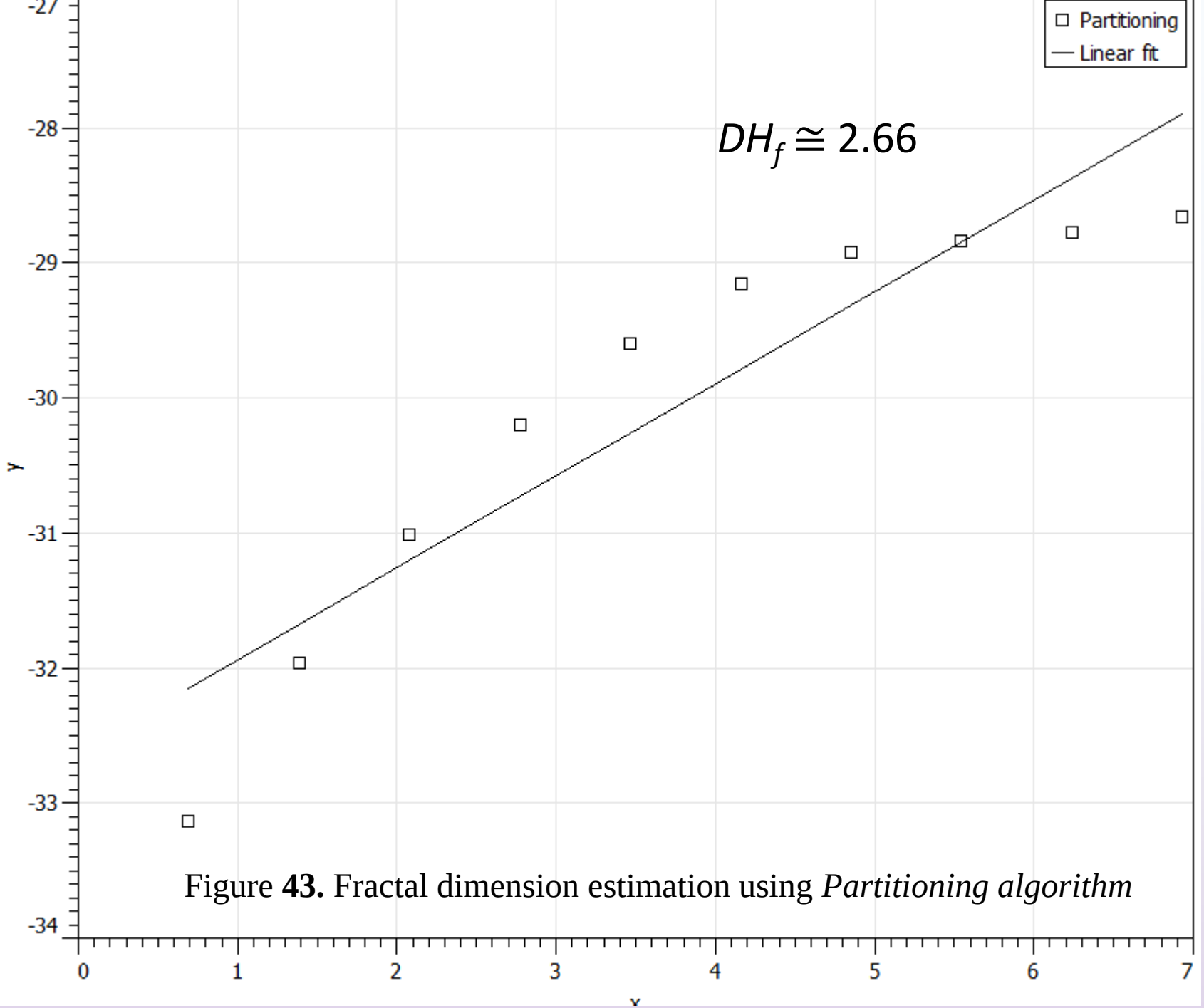

Figure **43.** Fractal dimension estimation using *Partitioning algorithm*

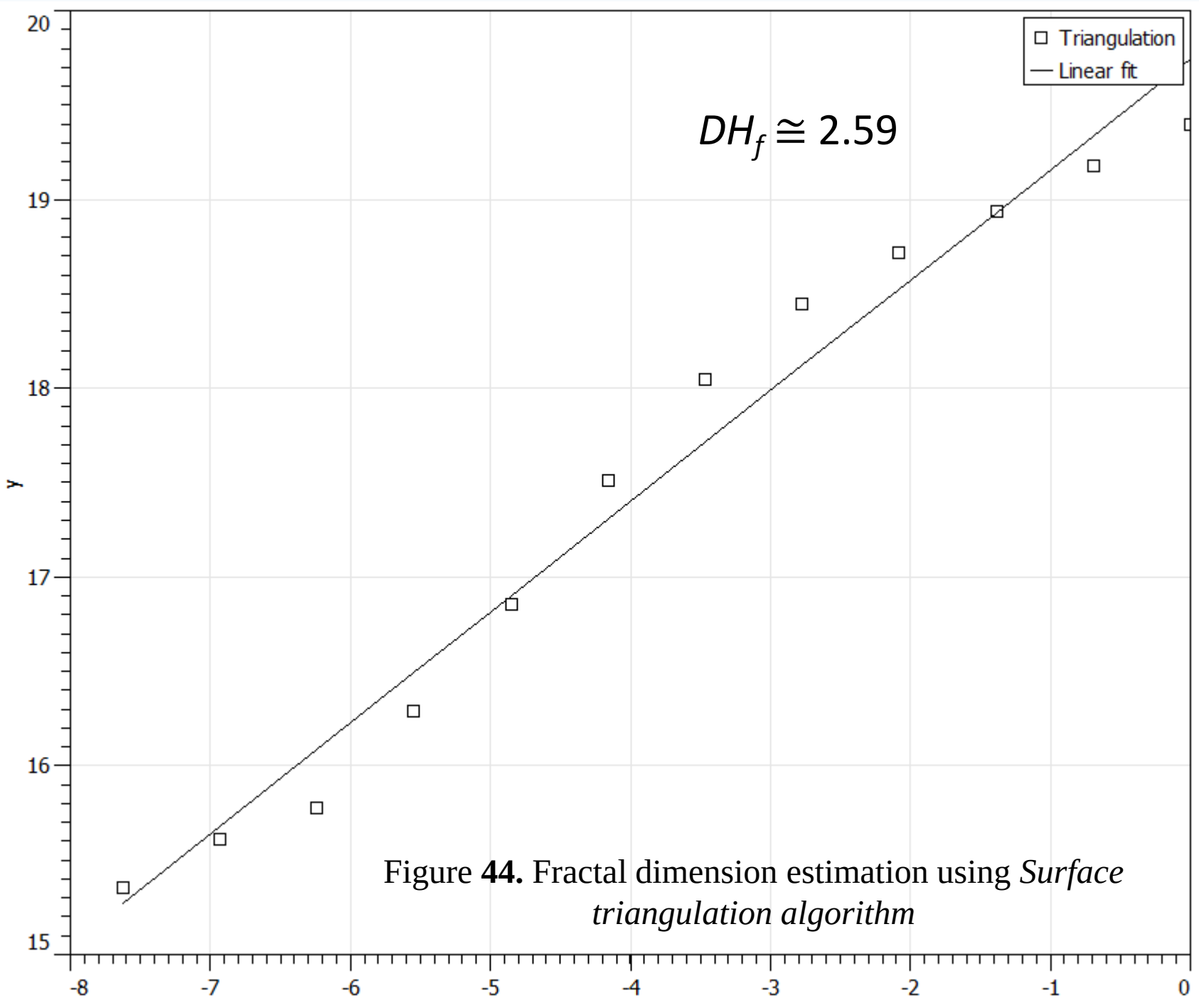

Figure **44.** Fractal dimension estimation using *Surface triangulation algorithm*

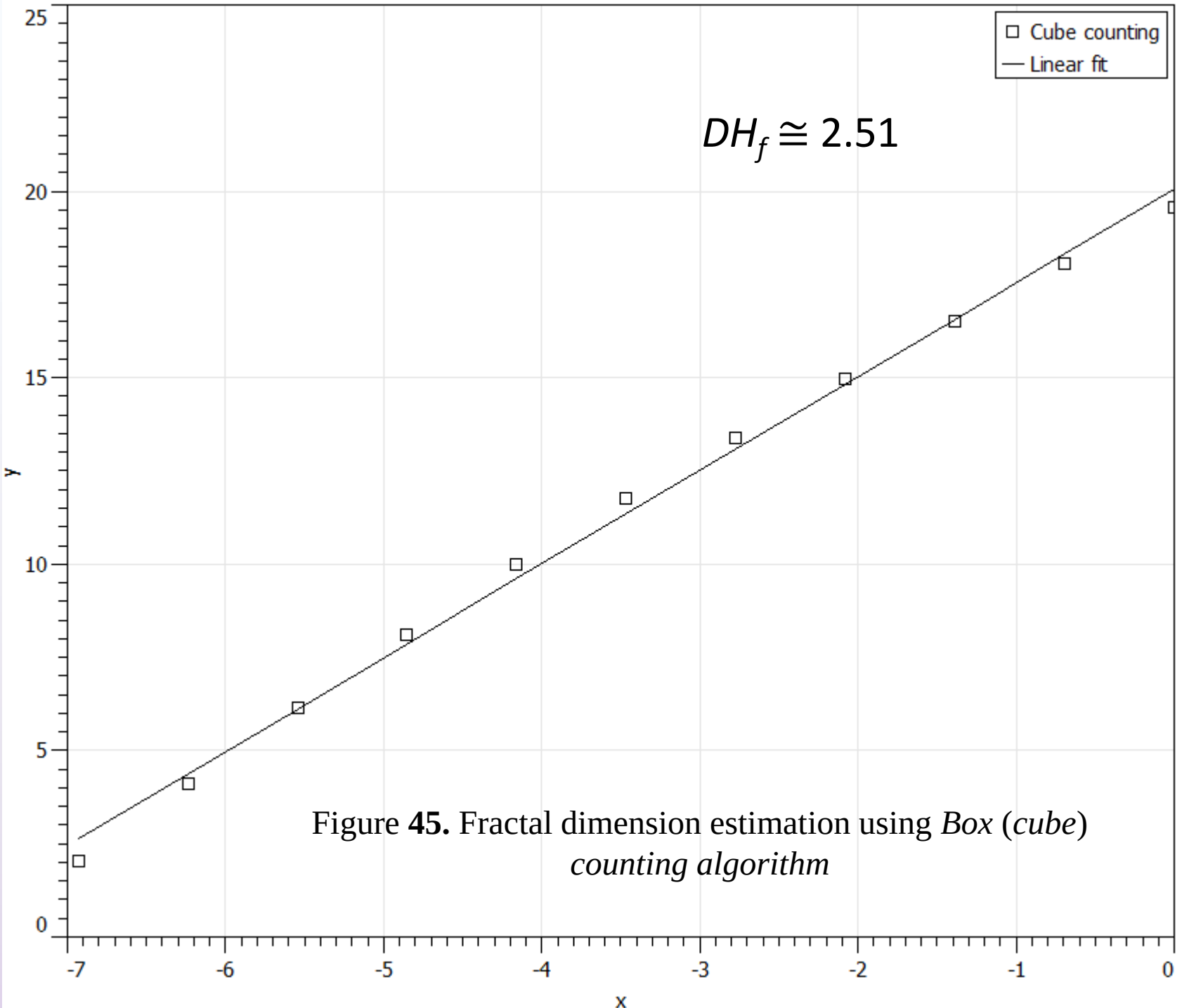

Figure **45.** Fractal dimension estimation using *Box* (*cube*) *counting algorithm*

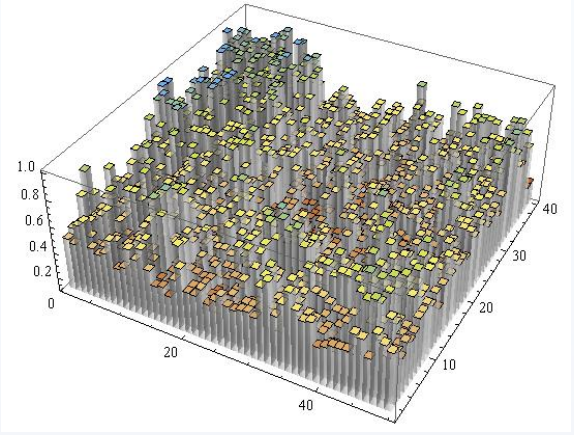

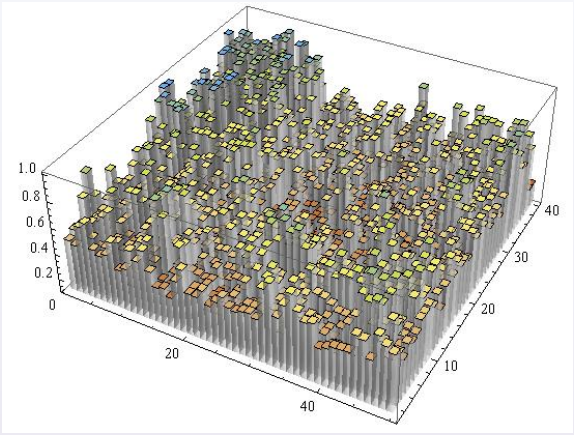

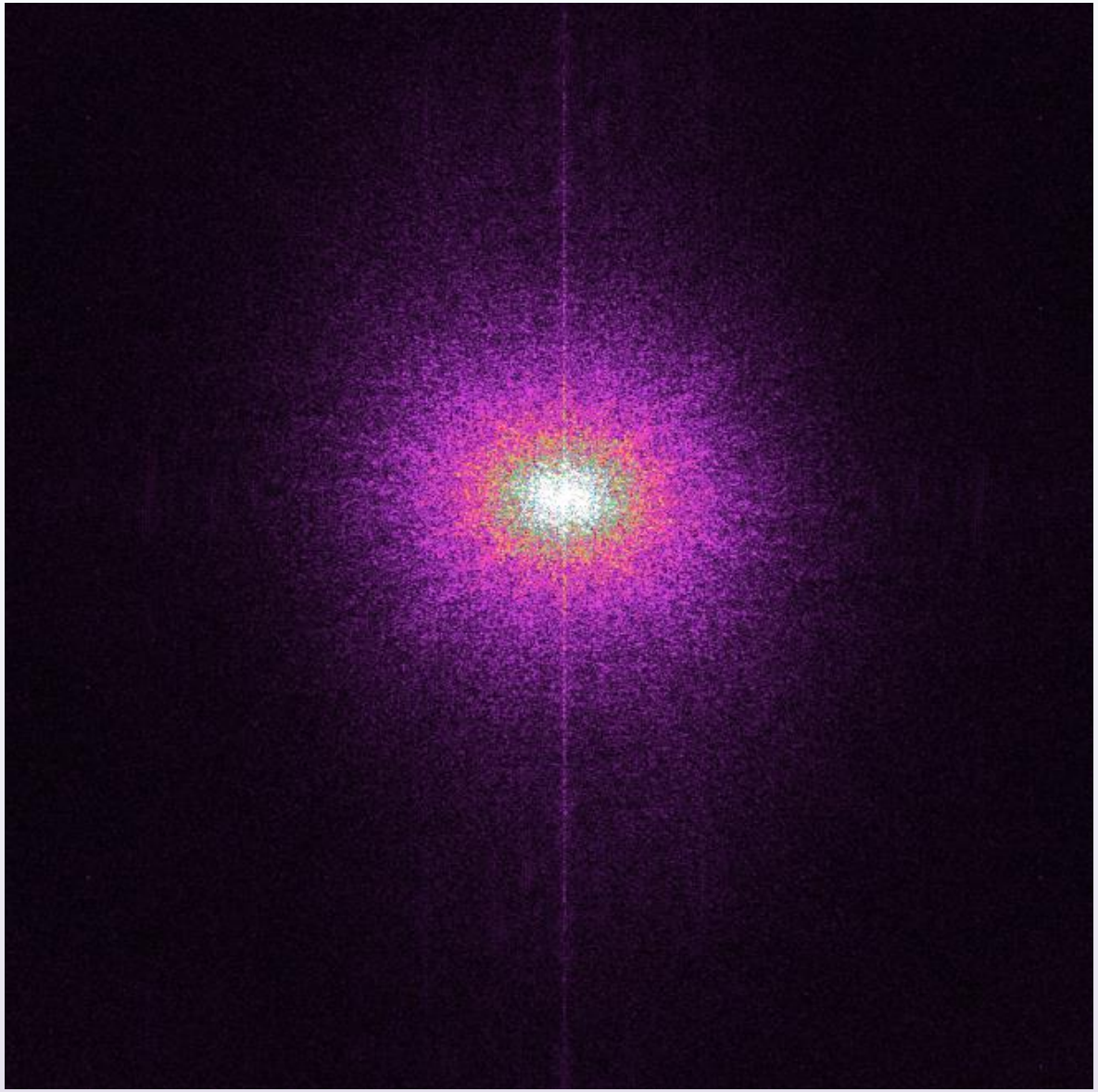

Figure **46.** The Fast Fourier transformation of the surface shows chaotic emerging of picks of different frequencies

Energy and fractals

World's need for energy imposed the whole spectra of technological challenges that further transform to scientific tasks. This chapter discusses the role of fractal geometry and analysis in energetic questions. In fact, some of the early fractal applications have been used as a tool in energy research, applying on diverse energy technologies, from photovoltaics to fuel cells and carbon capture.

Three items are essential regarding energetic questions:

i) *Free energy stocks location*;

ii) *Energy harvesting*;

iii) *Short and long term energy storage*;

What fractals and energy have in common?

I. Both fractals and energy are properties, energy is physical objects property, fractality is geometrical;

II. As well as energy, fractality is omnipresent, unlimited entity concerning space and time. There is a strong belief and many evidences that the whole Universe is permeated by fractal structures as well as by energetic fields;

III. Both entities, energy and fractality exist in micro and macro world. Any fractal is dividable down to nano-scale as well as the energy field;

IV. Energy is closely connected with geometry structures and especially with nano-geometry. Some energetic extremal problems as a solution have smooth, symmetric Euclidean objects, another have fractals;

V. If an energetic situation can be described by fractals, then potential energy corresponds to fractals constant in time while kinetic energy needs time dependent fractals;

VI. Energy spectrum and energy spectral density of some time series (signals), by the rule, has fractal structure;

In *i.*, term “geometry” as it is custom in plain language, understands “shape” rather than the science of geometry. In this sense, geometry is a property. And it is more present in everyday life than we are usually aware of. Just note that all our senses often convey information on the quality of some matter by interacting with some geometry or shape. The touch feeling of smooth or rough surface, olfactory or taste data generates according to geometry of particles, etc. With fair precision, our eye can distinguish metal from fur or wood from feather.

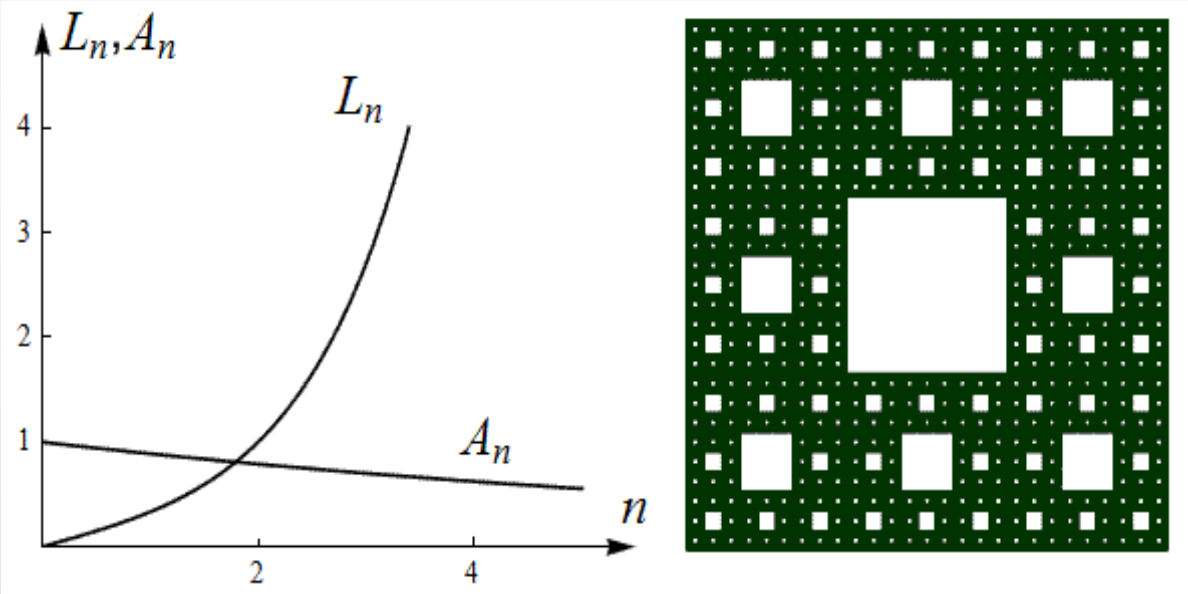

Figure **47.**

The Sierpinski carpet ($D_H \approx 1.8928$, when $n \to \infty$). While the length L_n (the sum of circumferences of all white squares) increases to infinity, the black area, A_n decreases to zero.

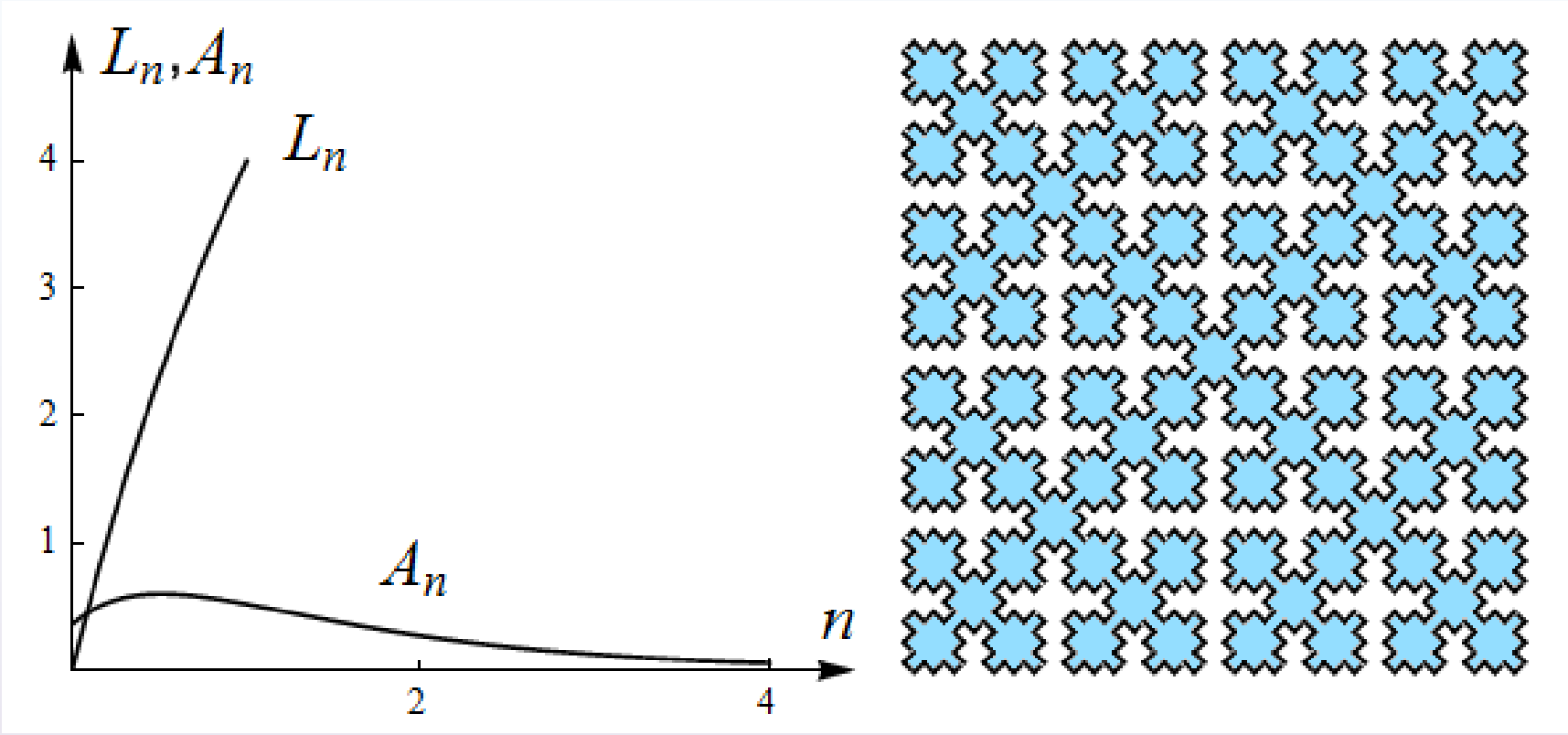

Figure **48.** The Sierpinski square curve ($D_H = 2$, when n goes to infinity) displays typical behaviour of fractal object. While one dimension (length L_n) increases unlimitedly another one (area it covers, A_n) decreases to zero.

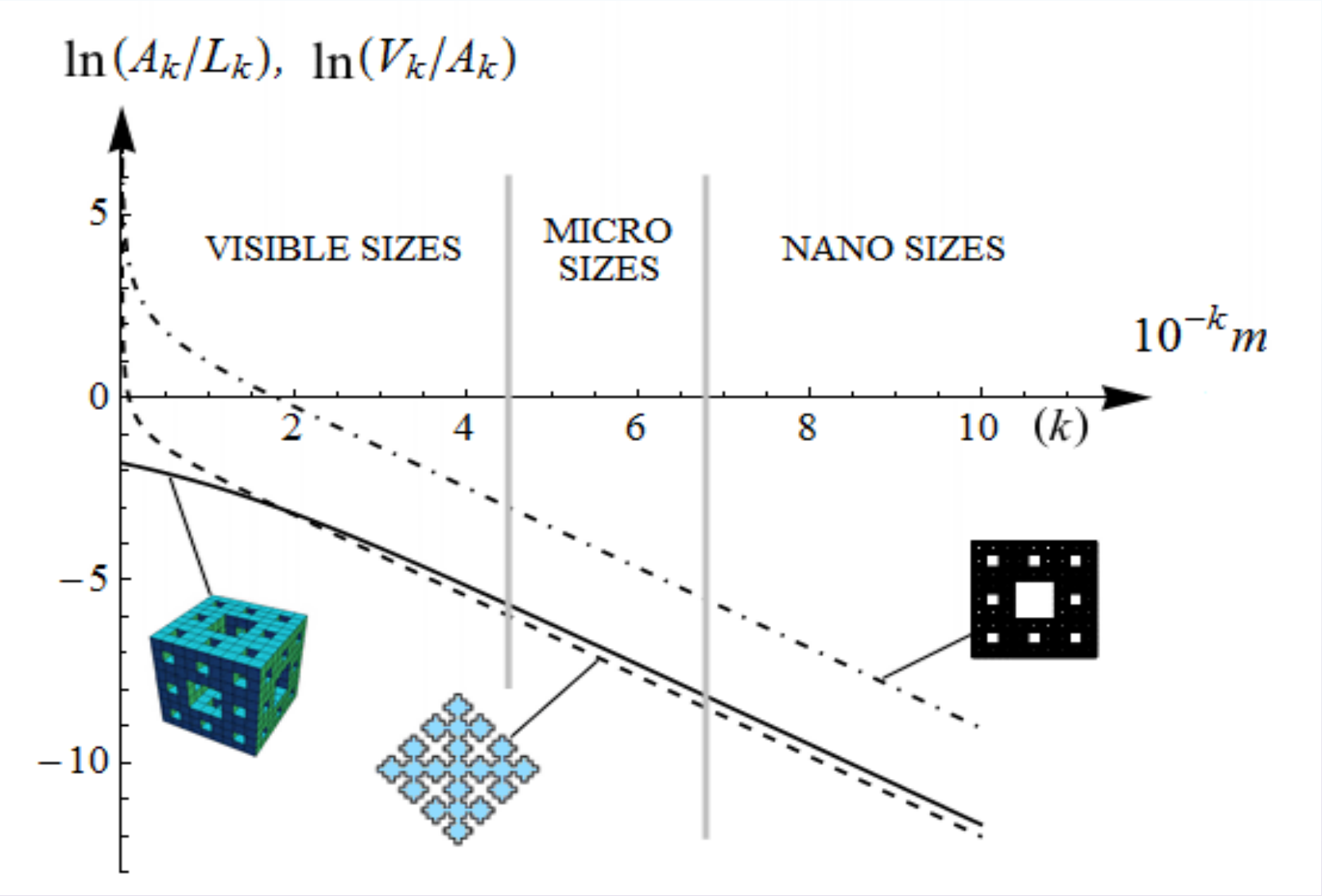

Figure **49.** The ratios area vs. length for Sierpinski quadratic curve and Sierpinski carpet as well as the ratio for Menger sponge in logarithmic scale and with $n = k \log_3 10$.

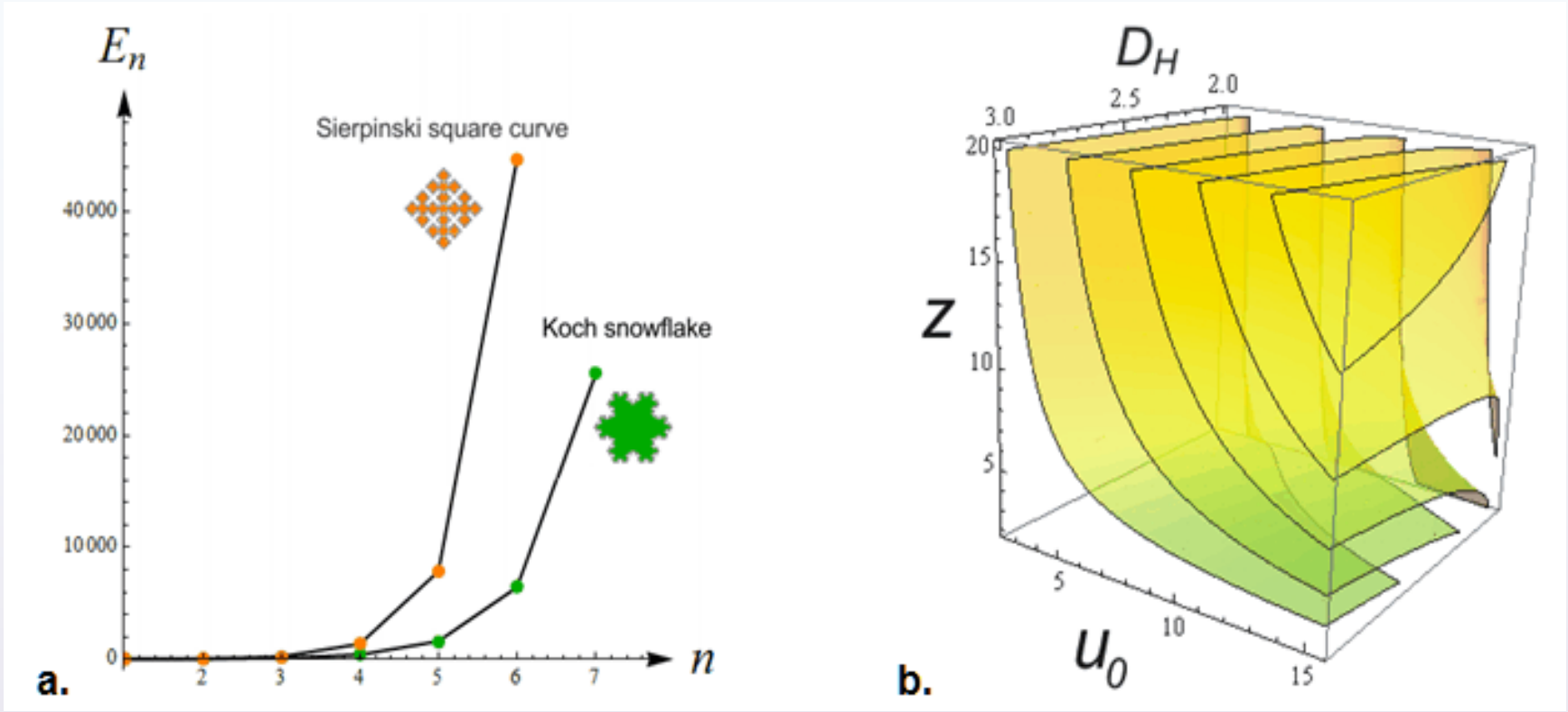

Figure **50. a.** Energy of fractal curves as function of iteration number n. The higher fractal dimension ensures higher energy; **b.** The wind profile logarithmic law with fractal correction (6) showing the average wind speed as function of friction velocity u_0, height z and fractal dimension of the surface D_H.

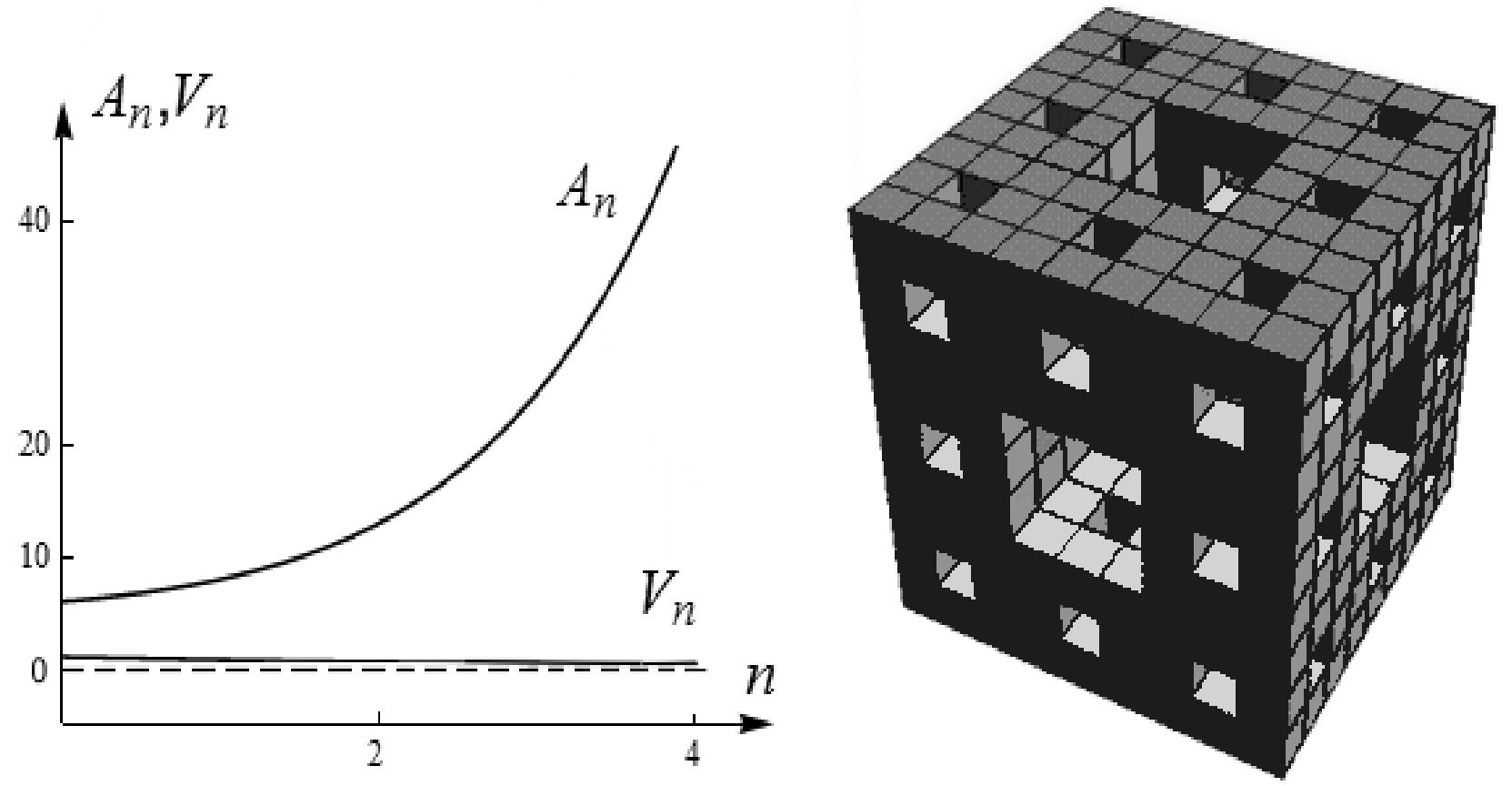

Figure **51.**

The Menger sponge fractal ($D_H \approx 2.7268$ when $n \to \infty$). In this case, the area A_n increases unlimitedly while the volume V_n decreases to zero.

So, if the ceramics is organized as composition of grains and pores, and if pores have distribution that follows Sierpinski Carpet fractal configuration, than

$$d_F = \frac{\ln 8}{\ln 3} = 1.8928...$$

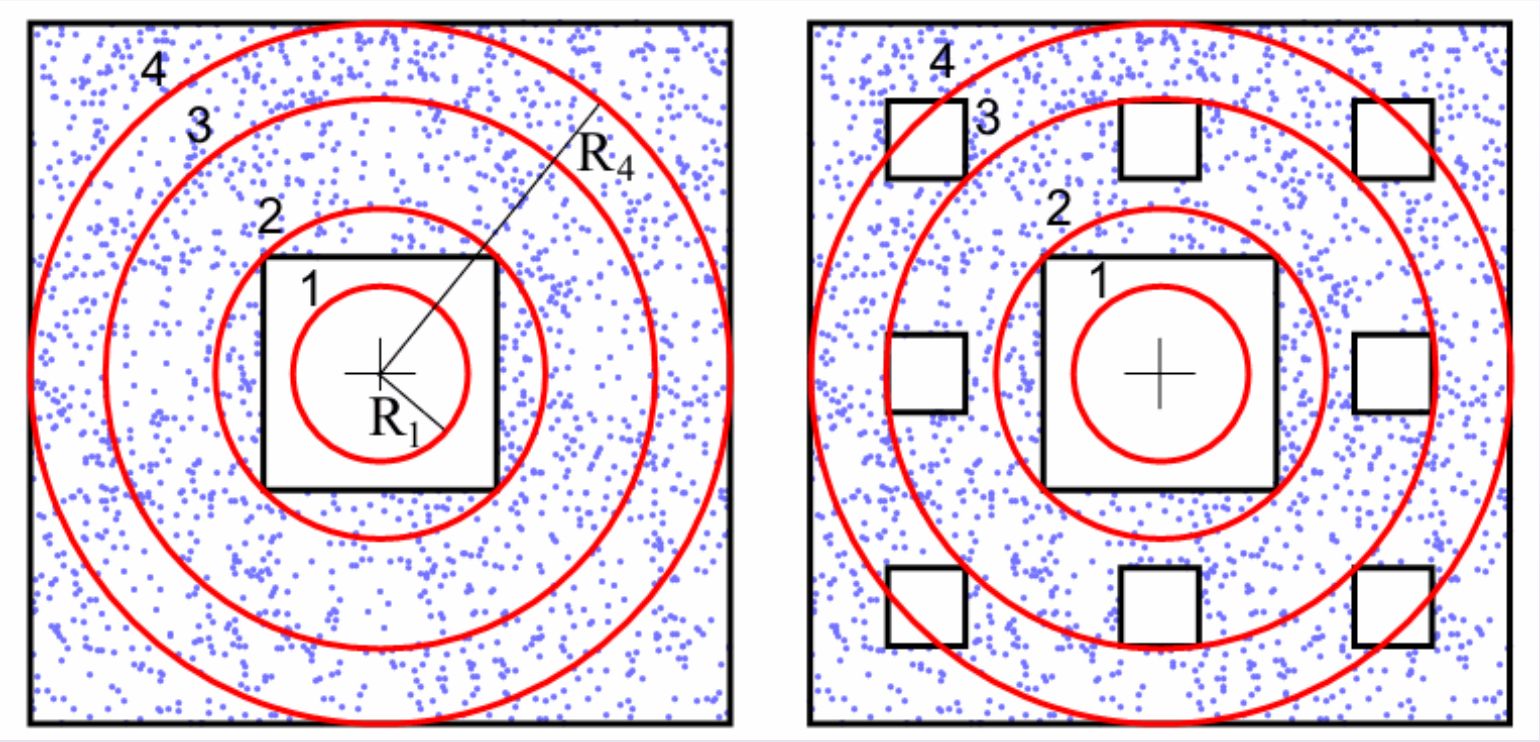

In this manner, the density of contacts is given by asymptotic formulae

$$\rho(a) \sim a^{\ln 8/\ln 3}, \quad \text{or} \quad \rho(a) = K \times a^{1.8928}.$$

Estimation of contact density via the volume $V = a^3$ is $\rho(a) = K \cdot V^{DH_f/3}$ which gives the number of contacts in V as

$$N(V) = K \cdot V^{1+\frac{1}{3}DH_f}$$

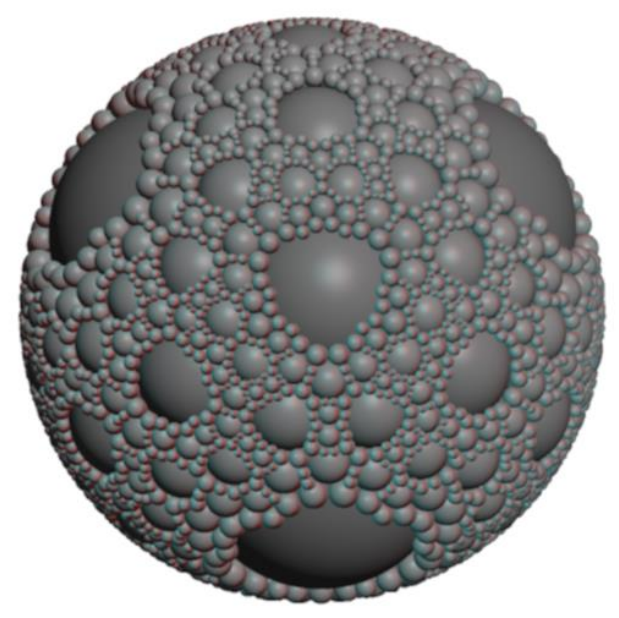

$DH_f = 2.4739$

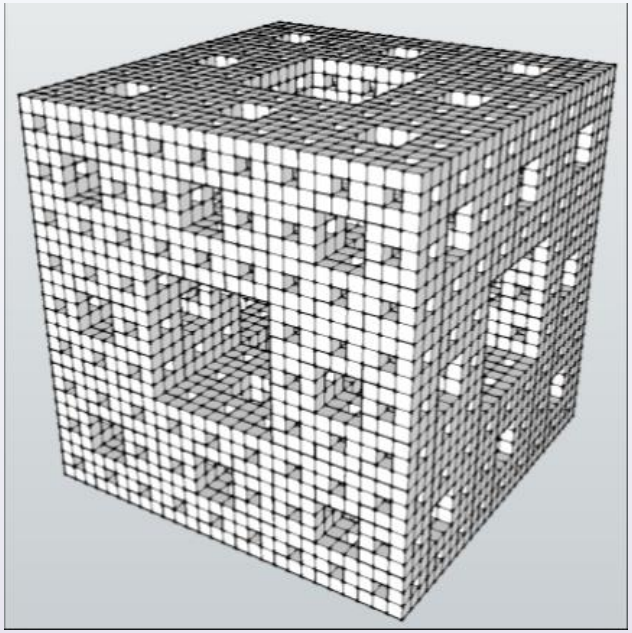

$DH_f = 2.7268$

Figure **52.** *Paradox*: Compariing the fractal dimensions of Apollonian fractal and Menger sponge fractal reveals that the last one is less porous than Apollonian packing, although it looks it has to be just the opposite.

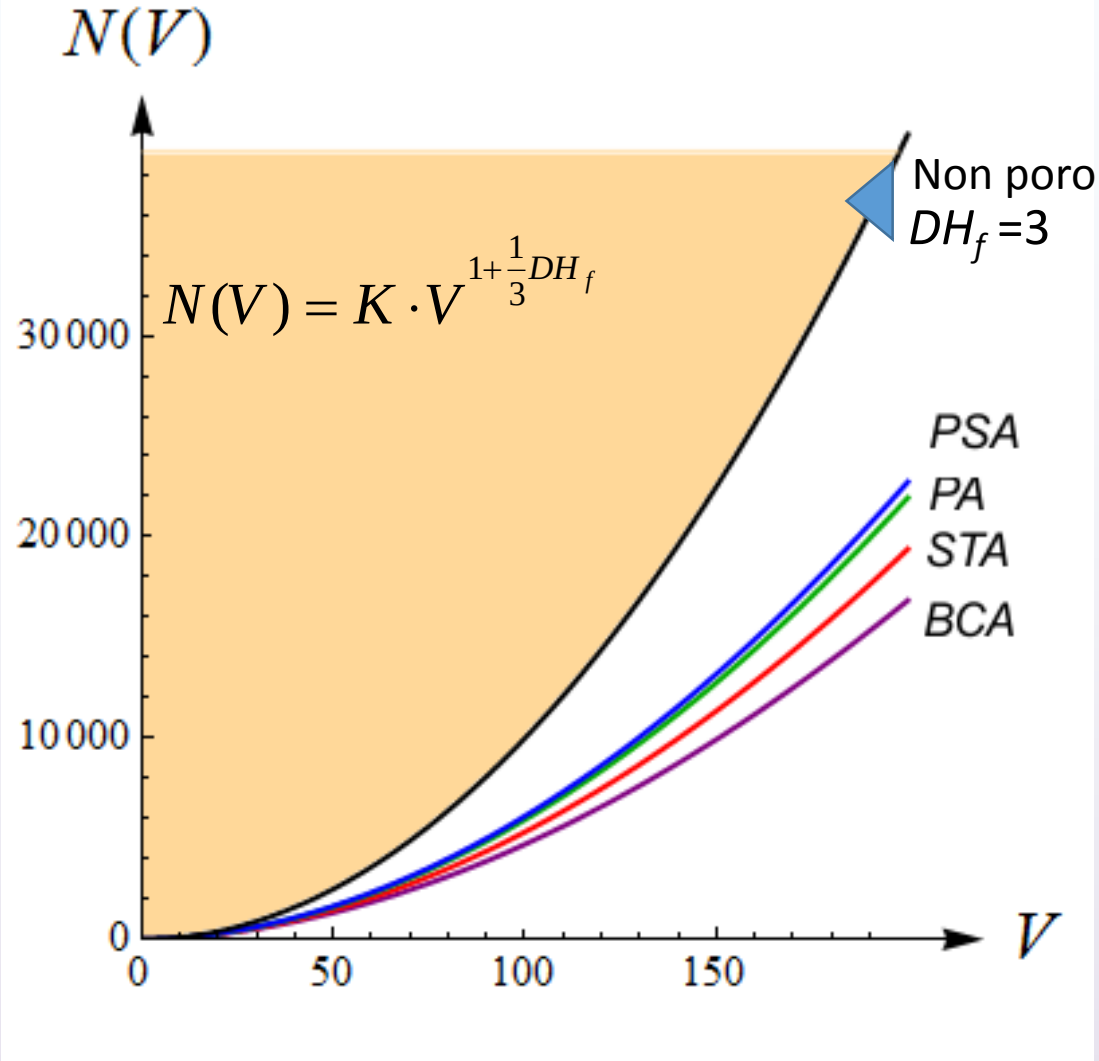

Figure **53.** The graphs for values of DH_f estimated by *Power spectrum algorithm* (PSA), *Partitioning algorithm* (PA), *Surface triangulation algorithm* (STA), and *Box counting algorithm* (BCA). The top curve represents is the theoretical upper limit DH_f =3 that corresponds to absolute dense material, without pores.

Minkowski-Hlawka Theorem

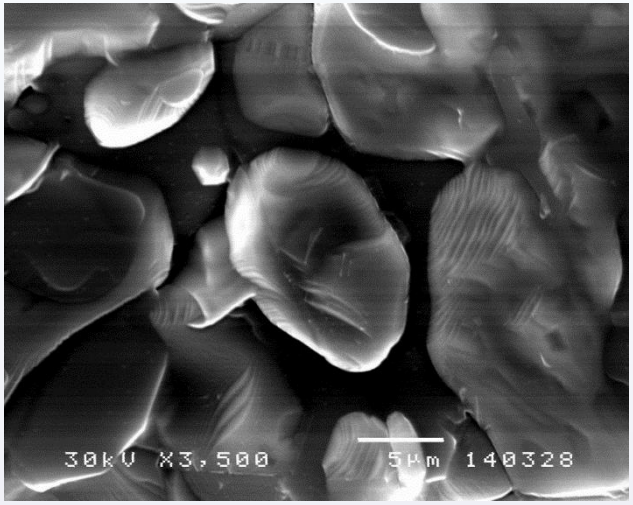

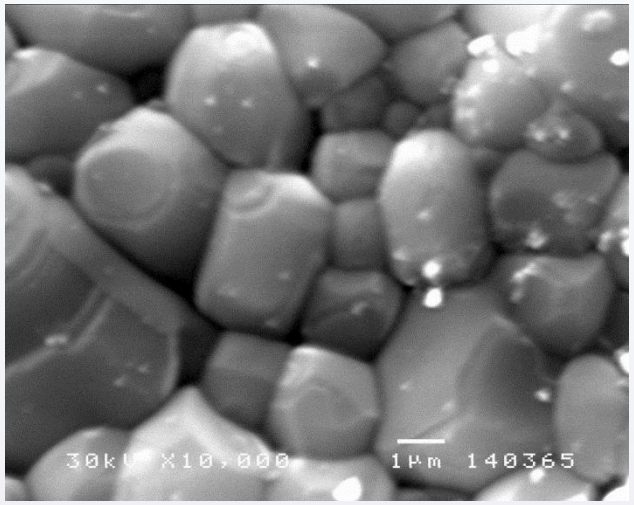

There exist lattices in *n*-dimensions having hypersphere packing densities satisfying

$$\rho = \frac{\zeta(n)}{2^{n-1}}$$

where

$$\zeta(n) = \frac{1}{(n-1)!}\int_0^\infty \frac{t^{n-1}}{e^t - 1}\,\mathrm{d}t = \frac{1}{1^n} + \frac{1}{2^n} + \frac{1}{3^n} + \cdots$$

is Riemann *Zeta function*. Property: $\zeta(2n) = \dfrac{(-1)^{n+1} B_{2n} (2\pi)^{2n}}{2(2n)!}.$

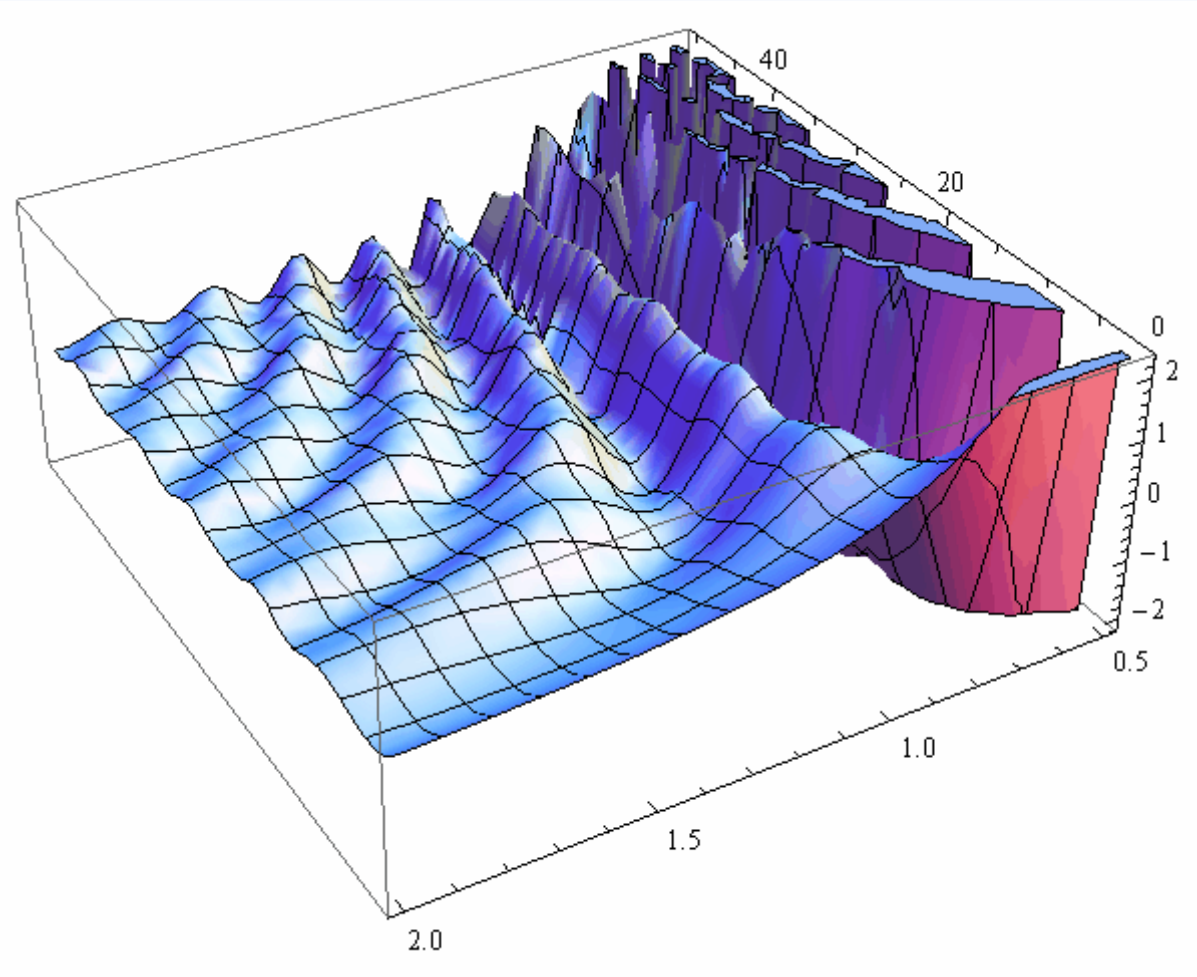

Figure **54.** The graph of Riemann Zeta function $\mathrm{Re}\{\zeta(3+i\,x,\,a)\}$ for 3D space i.e., around the point (3, a), when $0.5 < a < 2$.

Conclusion

The first aim of this scope is to review some ceramics sintered materials intergrain models including generalizations of Coble's two sphere intergrain contact model. In the initial sintering phase, two grains approximated by ellipsoids or polyhedrons, form a specific contact zone that is responsible for dielectric characteristics of $BaTiO_3$-ceramics. In this way, ellipsoid-ellipsoid, sphere-polyhedron and polyhedron-polyhedron Euclidean geometry models, have been developed. In addition, we offer a fractal extension of all of these models using fractal representation of grains. This representation is obtained as a stochastic subdivision of a regular polyhedron inscribed in a Coble's sphere, up to the certain extent. A short reflection on the Apollonian sphere packing is also given. Subdivision mechanism is flexible enough to give possibilities of changing fractal dimension of the grain, the real number that conveys information of irregularities on the grain's surface.

In the models being observed, the normal grain growth is independent from initial pressing pressure so that the results prove the conjecture that dielectric constant has a direct correlation with consolidation parameters (pressing pressure, sintering temperature and time). By simultaneous analysis of relative dielectric constant, the grain size and the capacitance distribution it can be obtained optimal intervals of technological parameters: lower sintering temperatures and higher pressing pressures.

Understanding the electrical properties of barium-titanate materials is important issue for modern devices applications and presents a challenge for simulation. In this study, the model of intergranular impedance is established using the equivalent electrical scheme characterized by a corresponding frequency characteristic. According to the microstructures we have obtained for $BaTiO_3$, sometimes doped with rare earth additives, the global impedance of a barium-titanate ceramics sample contains both a resistor and capacity component. The resistor and capacity component was presented as a “sum” of many clusters of micro-resistors and micro-capacitors connected in the tetrahedral lattice.

The positions of neighbouring grains for the four grain cluster have been defined and according to them the tetrahedral scheme of mutual electrical influence of $BaTiO_3$ grains has been established. The impedance model between clusters of ceramics grains has been presented and calculations of micro-capacitance generated in grain contacts of $BaTiO_3$ have been performed. By controlling shapes and numbers of contact surfaces on the level of the entire $BaTiO_3$–ceramic sample, control over structural properties of this ceramics can be done, with the aim of correlation between material electronic properties and corresponding microstructure.

High precision of the applied fractal nature mathematics opens the new perspectives to better intergranular capacity evaluation and micro-impedances spatial distribution understanding with the further miniaturization and electronic circuits integration frontiers. With this, we can proceed towards better components and devices packing because the semiconductor technology possibilities are already limited.

Presented investigations results in the materials structures analysis area, and the fractal nature domain are important for more precise description of contact surface in energy storage area and in materials consolidation for battery systems. These results confirm microstructure constituent's shapes, grains, reconstruction possibilities with Brownian motion particles application, by long term scientific research on the electronic materials fractal analysis. This is original contribution in the basic electrochemical thermodynamic parameters area by introducing the α, fractal correction function, having as the arguments three correction parameters α_S, α_P and α_M, as electrochemistry area functions, especially from the energy storage aspects and creating new approach towards intergranular capacity. This offers a solid base for the future procedure and further application, to create new perspectives and solutions for advanced miniaturization, electronic parameters multi-level integration, materials, components and circuits (especially *C*, *R*, *L*) characteristics, as well as new solutions for better components and electronic circuits packaging.

All of these are of huge importance for the new and alternative energy sources, as the new frontiers towards miniaturization, what is in the new experimental-theoretical approach frame in the new model line developed by the authors, which could consider as the electrochemistry area *Fractal microelectronics*. From the other side, this paper is a systematic approach to create the method for the wind motion and turbulences, prediction the fractal nature influence. In this way, we confirmed the new fractal frontiers in the area of alternative energy sources, what is very new, precise and powerful approach. The concept design main goal is to reach the inventive ideas for final products with best performances. Through this method and results, we are opening the Fractal microelectronic new frontiers and technological processes, especially specific intergranular relations within grains surfaces coatings. This enlightening the new future intergranular thin film's fractal nature microelectronics, from the one aspect, and also opening the new "window" towards that the sizes of the objects on the Earth, under the telescope from the space, are like microstructures under the microscope, from the other aspect regarding the fractal nature in the matter.

References

1. Coble, R.L., Effects of Particle-Size Distribution in Initial-Stage Sintering, *J. Am. Ceram. Soc*. **56** (9) 461–466 (1973)
2. Coble, R.L., Sintering of crystalline solids. I. Intermediate and final state diffusion models, *J. Appl. Phys*., **32,** 789–92, (1961).
3. Gibbs, J.W.: Collected Works, Longmans, New York, 1928.
4. Wulff, G. On the question of the speed of growth and the resolution of On the question of the speed of growth and the resolution of crystal surfaces (in German), *Z. Kristallogr*. 34 449–530, (1901).
5. Mitić, V.V., Structures and elektrical properties of $BaTiO_3$ ceramics, Begrade: Zadužbina Andrejević (in Serbian), 2001.
6. Kang, S.J. L., Sintering. Densification, Grain Growth, and Microstructure, Elsevier 2005.
7. DeJonge L., Rahman M.N., Sintering of Ceramics, Handbook of Advanced Ceramics, S.Sowmya et al. (Eds.), Elsevier (78s), 2003.

8. Cho, Y.K., Kang, S.L., Yoon, D.Y. Dependence of grain growth and grain-boundary structure on the Ba/ Ti ratio in $BaTiO_3$, *J. Am. Ceram. Soc.*, 87 119-124, (2004).
9. Zhang, D., Weng, G., Gong, S., Zhou D, The kinetics of initial stage in sintering process of BaTiO3 based PTCR ceramics and its computer simulation, *Materials Science and Engineering B*, 99 [1-3] 88-92, (2003).
10. Mitic, V.V., Paunovic,V.,Mancic, D.,, Kocic, Lj., Zivkovic, Lj., Pavlovic, V. B.. Dielectric Properties of $BaTiO_3$ Doped with Er2O3 and Yb2O3 Based on Intergranular Contacts Model. In Advances in Electroceramic Materials, ed. K. M. Nair, D. Suvorov, R. W. Schwartz, and R. Guo, 137–144. John Wiley & Sons, Inc. 2009.
11. Mitic, V.V., Pavlovic, V., Paunovic, V., Purenovic, J., Kocic, Lj., Jankovic, S., Antolovic,I., Rancic, D., Intergranular Properties and Structural Fractal Analysis of BaTiO3-Ceramics Doped by Rare Earth Additives. In: Advanced Processing and Manufacturing Technologies for Structural and Multifunctional Materials V, ed. Tatsuki Ohji, Mrityunjay Singh, Sujanto Widjaja, and Dileep Singh, 121–132., 2011.

12. Mitic, V.V., Pavlovic, V., Paunovic, V., Purenovic, J., Kocic, Lj., Jankovic, S., Antolovic,I., Rancic, D., Intergranular Properties and Structural Fractal Analysis of BaTiO3-Ceramics Doped by Rare Earth Additives. In: Advanced Processing and Manufacturing Technologies for Structural and Multifunctional Materials V, ed. Tatsuki Ohji, Mrityunjay Singh, Sujanto Widjaja, and Dileep Singh, 121–132., 2011.
13. Mitrovic, I., Mitic, V.V., $BaTiO_3$-Ceramics Electrical Model Based on Intergranular Contacts. *Journal of the European Ceramic Society* 21 (15): 2771-2775, (2001).
14. V. V. Mitić, Lj. M. Kocić, M.M. Ristić, The Fractals and $_{BaTiO3}$-ceramics sintering, 1997, *Key Engeneering Materials* 136, 1060-1063, (2001).
15. Mitić, V.V., Petković, P., Kocić, Lj., $BaTiO_3$-Ceramics Capacitance in Terms of Consolidation Parameters, Proc. of Micro Materials Conference and Exhibition Micro Mat 97, Berlin, 1103-1105, 1997.
16. Mitić,V., Živković, Lj., Effect of nonstoichiometry on the microstructure and electrical properties of $BaTiO_3$- ceramics, Proc. of the 12th Conference on glass and ceramics, Bulgarian Ceramic Society, Varna, Bulgaria, 479-484, 1997.

17. Mitić, V.V., Kocić, Lj.M., Ristić, M.M. The Fractals and $BaTiO_3$-Ceramics Structure, Extended Abstracts of the 5th Conference and Exhibition of the European Ceramic Society, Euro Ceramics V, Part 2, Versailles, France,. 1060-1063, 1997.

18. Nikolić, Z.S., Mitrović, I., Mitić, V.V. Computer Simulation of Neck Growth During Sintering Process, Proc. of the IX World Round Table Conference on Sintering held in Belgrade: Advanced Science and Technology of Sintering, edited by Stojanović et al., Kluwer Academic/Plenum Publishers, New York, pp. 61-66, 1999.

19. Mitić, V.V. Kocić, Lj.M. Mitrović, I.Z., Fractals in Ceramic Structure, Proc. of the IX World Round Table Conference on Sintering" held in Belgrade:Advanced Science and Technology of Sintering, edited by Stojanović et al, Kluwer Academic/Plenum Publishers, New York, pp. 397-402, 1999.

20. Mitić, V.V. Mitrović, I.Z., $BaTiO_3$ Structure Prognosis, Proc. of the IX World Round Table Conference on Sintering held in Belgrade: Advanced Science and Technology of Sintering, edited by Stojanović et al, Kluwer Academic/Plenum Publishers, New York, pp. 431-436, 1999.

21. Mitic, V.V., Pavlovic, V.B., Kocic, Lj., Paunovic, V., Mancic, D., Application of the Intergranular Impedance Model in Correlating Microstructure and Electrical Properties of Doped $BaTiO_3$*Science of Sintering*, 41 [3], 247-256, (2009).

22. Mitić, V., Paunović, V., Mancic, D., Kocic, Lj.,. Zivković, Lj., Pavlović, V.B., ″ Dielectric Properties of $BaTiO_3$ Doped with Er_2O_3, Yb_2O_3 Based on Intergranular Contacts Model, *Ceramic Transactions*, 204 137-144, 2009

23. Mancic, D., Paunovic, V., Vijatović, M., Stojanović, B. Zivković, Lj., Electrical characterization and impedance response of lanthanum doped barium titanate ceramics, *Science of Sintering*, 40 [3] 283-294, (2008).

24. Chen, J.H. Johnson, P.F., Computer Simulation of Initial Stage Sintering in Two-Dimensional Particulate Systems", P.E. Russell, Ed., Microbeam Analysis- 405-409, 1989,

25. W. Heywang, H. Thomann, Electronic Ceramics, London and New York, 1991.

26. Pontes, F.M., Pontes, D.S.L., Leite, E.R., Longo, E., Chiquito, A. J., Pizani, P. S., Varela, J.A., Electrical conduction mechanism and phase transition studies using dielectric properties and Raman spectroscopy in ferroelectric Pb0.76Ca0.24TiO3 thin films, *J. App. Phy.*, 94, 11, 7256. (2003).

27. Frenkel', Ya. I. On the surface crawling particles in crystals and the natural roughness of natural faces, JETP 16 (1), 1948.
28. Mitić, V.V., Fecht, H.J., Kocić, Lj., Materials Science And Energy Fractal Nature New Frontiers, Contemporary Materials (Renewable energy sources), VI, 2 (2015) Page 190-203.
29. Mitić, V.V., Paunović, V., Kocić, Lj. Fractal Approach to $BaTiO_3$-Ceramics Micro-Impedances, *Ceramic Int.*, Vol. 41−5, 6566–657 (2015).
30. Mandelbrot, B. B., The fractal geometry of nature, W. H. Freeman, New York 1983.
31. Boyd D. W., The osculatory packing of a three dimensional sphere, Canad. J. Math. 25, 303-322 (1973).
32. Borkovec M. et al., The Fractal Dimension of the Apollonian Sphere Packing, Fractals, Vol. 2, No. 4, 521-526 (1994).

33. V.V. Mitić, Lj.M. Kocić, M. Miljković, I. Petković, "Fractals and BaTiO3-Ceramics Microstructure Analysis", Mikrochim. Acta 15, Springer-Verlag, pp. 365-369, 1998.
34. Lj.M. Kocić, V.V. Mitić, M.M. Ristić, "Stereological Models Simulation of BaTiO3-Ceramics Grains", Journal of Materials Synthesis and Processing, Vol. 6, No. 5, pp. 339-344, 1998.
35. V.V. Mitić, Z.S. Nikolić, Lj. Kocić, M.M. Ristić, "Dielectric Properties of Barium-Titanate Ceramics as a Function of Grain Size, Advances in Dielectric Ceramic Materials", Ceramic Transactions, Vol. 88, 215-223, 1998.
36. Kaye B. H. , A Random Walk Through Fractal Dimensions, Wiley-VCH 1994.

Acknowledgements

This research is part of the project “Directed synthesis, structure and properties of multifunctional materials” (OI 172057). The authors gratefully acknowledge the financial support of Serbian Ministry of Education, Science and Technological Development for this work.